N° d'ordre :

الجمهورية الجزائرية الديمقراطية الشعبية

République Algérienne Démocratique et Populaire

وزارة التعليم العالي والبحث العلمي

Ministère de L'enseignement Supérieur et de La Recherche Scientifique

جامعة عين تموشنت بلحاج بوشعيب

Universite Ain Témouchent-Belhadj Bouchaib

Faculté: Sciences et Technologie
Departement: Génie Mécanique
Laboratoire: Laboratoire d'Hydrologie Appliquée et Environnement

THESE

Présentée pour l'obtention du **diplôme de DOCTORAT**
Domaine : Sciences et Technologie
Filière : Génie Mécanique
Spécialité : Énergétique

Par : BOUSMAHA Mouad

Intitulé

Etude et conception d'un système de distillation membranaire intégré pour la purification de l'eau et la production d'énergie.

Soutenue publiquement, le 18/12/2025, devant le jury composé de :

Nom & Prénom(s)	Grade	Qualité	Etablissement de rattachement
Mr. BOUNIF Abdelhamid	Pr	Président	Université Ain Temouchent-Belhadj Bouchaib
Mr. NEHARI Driss	Pr	Rapporteur	Université Ain Temouchent-Belhadj Bouchaib
Mr. SERIER Mohamed	Pr	Examinateur	Université Ain Temouchent-Belhadj Bouchaib
Mr. SAIM Rachid	Pr	Examinateur	Université Abou Bekr Belkaid- Tlemcen
Mr. LAOUDJ Samir	Pr	Examinateur	Université Djillali Liabes Sidi Bel Abbes
Mr. MERAD Laarej	Pr	Examinateur	Université Abou Bekr Belkaid- Tlemcen

Année Universitaire :2025/2026

N° d'ordre :

الجمهورية الجزائرية الديمقراطية الشعبية

People's Democratic Republic of Algeria

وزارة التعليم العالي والبحث العلمي

Ministry of Higher Education and Scientific Research

جامعة عين تموشنت بلحاج بوشعيب

University Ain Témouchent-Belhadj Bouchaib

Faculty of Science and Technology
Department of Mechanical Engineering
Applied Hydrology and Environment
Laboratory

THESIS

Presented to obtain the **3rd cycle DOCTORAL diploma**
Faculty: Science and Technology
Department: Mechanical Engineering
Specialty: Energetic

By : BOUSMAHA Mouad

Title of the thesis
Study and design of an integrated membrane distillation system for water purification and energy production

Supported publicly, the 18/12/2025, in front of the jury composed of:

Full Names	Grade	Quality	Establishment of attachment
Mr. BOUNIF Abdelhamid	Pr	President	University Ain Temouchent-Belhadj Bouchaib
Mr. NEHARI Driss	Pr	Supervisor	University Ain Temouchent-Belhadj Bouchaib
Mr. SERIER Mohamed	Pr	Examiner	University Ain Temouchent-Belhadj Bouchaib
Mr. SAIM Rachid	Pr	Examiner	University Abou Bekr Belkaid- Tlemcen
Mr. LAOUDJ Samir	Pr	Examiner	University Djillali Liabes Sidi Bel Abbes
Mr. MERAD Laarej	Pr	Examiner	University Abou Bekr Belkaid- Tlemcen

Academic year :2025/2026

Abstract

This study investigates the modeling, simulation, and performance analysis of a solar-assisted direct contact membrane distillation (DCMD) system for freshwater production in arid and semi-arid regions. A dynamic co-simulation approach, combining TRNSYS for solar thermal modeling and MATLAB for detailed DCMD module modeling, was developed and validated under real climate conditions in Ain Témouchent, Algeria. The system integrates flat-plate solar collectors (2 to 6 m^2), a 300-liter hot water storage tank, an auxiliary heater, and 0.5 m^2 of PVDF flat-sheet membrane modules. The DCMD module, modeled using heat and mass transfer equations, allows for co-current and counter-current operation. The simulation included two configurations: a basic system without heat recovery and an enhanced system with an economizer to recover residual heat from the membrane outlet.

The simulation results demonstrate the high performance and potential of the proposed solar integrated DCMD system for freshwater production. Membrane water production reached up to 13.57 $kg/m^2 \cdot h$, with an average daily yield of 54.28 liters during the standard 8-hour operation window. The solar fraction peaked at 71%, and the solar collector efficiency reached a maximum of 63% in July, indicating strong alignment with seasonal solar resource availability. The annual performance simulations indicated the best balance between energy efficiency, water productivity. The economizer successfully recovered thermal energy from the membrane outlet stream, preheating the incoming feed and significantly reducing thermal losses. This improved the overall thermal efficiency by reusing the membrane outlet heat, reducing system losses, increasing effective temperature at the feed inlet. and a daily water production increased from 54.28 liters/day to approximately 100 liters/day, despite a reduction in operating time from 8 hours to just 5 hours a clear indication of a more efficient desalination process.

The TRNSYS-MATLAB co-simulation framework proved to be a powerful and flexible tool for modeling, design, and performance optimization of solar-thermal desalination systems.

Keywords: *Solar desalination, Direct contact membrane distillation, Solar thermal energy, Heat recovery economizer, TRNSYS-MATLAB co-simulation.*

Résumé

Cette étude examine la modélisation, la simulation et l'analyse des performances d'un système de distillation membranaire à contact direct assistée par l'énergie solaire (DCMD) pour la production d'eau douce dans les régions arides et semi-arides. Une approche de co-simulation dynamique, combinant TRNSYS pour la modélisation thermique solaire et MATLAB pour la modélisation détaillée du module DCMD, a été développée et validée dans des conditions réelles à Aïn Témouchent, en Algérie. Le système intègre des capteurs solaires à plaque plate (2 à 6 m²), un réservoir de stockage d'eau chaude de 300 litres, un chauffage auxiliaire et 0,5 m² de modules à membranes planes en PVDF. Le module DCMD, modélisé à l'aide d'équations de transfert de chaleur et de masse, permet un fonctionnement en co-courant et contre-courant. La simulation comprenait deux configurations: un système de base sans récupération de chaleur et un système amélioré avec un économiseur pour récupérer la chaleur résiduelle à la sortie de la membrane.

Les résultats de la simulation démontrent la haute performance et le potentiel du système DCMD solaire intégré pour la production d'eau douce. La production d'eau par membrane a atteint jusqu'à 13,57 kg/m²·h, avec un rendement quotidien moyen de 54,28 litres pendant la fenêtre d'opération standard de 8 heures. La fraction solaire a atteint un pic de 71 %, et l'efficacité du capteur solaire a atteint un maximum de 63 % en juillet, indiquant une forte concordance avec la disponibilité saisonnière des ressources solaires. Les simulations annuelles de performance ont montré le meilleur compromis entre efficacité énergétique et productivité en eau. L'économiseur a permis de récupérer l'énergie thermique du flux de sortie de la membrane, préchauffant l'alimentation entrante et réduisant considérablement les pertes thermiques. Cela a amélioré l'efficacité thermique globale en réutilisant la chaleur de sortie de la membrane, en réduisant les pertes du système, en augmentant la température effective à l'entrée du fluide et en élevant la production quotidienne d'eau de 54,28 litres/jour à environ 100 litres/jour, malgré une réduction du temps de fonctionnement de 8 heures à seulement 5 heures, ce qui constitue une indication claire d'un processus de dessalement plus efficace.

Le cadre de co-simulation TRNSYS-MATLAB s'est révélé être un outil puissant et flexible pour la modélisation, la conception et l'optimisation des performances des systèmes de dessalement solaire thermique.

Abstract

Mots-clés: *Désalinisation solaire, Distillation membranaire en contact direct, Énergie thermique solaire, Économiseur de récupération de chaleur, Co-simulation TRNSYS-MATLAB*

ملخص

تبحث هذه الدراسة في نمذجة ومحاكاة وتحليل أداء نظام تقطير الأغشية المباشر بمساعدة الطاقة الشمسية (DCMD) لإنتاج المياه العذبة في المناطق الجافة وشبه الجافة. تم تطوير نهج محاكاة ديناميكي مشترك، يجمع بين TRNSYS لنمذجة الطاقة الشمسية الحرارية وMATLAB لنمذجة وحدة DCMD بالتفصيل، وتم التحقق من صحته تحت ظروف المناخ الحقيقي في عين تموشنت، الجزائر. يشتمل النظام على مجمعات شمسية مسطحة (2 إلى 6 م²)، وخزان لتخزين المياه الساخنة بسعة 300 لتر، وسخان مساعد، و0.5 م² من وحدات الأغشية المسطحة من مادة .PVDF وحدةDCMD ، التي تم نمذجتها باستخدام معادلات نقل الحرارة والكتلة، تسمح بالتشغيل المتوازي والعكسي. شملت المحاكاة تكوينين: نظام أساسي بدون استعادة الحرارة ونظام معزز مع موفر لاستعادة الحرارة المتبقية من مخرج الغشاء.

تُظهر نتائج المحاكاة الأداء العالي والإمكانات لنظام DCMD المدمج بالطاقة الشمسية المقترح لإنتاج المياه العذبة. وصل إنتاج الماء عبر الغشاء إلى 13.57 كجم/م²·ساعة، مع متوسط إنتاج يومي قدره 54.28 لتر خلال فترة التشغيل القياسية التي تبلغ 8 ساعات. بلغت نسبة الطاقة الشمسية ذروتها عند 71%، ووصلت كفاءة المجمع الشمسي إلى 63% كحد أقصى في يوليو، مما يشير إلى توافق قوي مع توافر الموارد الشمسية الموسمية. أشارت محاكاة الأداء السنوي إلى أفضل توازن بين كفاءة الطاقة وإنتاجية المياه. نجح الموفر في استعادة الطاقة الحرارية من تيار مخرج الغشاء، مما أدى إلى تسخين مسبق للتغذية الواردة وتقليل الخسائر الحرارية بشكل كبير. هذا حسن الكفاءة الحرارية العامة من خلال إعادة استخدام حرارة مخرج الغشاء، وتقليل خسائر النظام، وزيادة درجة الحرارة الفعالة عند مدخل التغذية. وزادت كمية المياه المنتجة يوميًا من 54.28 لتر/يوم إلى حوالي 100 لتر/يوم، على الرغم من تقليل وقت التشغيل من 8 ساعات إلى 5 ساعات فقط، مما يدل بوضوح على عملية تحلية أكثر كفاءة .

أثبت إطار المحاكاة المشتركة TRNSYS-MATLAB أنه أداة قوية ومرنة لنمذجة وتصميم وتحسين أداء أنظمة التحلية الشمسية الحرارية.

الكلمات المفتاحية: *التحلية الشمسية، التقطير الغشائي بالاتصال المباشر، الطاقة الشمسية الحرارية، جهاز استرداد الحرارة، المحاكاة المشتركة باستخدام* TRNSYS-MATLAB

Publications included in the thesis:

The present thesis is based on a summary of the following publications:

Journal Papers

Bousmaha, M., Remlaoui, A., & Nehari, D. (2025). *Modeling and co-simulation of an integrated solar heating system and direct contact membrane distillation module. Journal of Thermal Engineering, 11(1), 94-111*. https://doi.org/10.14744/thermal.0000906

Bousmaha, M., Belmonte, J. F., Nehari, D., Villena-Ruiz, R., Honrubia-Escribano, A., & Gómez-Lázaro, E. (2025). *Membrane distillation module powered by low-temperature solar thermal systems: Modeling and transient performance analysis. Desalination and Water Treatment, 101365*. https://doi.org/10.1016/j.dwt.2025.101365

Bekraoui, H., Nehari, D., Baki, T., & **Bousmaha, M.** (2023). *The Effect of Operating Parameters on Total Cross-membrane Flux in a PVDF Flat Sheet Membrane*. *Periodica Polytechnica Chemical Engineering, 67(3), 490-503*. https://doi.org/10.3311/PPch.21815

Conference papers

Bousmaha, M., Remlaoui, A., & Nehari, D. (2023). *Analyzing a counter-current direct contact membrane distillation system: Study and simulation*. The First Seminar on Engineering Materials and Energy Technologies, University of Relizane, Algeria.

Remlaoui, A., **Bousmaha, M.**, & Nehari, D. (2023). *Economic analysis of a self-contained solar-assisted direct contact membrane distillation system for seawater desalination*. The First Seminar on Engineering Materials and Energy Technologies, University of Relizane, Algeria.

Bousmaha, M., Remlaoui, A., & Nehari, D. (2022). *Mathematical modelling of desalination for production of drinking water using direct contact membrane distillation module*. The 1st International Conference on Water and Environment (ICWE'2022), University Mustapha Stambouli, Algeria.

Bousmaha, M., & Nehari, D. (2021). *Étude et simulation d'un système de distillation membranaire à contact direct (DCMD)*. The National Conference on Renewable Energies and Energy Efficiency (CNEREE), University Ahmed Draïa, Algeria.

Other publications related to this research but not included in the thesis:

Conference papers

Sereir, T., Remlaoui, A., **Bousmaha, M.**, & Nehari, D. (2023). *Dynamic simulation of forced circulation water heaters system (SWH) using the TRNSYS program*. The International Conference "Energy Transition and the Built Environment", University of Constantine 3, Algeria.

Remlaoui, A., **Bousmaha, M.**, Nehari, D., & Nehari, T. (2023). *Techno-economic analysis of a residential solar water heating (SWH) system*. The International Conference "Energy Transition and the Built Environment", University of Constantine 3, Algeria.

Remlaoui, A., Nehari, D., & **Bousmaha, M.** (2022). *Dynamic simulation and numerical analysis of solar water heating (SWH) system to evaluate and control auxiliary heating by recovering wasted energy*. The 1st International Symposium on Industrial Engineering, Maintenance and Safety, University Oran 2 Mohamed Ben Ahmed, Algeria.

Awards

Bousmaha, M., & Sandid, A. M. (2022). *Solar desalination*. Project presented at the 2nd edition of the EIC Energy Innovation Challenge competition (3rd Place Award), University Oran 2 Mohamed Ben Ahmed, Algeria.

Acknowledgement

I would like to express my deepest gratitude to my supervisor, **Prof. Driss Nehari**, for his continuous guidance, valuable insights, and unwavering support throughout the course of this research.

My sincere thanks go to **Juan Francisco Belmonte Toledo, Emilio Gomez-Lázaro, Raquel Villena-Ruiz,** and **Andres Honrubia-Escribano** for their warm welcome, collaboration, and support during my Erasmus+ internship at the University of Castilla-La Mancha, Albacete, Spain. Their guidance greatly enriched my academic and personal experience.

Special thanks to **Dr. Ahmed Remaloui** for his helpful advice and guidance, which were instrumental at several critical stages of this work.

I sincerely thank **Prof. Bounif Abdelhamid, Prof. Saim Rachid, Prof. Loudj Samir, Prof. Merad Laarej,** and **Prof. Serier Mohamed** for their time and valuable contributions as members of the dissertation committee.

I am also grateful to all the professors and administrative staff of the **University of Ain Témouchent** for their support and dedication throughout my academic journey.

Finally, I extend my appreciation to all who, in one way or another, contributed to the completion of this thesis.

Dedicated to

To my dear parents,
whose unwavering support and prayers have guided me every step of the way.

To my beloved sisters — Souhila, Ghania, and Douaa,
for their endless encouragement and love.

And to my friends,
for their companionship and support throughout this journey.

Thank you all.

MOUAD

Table of Contents

List of figures

Chapter IV

Chapter V

List of tables

Nomenclature

Abbreviation

AGMD	*Air-gap membrane distillation*
DCMD	*Direct contact membrane distillation*
HX	*Heat exchanger*
HVAC	*Heating, Ventilation, and Air Conditioning*
MD	*Membrane distillation*
PTFE	*Polytetrafluoroethylene*
PVDF	*Polyvinylidene fluoride*
RO	*Reverse osmosis*
SMD	*Solar membrane distillation*
SGMD	*Sweeping gas membrane distillation*
TES	*Thermal Energy Storage*
TR-PBOI	*Thermally rearranged polybenzoxazole-co-imide*
VMD	*Vacuum membrane distillation*

Greek Symbols

α	*Solar absorptance*	–
δ	*Thickness*	*m*
ε	*Porosity*	*%*
η	*Efficiency*	*%*
ρ	*Density*	kg/m^3

Subscript

amb	*Ambient*
aux	*Auxiliary energy*
coll	*Solar collector*
in	*Inlet*
load	*Total load to be met*
out	*Outlet*
sf	*Solar heat transfer fluid*
u	*Useful*
f	*Feed side*
i	*ith point*
k	*Tank number*
m	*Membrane boundary layer*
p	*Permeate side*
sat	*Saturation*
T	*Total solar radiation*

Symbol

A	*Membrane area*	m^2
Acoll	*Solar collector area*	m^2
Cm	*Water flux permeation coefficient*	$kg/m^2 \cdot Pa \cdot s$
Cp	*Specific heat capacity*	$kJ/kg \cdot K$
D	*Hydraulic diameter of the flow channel*	*m*
GT	*Total incident solar radiation flux*	W/m^2
L	*Total height of the water tank*	*m*
J	*Membrane water flux*	$kg/m^2 \cdot h$

P	*Pressure*	*Pa*
Q_c	*Conductive heat transfer through the membrane*	*W*
Q_f	*Convective heat transfer between feed and membrane*	*W*
Q_m	*Total heat transfer through the membrane*	*W*
Q_{aux}	*Auxiliary heating energy*	*kWh*
T	*Temperature*	*K*
ΔH_v	*Latent heat of vaporization*	*kJ/kg*
Q_{coll_u}	*Useful thermal energy from the solar collector*	*W*
$\dot{m}$	*Mass flow rate*	*kg/h*
F	*Solar fraction*	–
a_0	*Collector optical efficiency*	–
a_1	*1st-order efficiency coefficient (collector)*	$W/m^2 \cdot K$
a_2	*2nd-order efficiency coefficient (collector)*	$W/m^2 \cdot K^2$
b_0	*1st-order IAM coefficient*	–
h	*Heat transfer coefficient*	$W/m^2 \cdot K$
kg	*Thermal conductivity of vapor*	$W/m \cdot K$
kp	*Thermal conductivity of polymer*	$W/m \cdot K$
km	*Thermal conductivity of membrane*	$W/m \cdot K$
x	*Height from bottom of the water tank*	*m*
$xNaCl$	*Mole fraction of NaCl in feed solution*	–

General Introduction

1. General Introduction

Global demand for high-quality drinking water continues to grow, driven by rapid population growth and the increasing needs of the agricultural and industrial sectors. In response to this pressure, seawater desalination is emerging as a sustainable solution. However, conventional desalination techniques, such as reverse osmosis (RO), are highly energy-intensive, which limits their large-scale deployment, particularly in developing regions.

In this context, solar distillation presents itself as a promising alternative, particularly in regions with high levels of sunshine. Since 1872, projects have demonstrated that this process is economically viable when water needs are not excessive. Thanks to its privileged geographical position, Algeria has the largest solar resource in the Mediterranean basin, with annual sunshine exceeding 2,000 hours, reaching up to 3,500 hours in the Sahara. The total available solar energy is estimated at 169,400 TWh/year, or about 5,000 times the country's annual electricity consumption.

This thesis is part of this approach to exploiting renewable energies and focuses on membrane distillation (MD), a hybrid process combining the principles of thermal evaporation and membrane separation. More specifically, the study focuses on direct contact membrane distillation (DCMD), a simple, efficient configuration suitable for small and large scales applications for seawater desalination.

In the DCMD process, a hot solution (typically salt water heated using solar thermal collectors) is brought into contact with a microporous hydrophobic membrane, while a cold liquid circulates on the other side. The difference in vapor pressure across the membrane provides the driving force, causing evaporation on the hot side and vapor transfer across the membrane. The auxiliary energy required to operate the equipment (pumps, valves, etc.) can be supplied by photovoltaic modules.

2. Research Objectives

The main objective of this doctoral thesis is to conduct a numerical study of the membrane distillation (MD) process integrated with solar energy, with the aim of proposing a sustainable desalination solution suitable for isolated communities in coastal areas.

To address this issue, the study focused on several scientific parts:

An analysis of the membrane distillation process, with a particular focus on the direct contact membrane distillation configuration (DCMD), including operating principles, different types of membranes, and their characteristics.

The development and validation of a numerical model of the DCMD unit in MATLAB, then its integration into the TRNSYS dynamic simulation environment, with a view to studying its coupling with solar energy systems.

An evaluation of solar water heating (SWH) systems for heating feed water, analyzing the effect of auxiliary heating and thermal storage configuration, as well as modeling the permeate cooling system via TRNSYS.

The design and simulation of an integrated solar desalination system using DCMD, combining an energy loop (solar collector, tank, pumps, controllers) and a distillation loop.

Finally, an optimized design of a prototype solar-powered DCMD system, based on the simulation results, aimed at ensuring energy efficiency, technological simplicity, and economic feasibility.

3. Structure of the Thesis

Following this introduction, the content of this thesis is divided into four main chapters:

The first chapter is devoted to a review of the literature. It addresses the issue of access to drinking water in Algeria, identifying needs and challenges. It also presents the main existing desalination technologies, as well as desalination solutions coupled with renewable energies, highlighting their advantages and limitations in the local context.

The second chapter offers an in-depth study of the membrane distillation (MD) process. It details the operating principles, the different configurations (DCMD, AGMD, VMD, etc.), the characteristics of the membranes, the types of modules used, and the heat and mass transfer mechanisms. This chapter also introduces approaches for coupling MD with solar energy, highlighting their relevance for small-scale desalination applications.

The third chapter is devoted to modeling and dynamic simulation using TRNSYS software. It includes mathematical modeling of the DCMD process, as well as simulation of solar water heating systems (SDHW). The objective is to numerically represent the thermal and hydraulic behavior of the entire solar-DCMD system, also integrating an external model developed in MATLAB.

The fourth chapter presents and analyzes the numerical results obtained from these simulations. In particular, it examines the influence of feed temperature on permeate flow rate, as well as the impact of solar-DCMD system parameters (e.g., solar collector area or storage configuration) on technical performance indicators and distilled water production.

Finally, a general conclusion summarizes the main results obtained and proposes research prospects for the optimization and experimental implementation of solar distillation membrane desalination systems.

Chapter I: Literature Review

1. Introduction

Water constitutes the hydrosphere. The Earth is 97% salt water and 3% fresh water, of which 2.4% is in the form of ice, and the fresh water present in lakes and rivers is negligible. This quantity is shown in Table I. 1. Therefore, less than 1% of the total amount of water on the planet is available for human use. Furthermore, the needs of the population in some countries exceed the available water resources, which explains why in some cases the price of a liter of bottled water can be 4 to 5 times higher than that of a liter of gasoline [1].

Table I. 1: Global water volume [1]

Water	***Volume (10^{15} m^3)***	***Total***
Oceans	*1350*	*97%*
Glaciers	*33*	*2.4%*
Groundwater	*8*	*0.6%*
Lakes	*0.1*	*0.01%*
Water in soil	*0.07*	*0.01%*
Water in the atm	*0.013*	*0.001%*
Rivers	*0.0017*	*0.0001%*
Total	*1391*	*100%*

2. Water in Algeria (Problems and solutions)

Water is important for all living things and is a key part of keeping ecosystems in balance and helping people grow. Where people live and how businesses grow depend on how available it is. Water management, including treating wastewater, is very important as water becomes scarcer, especially in Africa and Southeast Asia. Today, the average person uses about 250 m^3 of water per year, but there are big differences between countries. Most of the water is used for farming and industry, and only about 12% is used at home. Over the last 50 years, the need for more water has led to a lot of thinking about how to manage it. This needs the right policies,

rules, and money, as well as treatment and analysis technologies. This study focuses exclusively on the technological aspect of water treatment.

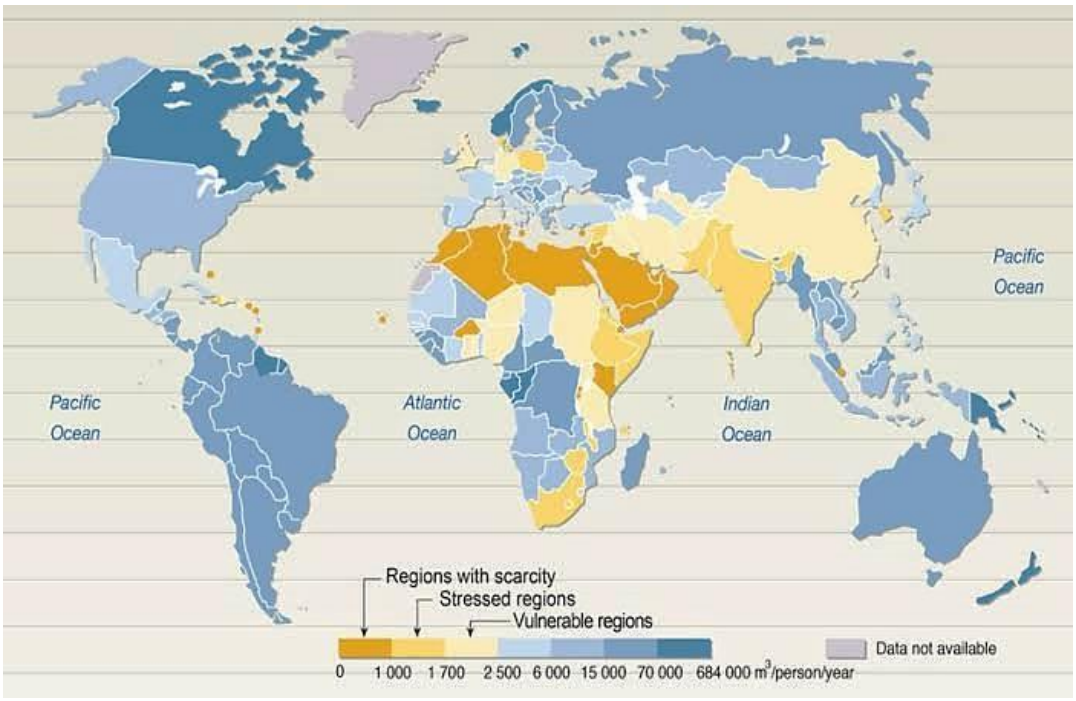

Fig I. 1: Water availability in the world [2].

2.1 Drinking water

Drinking water must meet specific physical, chemical, biological, and sensory quality criteria. In particular, it must be clear, tasteless, odorless, and pleasant to drink. However, these criteria may vary depending on the context. The World Health Organization (WHO) proposes international standards to ensure the safety of water intended for human consumption. According to these recommendations, salinity must not exceed 0.5 g/L, chlorine 200 mg/L, calcium 75 mg/L, magnesium 50 mg/L, and sulfates 150 mg/L [2].

The demand for fresh water is increasing by 4 to 5% annually, while available natural resources remain limited and are even declining due to increasing pollution. This imbalance points to a future where demand will far exceed supply. In Algeria, the population has grown from 23 million in 1987 to approximately 46 million in 2025, resulting in a substantial increase in water demand. Consumption for domestic and industrial use reaches around 5 billion m³, while the resources mobilized do not

exceed 2 billion m³. It is therefore urgent to mobilize an additional 3 billion m³ over the next two decades, not counting agricultural needs or losses due to leaks.

2.2 Problems

Algeria faces significant challenges in providing drinking water due to several key factors. Firstly, the country's water resources are limited and distributed unevenly, making them increasingly difficult to exploit and raising pollution risks. Secondly, the continuous degradation of water quality, especially in hilly areas where most surface water is located, is exacerbated by domestic and industrial pollution. Thirdly, the rapid growth of the population puts additional pressure on existing water infrastructure, particularly in densely populated coastal areas and major urban centers. With a population exceeding 35 million, urgent and sustainable solutions to these issues are required.

2.3 Solutions

With global population growth, the shortage of fresh water is becoming a major challenge, particularly in arid regions. Desalination of seawater and brackish water appears to be an effective solution for boosting drinking water resources, especially during periods of drought. This solution also offers certain advantages, including reduced use of chemicals and low sludge production compared to conventional river water treatment methods.

2.4 Seawater

Even though water exists on Earth in many forms, its overall amount remains constant because of the water's natural cycle. However, more than 97% of this resource is found in the oceans, which cover roughly 71% of the Earth's surface, primarily in the southern hemisphere. Thus, the ocean is a nearly limitless, but salted, water reserve.

2.4.1 Seawater properties

One of the most important characteristics of seawater is its salinity, which is its total salt content (sodium and magnesium chlorides, sulfates, carbonates).

The average salinity of seawater is approximately 35 g/L, mainly composed of the following salts [3].

Table I. 2: Average Composition of Seawater Salinity

Compound	***Average Concentration (g/L)***
NaCl (Sodium chloride)	*27.20*
$MgCl_2$ (Magnesium chloride)	*3.80*
$MgSO_4$ (Magnesium sulfate)	*1.70*
$CaSO_4$ (Calcium sulfate)	*1.26*
K_2SO_4 (Potassium sulfate)	*0.86*
Total	***≈ 35.00***

Salinity concentration may vary in enclosed or semi-enclosed seas, as shown in Table I. 3. In addition, the average pH of seawater ranges from 7.5 to 8.4, indicating that it is slightly basic [3].

Table I. 3: Salinity concentrations in selected enclosed seas.

Sea	***Salinity (g/L)***
Mediterranean Sea	*36 – 39 g/L*
Red Sea	*~40 g/L*
Caspian Sea	*13 g/L*
Dead Sea	*270 g/L*
Arabian Gulf	*36 – 39 g/L*

2.4.2 Saltwater

There are various types of saltwater found in nature, each with different salinity concentrations. These include seawater, brackish water and other saline waters, which are detailed below in Table I. 4. Brackish water is a type of non-potable saline water with lower salinity than seawater. It typically contains between 2,000 and 10,000 mg/L of dissolved salts. It is often found in underground sources,

acquiring its salt content through the dissolution of minerals present in the soil and rocks through which it flows. The composition of brackish water depends on geological characteristics and the rate of water circulation.

Table I. 4: Saltwater classification [2].

Water Type	***Salinity (mg/L)***
Pure water	*< 500*
Slightly brackish water	*1,000 – 5,000*
Moderately brackish water	*5,000 – 15,000*
Very brackish water	*15,000 – 35,000*
Seawater	*35,000 – 42,000*

2.5 Seawater desalination

2.5.1 Introduction

Desalination is a process that removes dissolved salts and other impurities (minerals, heavy metals, organic matter, and pathogens) from seawater, brackish water, or treated wastewater to produce fresh water suitable for human consumption or irrigation. This process reduces the salinity of the water often measured by total dissolved solids (TDS) concentration to a level below 500 mg/L, in accordance with drinking water standards [3].

Although seawater desalination is an effective solution to freshwater shortages, the process has some limitations. The process requires high energy consumption and has significant environmental impacts, such as the discharge of concentrated, sometimes hot, brine into the sea or soil. Furthermore, the use of chemicals for facility maintenance, the potential release of heavy metals and the absence of clear regulations regarding the quality of desalinated water present significant challenges.

Despite its technical and environmental limitations, desalination remains a reliable and promising solution for alleviating the shortage of fresh water in regions facing water shortages.

2.5.2 History

The desalination of seawater for the production of drinking water has been practised since ancient times, particularly through evaporation. However, desalination did not become widespread until the late 1940s, when thermal distillation technologies were developed. The first industrial desalination plants were built in the 1950s, primarily in the Middle East.

Reverse osmosis (RO) was introduced to desalination in the late 1960s. Then, in the 1970s, new membrane-based technologies such as electrodialysis (ED) and RO began to be exploited commercially.

Since 2001, RO has become the world's most widely used desalination technology, accounting for around 53% of global water production capacity. By 2003, almost 75% of new desalination plants had adopted this technology. Large-scale RO plants were commissioned in 2005, including the Wadi Ma'in plant in Jordan (150,000 m^3/day) and the Algiers plant in Algeria (200,000 m^3/day) [2].

2.5.3 Commun problems in desalination

The problems associated with desalination plants are both technical and environmental. On the technical side, a number of difficulties can be encountered, such as membrane fouling, equipment corrosion, clogging (colmatage), and scaling [4].

Corrosion, caused by high chloride ion content, high conductivity and the presence of dissolved oxygen or marine organisms, affects plant durability.

Scaling also one of common problems in desalination, caused by the precipitation of mineral salts on exchange surfaces, can be controlled by process adjustments (pressure, heat) or water pre-treatment (addition of acid, inhibitors).

Clogging is another issue which results from the presence of suspended organic matter that clogs surfaces, reducing system performance.

3. Main water desalination technologies

According to the principle of operation, current water desalination technologies are divided into two types:

- Thermal processes including a change of phases: distillation
- The membrane processes: electrodialysis, reverse osmosis and membrane distillation.

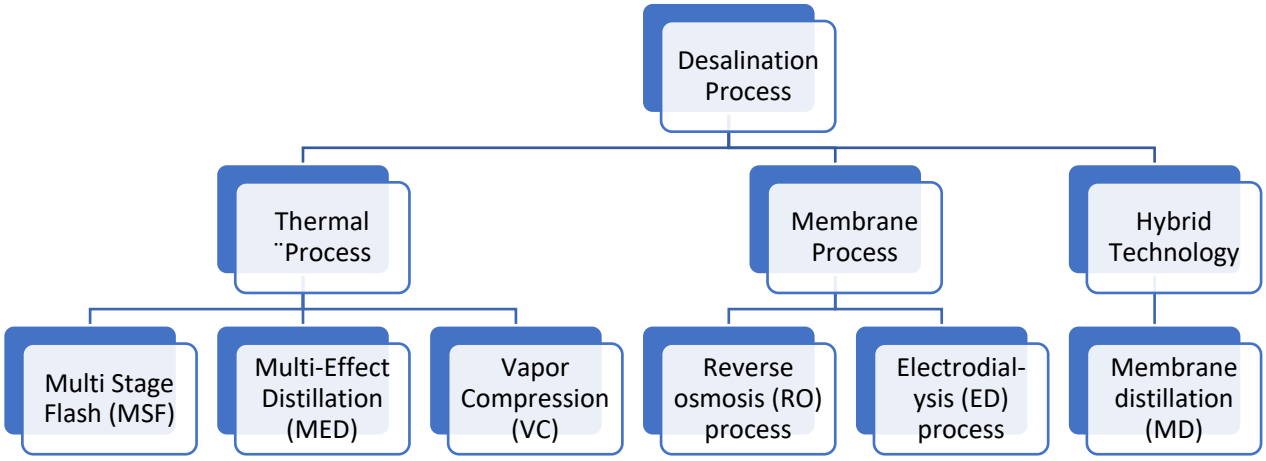

Fig I. 2: Main water desalination processes.

3.1 Thermal distillation technologies

3.1.1 Multi stage flash (MSF) process

The multi-stage distillation (MSF) process is based on the instant vaporization of seawater, also known as flash distillation. After pre-treatment, the seawater is heated to around 110°C using a heater. It is then introduced into a first chamber at reduced pressure, causing rapid evaporation. The resulting steam condenses on cooled surfaces, forming reclaimed fresh water (see Fig I. 3).

This mechanism is repeated through several successive chambers, each with a lower pressure than the previous one, enabling progressive distillation without the need for pumps between stages [5]. This process produces around 25,000 m^3 of fresh water per day, with low salinity (50 to 100 mg/L), and moderate energy consumption of 1 to 3 kWh/m^3.

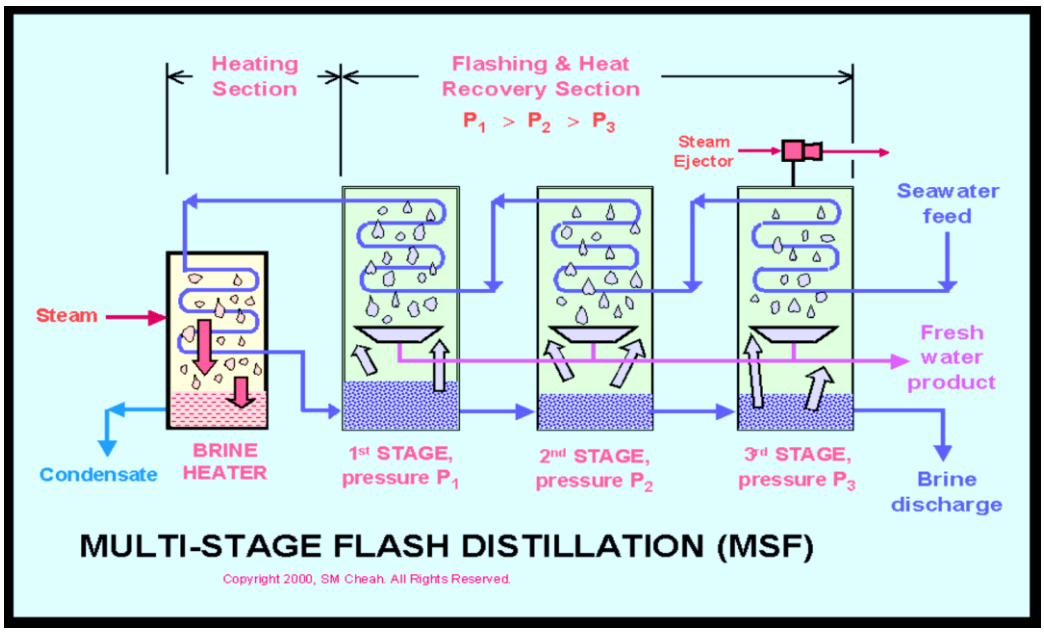

Fig I. 3: Multi-stage flash distillation [5].

3.1.2 Multi-effect distillation (MED) process

Multi-effect distillation (MED) is based on a series of cells that operate according to the single-effect principle. In the first cell, which has the highest temperature, a heat transfer fluid causes the seawater to boil. The resulting steam is then used as a heat source in the next cell, which operates at a slightly lower pressure to enable further evaporation [5].

This process is repeated through several successive stages, with each chamber benefiting from the heat of the steam produced in the previous stage. This cascade system ensures the efficient use of thermal energy (see Fig I. 4).

The MED method produces 10,000–25,000 m³ of fresh water per day with very low salinity (1–50 mg/L) and energy consumption of 1–2 kWh/m³ [5].

3.1.3 Vapor compression (VC) process

Vapor Compression (VC) distillation uses a compressor to recycle the steam produced. Seawater is brought to the boil in a thermally insulated chamber. The steam generated is then compressed, raising its temperature and saturation pressure. By condensing on a tube bundle at the base of the enclosure, this steam releases heat, which is used to evaporate more seawater (see Fig I. 5).

Although more energy-intensive, this process produces around 5,000 m³ of fresh water per day, with a final salinity of between 1 and 50 mg/L, for an energy consumption of 12 to 17 kWh/m³.

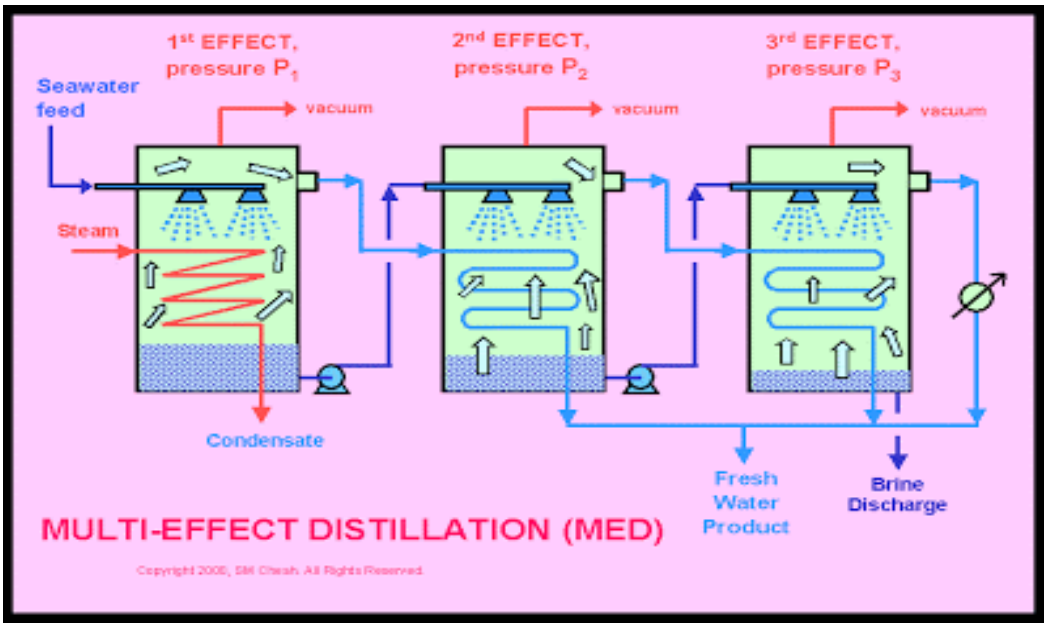

Fig I. 4: Multi-Effect distillation (MED) [5].

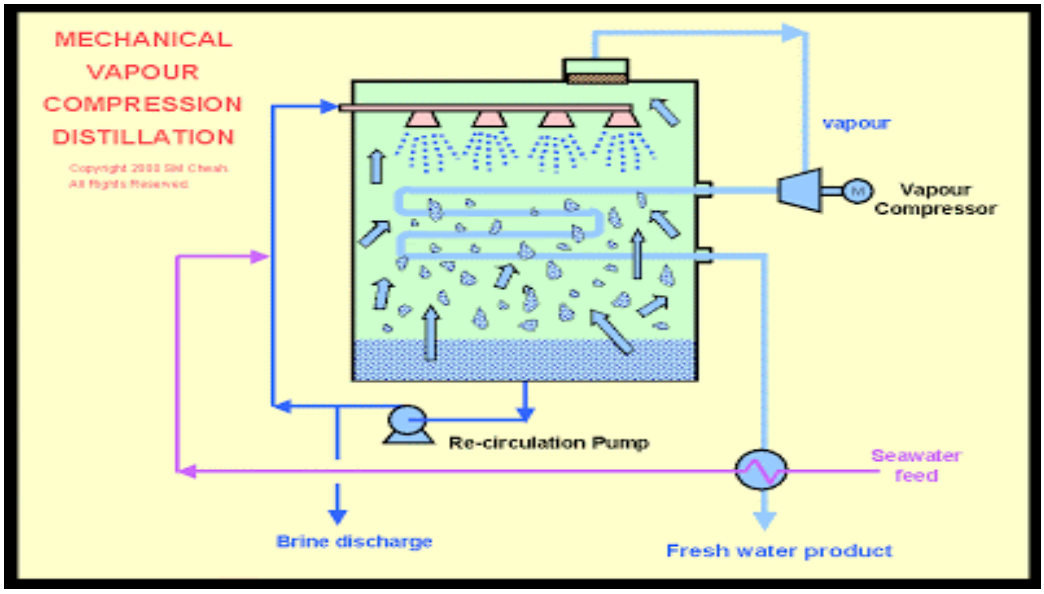

Fig I. 5: Vapor compression (VC) [5].

3.2 Membrane desalination technologies

3.2.1 Electrodialysis (ED) process

Electrodialysis (ED) is an electro-membrane process used to demineralize solutions containing ions. Under the effect of an electric field applied between two electrodes, the ions present in the water migrate through alternating anion and cation exchange membranes. This process results in the accumulation of salts in one compartment (brine) and their reduction in another (desalinated) as illustrated in Fig I. 6 Because of its high energy consumption, electrodialysis is mainly reserved for the treatment of brackish water with a salinity of less than 3 g/L [6].

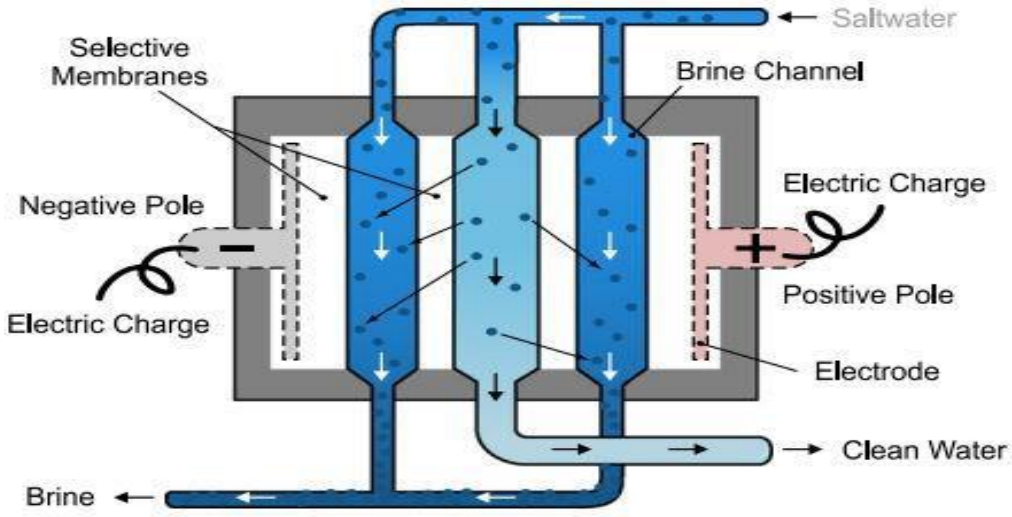

Fig I. 6: Electrodialysis (ED) process [7].

3.2.2 Reverse osmosis (RO) process

Osmosis refers to the natural movement of a solvent, such as water, across a semipermeable membrane from a region of low solute concentration to one of higher concentration, resulting in osmotic pressure. In reverse osmosis (RO), this process is reversed by applying an external pressure greater than the osmotic pressure, forcing water to move from the concentrated solution to the dilute side, thereby further concentrating the saline solution [8].

Reverse osmosis (RO) is a process for separating water and dissolved salts using semi-permeable membranes under high pressure, generally 54-80 bar. The

process is carried out at room temperature, with no phase change. Only very small water molecules can pass through the polymer membranes, while larger particles (dissolved salts, organic molecules) are retained, as illustrated in Fig I. 7 and Fig I. 8.

Reverse osmosis operates solely on electrical energy, mainly used to power high-pressure pumps. The water produced has a low salinity, around 0.5 g/L [9].

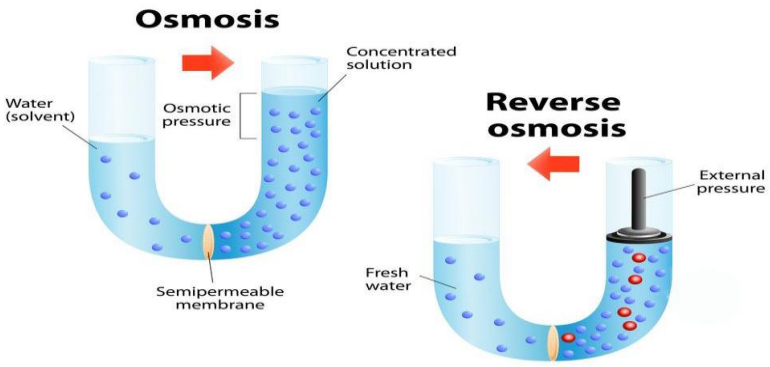

Fig I. 7: Reverse osmosis phenomenon [5].

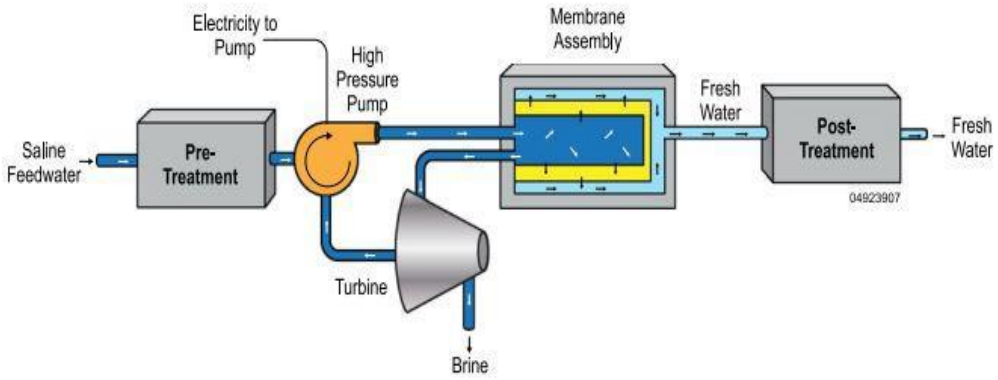

Fig I. 8: Reverse osmosis process [7].

3.3 Hybrid technology (membrane distillation process)

Membrane distillation (MD) is a thermal driven process combining both the thermal distillation process and a membrane process, MD based on the difference in vapor pressure between a hot solution and a cold surface. Feed water, in contact with a hydrophobic membrane, evaporates at moderate temperatures (often below 80°C), then passes through the membrane as vapor before condensing on the other side [10].

Different configurations exist depending on how the vapor is condensed:

- Direct contact membrane distillation (DCMD)
- Air gap membrane distillation (AGMD)
- Vacuum membrane distillation (VMD)
- Gas sweeping membrane distillation (SGMD)

DCMD, the most commonly studied, is simple to use but suffers from low energy efficiency due to conduction heat losses. AGMD, by inserting a stagnant air space between membrane and cold surface, improves thermal efficiency, but still faces technical challenges such as energy consumption, the development of specific membranes and the design of high-performance modules. Other innovative variants have also been developed, such as LGMD, PGMD, MGMD or CGMD [5], [11].

4. Renewable energies sources in desalination.

Desalination is an energy-intensive process which is traditionally powered by fossil fuels and contributes to greenhouse gas emissions. In the context of the energy transition and climate change, using renewable energy sources, particularly solar energy (photovoltaic and thermal), is a sustainable alternative for powering desalination systems, particularly in sunny regions such as the MENA zone, including Algeria [12].

Despite its great potential, desalination based on renewable energy remains very limited worldwide, accounting for only around 0.02% of total usage [13]. Integrating solar energy would enable the autonomous production of drinking water with a low environmental impact, particularly in rural or isolated areas. However, further efforts are needed to improve the efficiency of these technologies and reduce their costs, which are currently higher than those of conventional processes.

Solar desalination thus represents a promising long-term solution for addressing water shortages while reducing dependence on fossil fuels.

Renewable energies can be effectively coupled with various desalination technologies. This combination makes it possible to meet the energy and environmental challenges posed by conventional methods, while offering solutions suited to isolated or sunny areas. Fig I. 9 provides a comprehensive illustration of the different ways in which renewable energies can be combined with desalination processes.

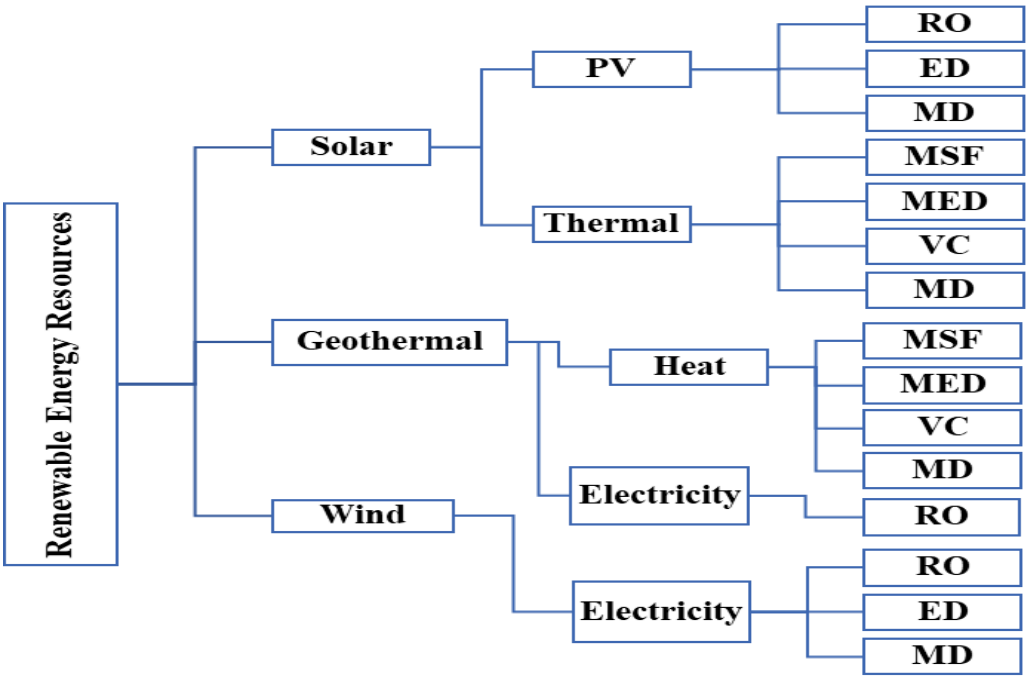

Fig I. 9:Combinations of renewable energy sources with desalination.

4.1 Solar energy

Many areas that are abundant in sunlight, such as coastal regions, suffer from a shortage of fresh water. Solar desalination of seawater or brackish water is a sustainable solution to this problem. The integration of solar energy into desalination processes has been the subject of extensive study, notably through two main approaches: thermal collectors and photovoltaic systems [5].

Solar desalination represents an interdisciplinary field of research, involving energy engineering, materials science and water resource management. Although a number of configurations have been proposed, their effectiveness is highly dependent on operating conditions and design criteria.

These technologies offer viable solutions for stand-alone installations, particularly in isolated regions with high levels of sunshine. It can be harnessed through solar distillation, for example, or coupled with thermal processes such as multi-effect distillation (MED) to produce drinking water. Solar basins and parabolic concentrators are among the most commonly used configurations [14], [15].

However, integrating solar energy into MED processes is less competitive than using fossil fuels, except in regions with high levels of sunshine, where it can

be a viable alternative. Photovoltaic (PV) panels are currently the most promising solar technology. By converting solar energy directly into electricity, they can efficiently power desalination systems, particularly those based on reverse osmosis (RO). In recent years, numerous small photovoltaic units have been installed, and PV RO systems are now the subject of commercial developments and numerous studies [16].

4.2 Wind power

Wind energy, harnessed by wind turbines, generates mechanical energy that can be converted into electricity. For optimum performance, wind speeds generally need to exceed 5 m/s. This makes wind-powered desalination a particularly attractive solution for windy coastal areas, such as the Canary Islands, where this energy is already harnessed for both electricity generation and seawater desalination [17].

Wind power is particularly well suited to batch or scalable processes such as electrodialysis (ED) and mechanical vapor compression (VC). On the other hand, its direct integration into reverse osmosis (RO) systems is more complex, due to the latter's need for continuous and stable operation. Consequently, the efficient use of wind energy in desalination requires significant investment in energy sizing and storage [18].

4.3 Geothermal energy

Geothermal energy, which is derived from the Earth's internal heat, can be harnessed in three forms: thermal energy, hydraulic energy, and methane gas. It can be used directly to power thermal desalination processes, such as MED and MSF, or indirectly to generate electricity [19]. This source has the advantages of stability and continuous availability, making it ideal for the regular operation of desalination plants. However, its exploitation is dependent on local geology and requires substantial initial investment.

Depending on feedwater quality, energy availability and system size, various renewable energy sources can be combined with specific desalination technologies. The Table I. 5: Combinations of renewable energy and desalination [20] outlines the recommended combinations for different parameters.

Table I. 5: Combinations of renewable energy and desalination [20]

Feed Water Quality	***Water Product***	***RES***	***System Size***	***Combination***
Seawater	*Distillate*	*Solar*	*-*	*Solar Distillation*
	Distillate	*Solar*	*-*	*MED*
	Distillate	*Solar*	*-*	*ST–MED*
	Potable	*Solar*	*Small*	*PV–RO*
	Potable	*Solar*	*Small*	*PV–ED*
	Potable	*Wind*	*Small & Medium*	*Wind–RO*
	Potable	*Wind*	*Small & Medium*	*Wind–ED*
	Potable	*Wind*	*Medium & Large*	*Wind–VC*
	Potable	*Geothermal*	*Medium & Large*	*Geothermal–MED*

5. Solar energy integrated with desalination

Solar energy can be converted into thermal or electrical energy. Thermal energy is usually produced locally using solar stills or solar thermal energy collection systems. As for electrical energy, it can be generated on-site by photovoltaic (PV) conversion or through solar thermal power plants.

5.1 Direct solar thermal distillation (solar stills)

This technology, used for several decades, is based on the greenhouse effect principle. A solar still usually consists of a shallow basin filled with saline or brackish water, covered by a tilting transparent roof that acts as a condenser. Solar radiation penetrates through the blanket, heats the water and causes it to evaporate. The water vapor then condenses on the inner surface of the roof and flows into a collecting channel.

The average production of a conventional solar still generally varies between 4 and 6 liters per day. Many improvements have been made over time, as the optimization of the configuration of the basin, addition of wicks to improve absorption, and using multiple layers of glass or even the coupling with solar thermal collectors to increase efficiency [2]. Due to their simplicity, low cost and autonomy, solar stills are a viable and competitive solution for the supply of drinking water in

rural or remote areas, particularly where demand is low and occasional [20], [21], [22]. Fig I. 10 illustrates an overview of solar still and different types of this process.

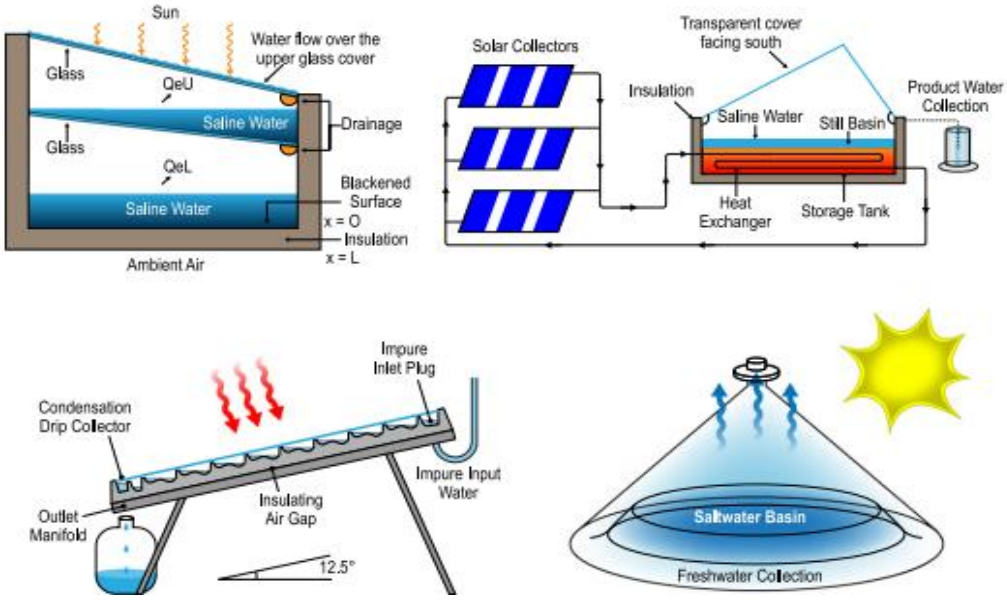

Fig I. 10: Solar still overview [7]

5.2 Solar pond

A solar pond is a saltwater basin that functions as a large scale solar thermal energy collector, with an integrated heat storage system to supply thermal energy [23] . Desalination using a solar pond is a promising renewable energy solution for producing large quantities of fresh water. Study carried out as part of the "El Paso" solar pond project (1987-1992) focused on the technical feasibility of thermal desalination integrated with solar ponds [2]. Thermal desalination processes, such as MSF and MED, can use the heat supplied by solar ponds to heat the salt water feed, without emitting greenhouse gases [24] (see Fig I. 11).

5.3 Solar membrane distillation

The solar energy required to power the membrane distillation (MD) process can typically be supplied by various thermal collector technologies:

- Flat plate collectors (FPC)
- Evacuated tube collectors (ETC)
- Compound parabolic concentrators (CPC)

- Salt gradient solar ponds (SGSP)
- Solar stills.

In addition to heat, MD requires electricity to power pumps and other equipment. This electricity can be supplied by the grid, via an auxiliary diesel generator (assisted system), or by photovoltaic (PV) collectors coupled to batteries and inverters (autonomous system). Fig I. 12 shows an example of a solar-powered MD system [25].

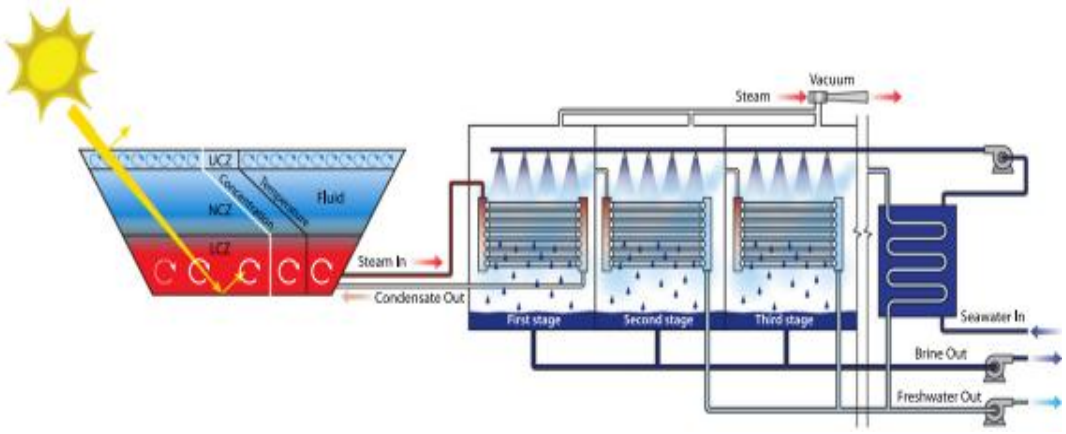

Fig I. 11: Solar Pond integrated with MED process [7].

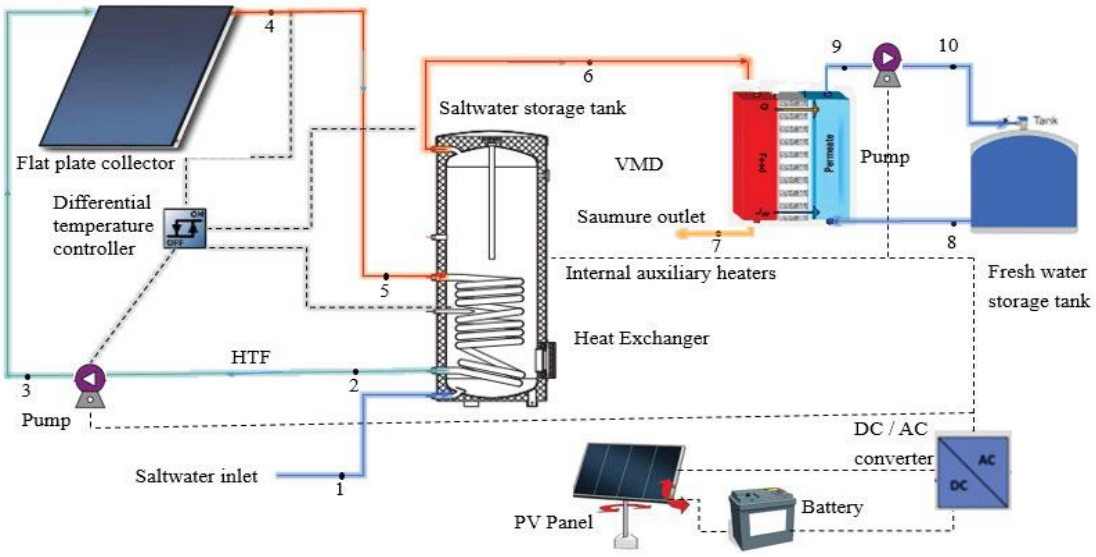

Fig I. 12: Diagram flow of a MD system powered by solar energy [26].

5.4 Solar thermal CSP

Concentrating Solar Power (CSP) technologies are based on the concentration of solar radiation using moving mirrors to produce high-temperature heat. This heat

is then fed into conventional thermal cycles (steam turbines, Stirling engines, etc.) to generate electricity. The four main CSP technologies are: parabolic trough mirrors, Fresnel mirrors, solar towers and dissipation turbine systems [7]. Although their main purpose is electricity generation, these systems can be effectively coupled with desalination processes. The parabolic trough system is currently the most suitable for CSP/desalination coupling, particularly with MED and RO processes.

5.4.1 CSP/MED

In this configuration, the steam produced (around 380°C) first feeds a turbine to generate electricity, then is reused at a lower temperature (70°C) to feed a MED unit (see Fig I. 13). This coupling was tested at the Almería solar platform (PSA) in Spain in the 1990s, and improved in the European AQUASOL project (2002), aimed at reducing costs and energy consumption. Although technologically mature, this solution remains costly compared with conventional desalination processes [7].

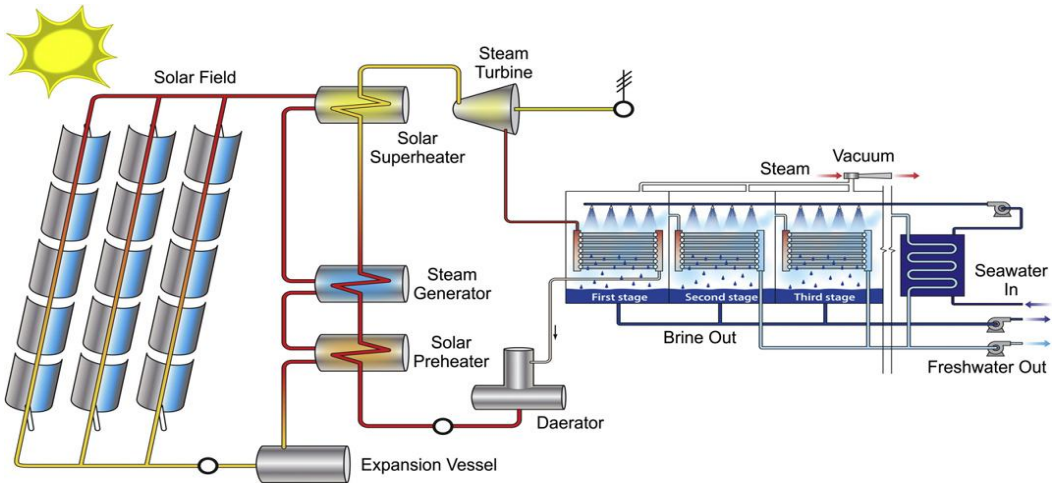

Fig I. 13: CSP/MED integrated system [7].

5.4.2 CSP/RO

For this system the heat generated by the CSP is converted into electricity to power the pumps required for the RO system (see Fig I. 14). A previous internal studies by Bechtel Power Corp.[27] have shown that this configuration is more energy-efficient and more effective than CSP/MED.

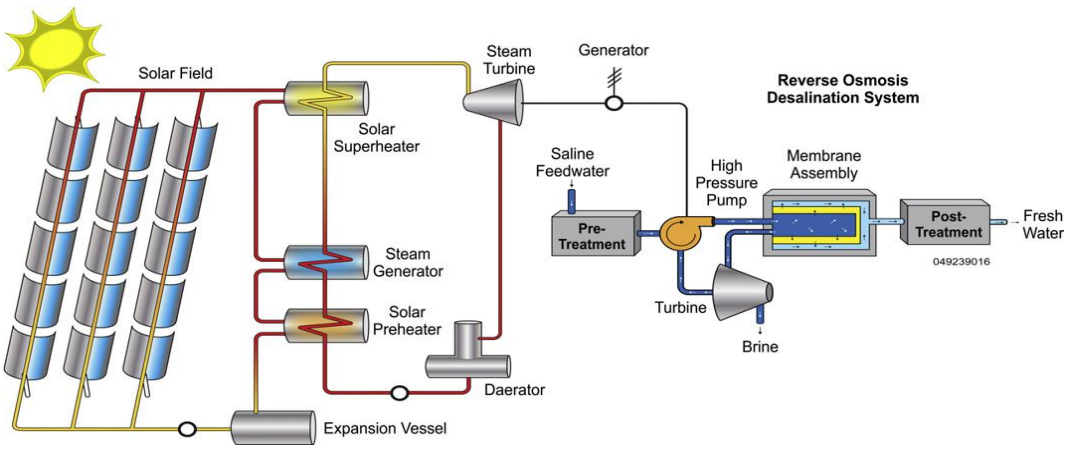

Fig I. 14: CSP/RO integrated system [7].

5.5 Solar-photovoltaic-coupled desalination

Photovoltaic (PV) cells are semiconductor devices, typically made of crystalline or amorphous silicon, that can convert sunlight directly into direct current (DC) electricity. This electricity can then be used to power various desalination processes.

5.5.1 PV/RO

In reverse osmosis (RO), the energy produced by solar panels is used to power the pumps that generate the pressure required for water to pass through membranes. A PV/RO system usually consists of PV panels, an inverter, an RO desalination unit, and a storage tank. This system is ideal for remote locations and highly efficient in sunny regions (see Fig I. 15).

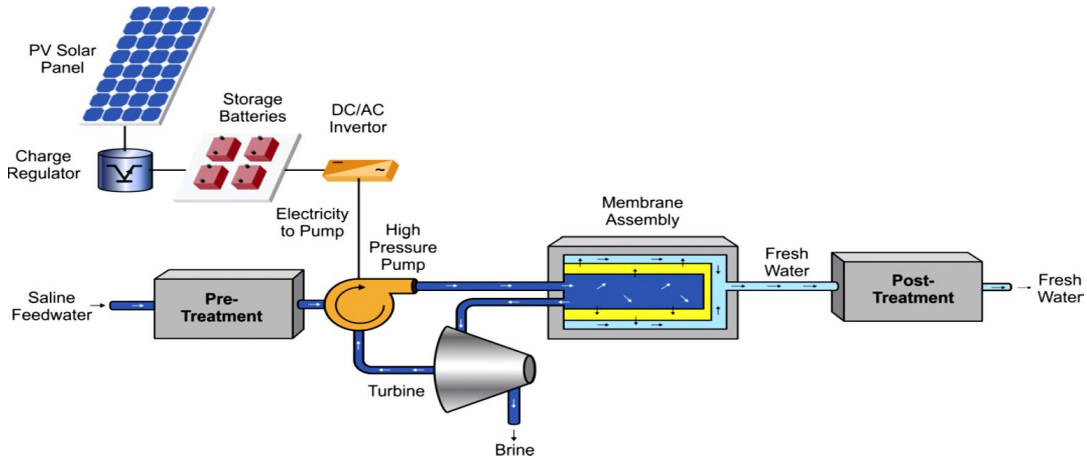

Fig I. 15: Schematic diagram of PV/RO process [7].

5.5.2 PV/ED

The electrodialysis (ED) system also uses direct current (DC), making it compatible with PV installations without the need for complex current transformation. Only a low-pressure pump is required, making this a cost-effective solution for treating low-concentration brackish water (less than 2500 ppm). The block diagram of this system is shown in Fig I. 16

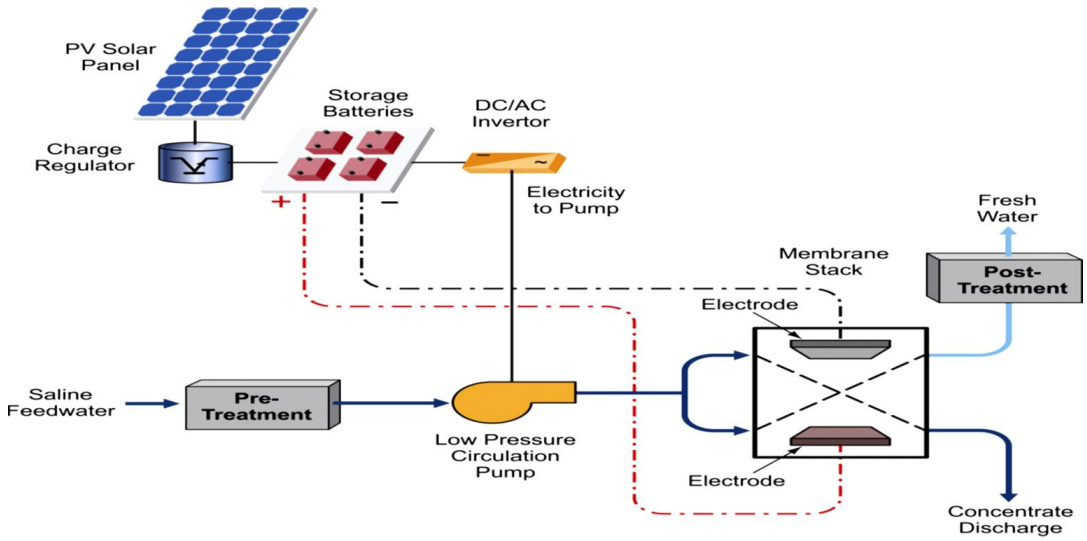

Fig I. 16: Schematic diagram of PV/ED process [7].

6. Overall Comparison of Desalination

Before selecting an appropriate desalination system, it is important to consider the various technologies available, including thermal and membrane processes. This section provides a comparison of the main desalination methods and their respective advantages and disadvantages to assist in making an appropriate choice based on specific requirements and operating conditions.

6.1 Thermal processes comparison

Thermal desalination processes, such as MSF, MED and VC, differ mainly in their energy efficiency, operating flexibility, investment requirements and specific fields of application.

MSF process is a mature technology widely used for large-scale installations. It is robust, requires little pre-treatment and can handle highly saline waters (up to

70,000 mg/L). However, it is energy intensive, with high pump consumption (around 4-5 kWh/m³), high brine production and significant greenhouse gas emissions. Scaling in the tubes is frequent, and its modulation capacity is limited, making it inflexible in the event of variations in demand. Moreover, in the event of leakage, the risk of contamination of fresh water by seawater is high, compromising product quality.

In comparison, the MED process offers numerous advantages. It operates at low temperatures (< 70°C), which reduces the problems of corrosion and scaling, energy in MED is more efficient (2 to 3 kWh/m³) and requires lower investments (10 to 20% less than MSF). Its operating flexibility is noteworthy, with a 15%-100% of capacity production for the nominal load without affecting performance, unlike the MSF. In case of leaks, the MED also offers better health safety, as the steam passes into the seawater. MED main drawback remains the limited unit size of the plants, although recent advances now make it possible to reach up to 22,500 m³/day per unit [2].

Finally, the VC process is particularly well suited to small-scale plants. It offers low energy consumption, simple operation with few components, and great adaptability to water sources of different salinities. It is well suited to isolated sites or sites with variable demand, and has a limited environmental impact. Still, it is dependent on electrical power to run the compressors, which can increase operating costs, and is less suited to large capacities. Pre-treatment of the feed water is often necessary to maintain the quality of the water produced.

6.2 Membrane processes comparison

RO and ED are two membrane desalination technologies with distinct properties that make them appropriate for specific application scenarios. Since the 1990s, reverse osmosis has undergone significant improvements, particularly in terms of membrane performance, investment cost reduction, and energy efficiency. It has a high rejection rate of salts, minerals, and organic compounds, making it the most popular method for desalinating seawater and brackish waters. However, it operates under high pressures, making the process relatively energy-intensive. It is

also susceptible to fouling and clogging of the membranes, which can result in high maintenance expenses.

Electrodialysis, on the other hand, stands out for its minimal energy consumption, making it ideal for treating low-salinity waters. It does not require high pressures, hence reducing the demand for pumps. ED also allows for selective ion separation, which is particularly useful for producing demineralized water with a composition similar to that of raw water, while maintaining its "living" properties. It can also be used to concentrate brines and recover salt. However, this method is sluggish to develop and remains constrained by fouling concerns and implementation difficulty, particularly in heavily laden environments.

In conclusion, whereas RO is often preferred for its ability to produce vast amounts of drinking water, ED remains competitive for low-mineral brackish water, particularly in inland applications, when the quality of produced water and brine valorization are significant factors.

7. Conclusion

In this chapter, we presented an overview of the major desalination technologies on the market, highlighting their potential for integration with energy production systems. This combination allows for the simultaneous production of fresh water and electricity; however, the most appropriate technology is determined by a number of factors. It is therefore necessary to examine the various possibilities available in order to identify the most appropriate solution. Once this decision has been made, detailed thermodynamic and economic studies applied to various geographical contexts should be able to prove the relevance of the chosen procedure.

In this regard, the study will focus in the next chapter on a configuration based on membrane distillation (MD) integrated with solar thermal energy.

Chapter II: Membrane distillation

1. Membrane distillation (MD)

1.1 Introduction

Membrane distillation (MD) is a new technology that shows a lot of promise for desalination and treating wastewater. It works by using a vapor pressure differential through a hydrophobic membrane to separate the parts of a liquid combination. MD is different from traditional thermal distillation methods because it uses a membrane as a physical barrier. The membrane only lets water vapor through and keeps liquid water, dissolved salts, and other non-volatile compounds from getting through. The most typical way to do this is to heat the feed side and keep the permeate side cold. This generates a temperature difference that causes vapor to pass through the membrane pores [28]. MD is an encouraging technique that works at lower temperatures, typically between 50°C and 90°C, making it cooler than conventional distillation and operating at significantly lower pressures than the RO process [29].

1.2 History of membrane distillation

Bruce R. Bodell patented MD in 1963 in the U.S. His invention provided a device that uses a heat-resistant silicone rubber membrane that is permeable to water vapor but impermeable to liquid water and contaminants to produce potable water from saline water [30].

Findley published the first scientific work on membrane distillation in 1967, looking at gumwood, aluminum foil, cellophane, silicon, and Teflon membranes. He defined the essential concepts of direct contact membrane distillation (DCMD) and specified the membrane parameters required for efficient MD [31], [32].

In 1967, Weyl also proposed an innovative strategy to improving water desalination efficiency that focused on polytetrafluoroethylene (PTFE) hydrophobic membranes and hybrid membranes. His work includes membranes constructed of PTFE, polyethylene, polypropylene, and polyvinyl chloride, which were frequently coated to increase hydrophobicity [33].

Bodell advanced the technology with a 1968 continuation patent, which described tubular silicone membranes and introduced the sweeping gas membrane distillation (SGMD) design, in which air sweeps water vapor for external condensation [30].

1.3 Principal of membrane distillation

MD is a thermally driven separation technique that uses a microporous hydrophobic membrane to create a physical barrier between two phases: a hot feed solution and a cold permeate, which can be liquid or gas. The temperature difference across the membrane creates a vapor pressure gradient, driving the transport of vapor molecule typically water vapor in applications involving the concentration of non-volatile solutes through the membrane pores as illustrated in Fig II. 1

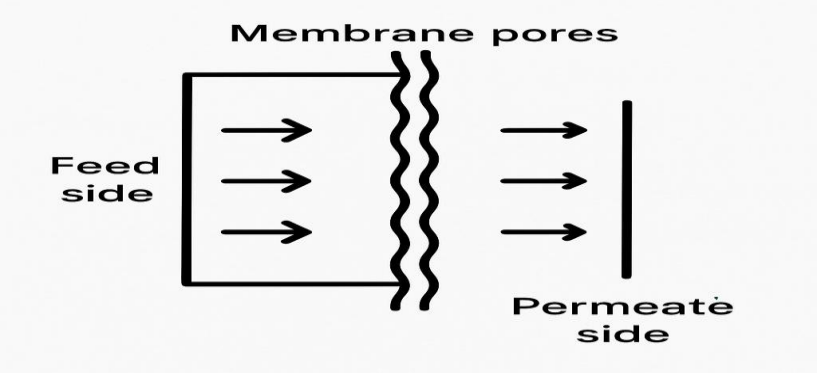

Fig II. 1: Principle of Membrane Distillation.

1.4 Advantages and disadvantages of membrane distillation

Table II. 1: Advantages and disadvantages of membrane distillation.

Advantages	***Disadvantages***
- *Low operating temperatures (<80-90 °C).* - *Low operating pressures.* - *Excellent ability to reject non-volatile solutes, ions, macromolecules, and colloids.* - *Possibility to treat very saline, which are difficult to treat by reverse osmosis.* - *Reduced chemical contact with the process solution and required less vapor space than traditional distillation.*	- *Lower permeate flux than conventional processes like reverse osmosis.* - *Fouling and wetting of hydrophobic membranes can reduce the efficiency and lifespan of the membranes.* - *Often requires pre-treatment of the feed water to avoid clogging and wetting.*

2. Membrane distillation configurations

Once the vapor has passed through the membrane, there are several methods for condensing this vapor. These methods offer a variety of MD configurations, including: Direct contact membrane distillation (DCMD), Air Gap Membrane Distillation (AGMD), Vacuum Membrane Distillation (VMD), and Sweeping Gaz Membrane Distillation (SGMD). Each configuration depends on how to collect the distilled water or the vapor in permeate side.

2.1 Direct contact membrane distillation (DCMD)

The direct contact membrane distillation (DCMD) process is based on direct contact between the feed solution and the surface of a hydrophobic membrane as depicted in Fig II. 2. Only water vapor can travel through the membrane during this procedure, while liquid water cannot due to the membrane's hydrophobic characteristics [34].

The operation of DCMD is dependent on the differential in vapor pressure between the two sides of the membrane. The feed solution, which is often saline or polluted water, is heated, resulting in water vapor in contact with one side of the membrane. On the other hand, a cold surface or cooling liquid permits the vapor to condense after passing through the membrane. This condensation produces a pure distillate, or liquid water free of impurities [28].

To ensure vapor transfer, there must be a considerable temperature differential between the hot solution and the cooling liquid, resulting in a vapor pressure gradient. The hydrophobic membrane is critical in preventing liquid water from passing through, avoiding mixing between the feed solution and the distillate. This process provides proper separation of impurities and pollutants. Furthermore, the hydrophobic membrane must be carefully selected and maintained on a regular basis to ensure its long-term performance, particularly to limit fouling and degrading phenomena that could jeopardize the process's efficiency [35].

2.2 Air gap membrane distillation (AGMD)

Air gap membrane distillation (AGMD) is a thermal separation technique that incorporates an air gap between the permeate solution and the membrane surface. Similar to other membrane distillation arrangements, a hydrophobic membrane is employed, permitting only the transit of water vapor molecules while obstructing the ingress of liquid water [34] (see Fig II. 2).

The functioning of AGMD is depending upon a vapor pressure differential created by a temperature gradient between the heated solution, often saline or polluted water, and a cold surface positioned on the opposite side of the membrane. The water vapor generated upon contact with the membrane permeates it in gaseous form, then diffusing across the air space before condensing on a cold surface or a cooling liquid. This phenomenon leads to the creation of a refined distillate [36], [37].

The air space serves a crucial function by working as an insulating layer, minimizing thermal losses by conduction through the membrane. This layer, however, also adds resistance to mass transfer, potentially restricting vapor movement. Furthermore, the gas gap guarantees the absence of direct contact between the feed solution and the condensation surface, thereby minimizing the possibility of membrane wetting and enhancing process stability [36], [37].

The hydrophobic membrane employed in AGMD must be meticulously chosen for its resistance to fouling and degradation to guarantee sustained performance. Furthermore, the design of AGMD systems must consider the meticulous regulation of the air gap's thickness and stability, as these factors directly affect energy efficiency and process productivity.

2.3 Vacuum membrane distillation (VMD)

Vacuum membrane distillation (VMD) is an innovative form of thermally assisted membrane distillation, where a hydrophobic membrane is employed with a vacuum on the permeate side to enhance the selective transport of water vapor. This arrangement facilitates the maintenance of a significant vapor pressure differential across the membrane, hence enhancing the unidirectional transmission of the vapor

phase. The membrane functions as a selective barrier due to its hydrophobic characteristics, permitting the passage of water vapor while keeping non-volatile solutes and liquid water, so assuring successful separation [38], [39].

The operational idea relies on two driving forces: a temperature gradient established between the feed side (hot) and the permeate side (cold), and a decrease in partial vapor pressure achieved through vacuum application. The feed solution, typically saline or polluted water, is heated until the water vapor contacts the membrane's surface. The introduction of a vacuum on the permeate side reduces the saturation pressure, hence enhancing the vapor flow through the membrane [40]. The vapor is subsequently condensed on a chilled surface, resulting in the retrieval of a high-purity distillate.

A significant advantage of VMD is its capacity to enhance permeate flux relative to alternative membrane distillation configurations, while minimizing the likelihood of membrane wetting, contingent upon the stringent regulation of operational parameters especially feed temperature and vacuum pressure [11], [39]. This method is especially appropriate for high-value applications, including industrial wastewater treatment, concentration of thermosensitive fluids, and low-energy desalination.

2.4 Sweeping gas membrane distillation (SGMD)

Membrane distillation with sweep gas (SGMD) is a more advanced method of membrane distillation that employs an inert gas flow (often air or nitrogen) to improve vapor transport and process yield. A hydrophobic membrane, like other types of membrane distillation, allows only water vapor to flow through while keeping liquid water and non-volatile solutes [12].

The SGMD idea is based on the formation of a concentration gradient strengthened by a sweep gas flow that flows from the permeate side parallel to the membrane's surface. This gas transports water vapor molecules outward, lowering their partial pressure on the permeate side and ensuring a continuous driving force across the membrane [40]. Unlike in other arrangements, the vapor is not instantly condensed after passing through the membrane, but rather transferred to an external condenser and collected as distillate.

In a typical process, a feed solution (saline or contaminated water) is heated to generate steam. This steam comes into contact with the hydrophobic membrane, passes through its pores due to the vapor pressure gradient, and is taken away by the sweep gas on the permeate side. This dynamic prevents vapor saturation at the membrane, allowing for more consistent and efficient diffusion [11].

Despite the somewhat increased complexity of the system, the SGMD provides several advantages, including reduced flow losses due to quick condensation, improved process control, and adaptation to various types of pollutants. To reduce energy losses, it is necessary to carefully manage gas flows and optimize thermal efficiency.

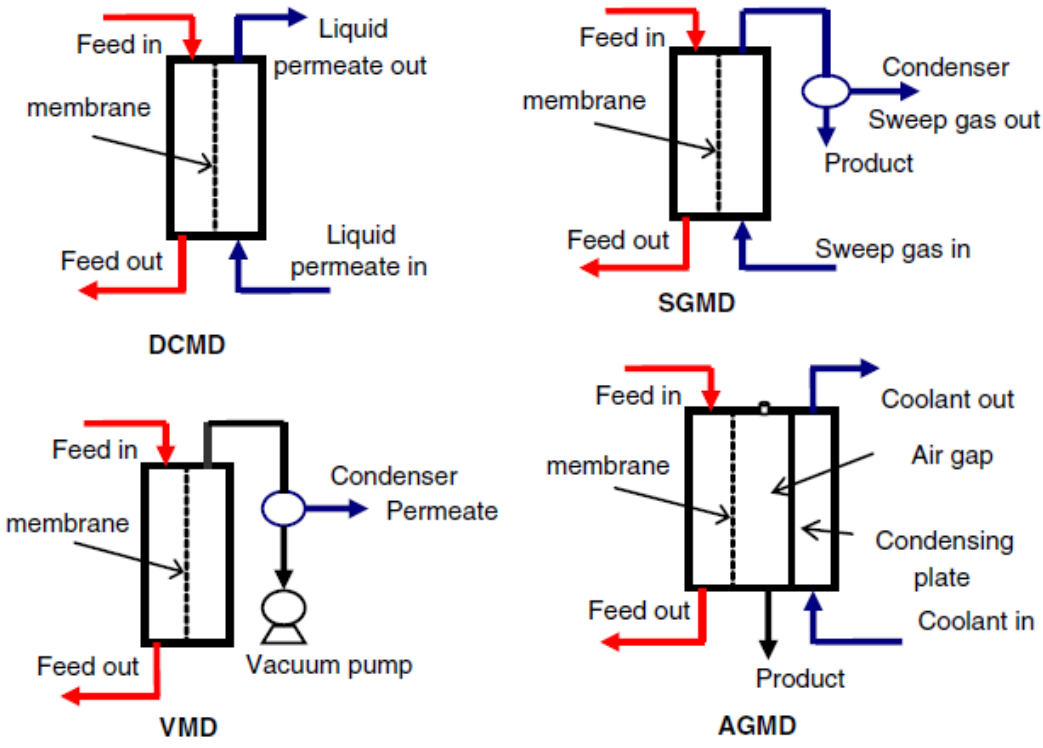

Fig II. 2: MD configurations [34].

3. Comparison of MD configurations

Table II. 2: Key principle, advantages, and disadvantages of MD

MD type	***Key principle***	***Advantages***	***Disadvantages***
DCMD	*Direct contact between the hot feed solution and the membrane, and between the membrane and cold permeate.*	*Simple design, high permeate flux, effective for saline water desalination.*	*Heat loss by conduction, relatively high energy consumption.*
AGMD	*Presence of an air gap between the membrane and the condensation surface.*	*Reduced heat loss, lower risk of membrane wetting, suitable for complex feed solutions.*	*Additional mass transfer resistance, lower permeate flux.*
SGMD	*Use of an inert gas to carry vapor away, with external condensation.*	*Reduced mass transfer resistance, good for volatile compounds.*	*Permeate dilution by the gas, higher energy consumption.*
VMD	*Application of vacuum on the permeate side to lower pressure and increase vapor flux.*	*High flux, suitable for highly saline waters, reduces membrane wetting risk.*	*Higher risk of membrane wetting, requires smaller pore membranes, more complex system design.*

Due to its simplicity, the DCMD technique is frequently utilized in modelling research and experimental development. Indeed, the DCMD arrangement requires direct contact between the two fluids on each side of the membrane, making it easier to formulate heat and mass transfer equations. This simplicity enables the creation of more accessible and stable mathematical models, which facilitates process simulation, optimization, and control. Furthermore, the membrane compositions employed in DCMD (typically in PTFE or PVDF) are well-known and stable, making it easier to analyze the physical processes involved.

Although DCMD has higher energy losses than other designs, such as AGMD or VMD, its operational efficiency and ease of modeling make it a popular choice for basic and applied research, particularly in theses and technological development projects.

In addition to traditional configurations such as DCMD, AGMD, VMD, and SGMD, several innovative membrane distillation configurations have been

developed to increase energy efficiency and permeate flow. The material gap membrane distillation (MGMD) arrangement improves on AGMD by incorporating specialized materials between the membrane and the condensation surface to maximize thermal transfers [34]. The permeate gap membrane distillation (PGMD), a mix of DCMD and AGMD, offers a permeation space that decreases conductive thermal losses while increasing overall system efficiency [41]. Multi-effect membrane distillation (MEMD) uses many stages within the same module, with internal heat recovery, to reduce specific energy consumption [42]. Finally, the vacuum multi-effect MD (VMEMD) arrangement combines the benefits of vacuum and many effects to improve thermal performance and energy efficiency [43]. These advancements show an increasing interest in enhancing membrane distillation, particularly in high-efficiency sustainable desalination applications [11], [34].

4. Membrane materials and characteristics

In the membrane distillation (MD) process, hydrophobic microporous membranes (non-wetting) are generally made from polytetrafluoroethylene (PTFE), polypropylene (PP), or polyvinylidene fluoride (PVDF). To ensure optimal performance, these membranes must exhibit low mass transfer resistance as well as low thermal conductivity to limit heat loss through the membrane. Moreover, they must offer good thermal stability at high temperatures and high resistance to aggressive chemical agents, particularly acids and bases.

Other new materials are being investigated as replacements for old polymers in membrane distillation, and thermally rearranged polybenzoxazole-co-polyimide (TR-PBOI) has showed promising results due to its high thermal stability, higher hydrophobicity, and improved mechanical strength. Kim et al. found that TR-PBOI outperformed conventional materials in terms of water vapor permeability and long-term operational stability [44].

4.1 Liquid entry pressure (LEP)

The liquid entry pressure (LEP) is a critical parameter in membrane distillation processes, as it defines the maximum pressure beyond which the feed

liquid risks penetrating the hydrophobic pores of the membrane. Such infiltration would compromise the vapor/liquid separation, thereby affecting the performance of the process. The LEP is primarily determined by the membrane's maximum pore size, hydrophobicity, and feed solution composition. Indeed, the presence of organic solutes reduces the liquid's surface tension, greatly lowering the LEP. Typically, commercial membranes used in membrane distillation have LEP values ranging from 1-4 bar [45]. LEP can be increased by using materials with low surface energy, a high contact angle, and tiny pore size. Franken et al. [46] provided the following equation for estimating the LEP (Eq.(1)):

$$LEP > P_f - P_p = \frac{-2B\gamma_1 cos\theta}{r_{max}} \quad (1)$$

Where P_f and P_p are the two hydraulic pressures on feed and permeate side (MPa), B is the geometric pore coefficient (=1 for cylindrical pores), γ_1 is the liquid surface tension (N/m), θ is the contact angle and r_{max} is the maximum pore size (m).

4.2 Membrane thickness

The membrane thickness (δ) has a significant impact on the performance of membrane distillation systems since it directly effects permeate flux and mass transfer resistance. In general, increasing membrane thickness reduces permeate flux because of increased resistance to vapor movement through the membrane [47]. However, this effect can be accompanied by significant benefits: a thicker membrane reduces thermal losses by conduction while decreasing the chance of wetness, potentially extending the membrane's operational lifespan. A previous investigation found that a thickness of 30-60 μm is optimal for balancing thermal performance and mass transmission [48]. It is crucial to note that in stagnant air membrane distillation systems (AGMD), the impact of membrane thickness can be ignored, with the intermediate air layer acting as the primary limiting factor.

4.3 Thermal conductivity

The thermal conductivity of a membrane used in membrane distillation is typically calculated using the thermal conductivities of the polymer k_p and the gas contained in the pores k_g, which is often air. The parameter k_p is affected by a number of parameters, including temperature, material crystallinity, and crystalline structure. However, the hydrophobic polymers usually utilized in MD membranes have identical heat conductivity characteristics. At 23°C, PVDF, PTFE, and PP had thermal conductivities of 0.17–0.19, 0.25-0.27, and 0.11-0.16 W/m·K, respectively [49]. To account for the material's bicomponent structure, the effective thermal conductivity of a membrane is often calculated as a volume average of k_p and k_g [50], the membrane conductivity can be calculated using Eq.(2):

$$k_{mem} = (1 - \mathcal{E}).\, k_p + \mathcal{E}.k_g \tag{2}$$

where, $\mathcal{E}$ is membrane porosity and k_p , k_g are the thermal conductivity of the solid (polymer) and gas in pores, respectively.

4.4 Membrane porosity and tortuosity

The porosity of a membrane, abbreviated as, is defined as the ratio of the volume of the pores to the overall volume of the membrane. A high porosity increases the available evaporation surface, encouraging increased permeate flow while lowering heat loss through conduction. In other words, higher porosity improves membrane performance in terms of mass transport and thermal efficiency. Porosity can be determined using the Smolder-Franken equation [51] (see Eq.(3)):

$$\mathcal{E} = 1 - \frac{\rho_m}{\rho_p} \tag{3}$$

Where ρ_m and ρ_p are the densities of the membrane and polymer, respectively.

Tortuosity (τ) refers to the deviation of the pore structure from the ideal cylindrical geometry. A high tortuosity indicates longer and more complex diffusion paths, reducing permeate flow. Mackie and Meares [19] proposed the most generally used correlation for estimating tortuosity, which is expressed in Eq.(4):

$$\tau = \frac{2-\varepsilon}{\varepsilon} \quad (4)$$

There are numerous commercial membranes used in membrane distillation. Table II. 3 shows a representative sample of membranes frequently available on the market, together with their key technical properties.

Table II. 3: Commun commercial membranes [52].

Membrane	***Manufacturer***	***Material***	***Thickness (µm)***	***Pore Size (µm)***	***Porosity (%)***	***LEP (bar)***
TE35	Schleicher &	PTFE	120	0.2	75	4
LCWP	Schnell	PTFE	125	5	58	2
TF200	Millipore	PTFE	175	0.2	80	0.7
TF450	Gelman	PTFE/PP	175	0.45	80	1.4
TF1000	Gelman	PTFE/PP	150	1	80	0.5
	Gelman					

In general, based on earlier research [2], [51], [52] identified a list of key requirements that a membrane should meet to be appropriate for membrane distillation (MD) applications.

- The membrane can be made up of one or more layers, but at least one of them must be porous and made of a hydrophobic material.
- The pore size should be between 10 nm and 1 µm, and porosity should be maximized, as higher porosity or larger pore sizes improve permeate flux in MD. On the other hand, to prevent pore wetting, the membrane should have a high LEP, which is best achieved by utilizing materials with low surface energy, high hydrophobicity, and tiny maximum pore diameters.
- A low tortuosity factor is preferable, as higher tortuosity can limit mass transfer and thus lower permeate flux.
- Single-layer membrane thickness must be tuned. Thicker membranes can limit mass and heat transfers.
- The membrane material's thermal conductivity should be as low as feasible to reduce heat loss. Although most commercial membranes have thermal conductivities from 0.04 to 0.06 W/m·K, overall thermal stability is important.

- The membrane material should be highly chemically resistant to a variety of feed solutions. If cleaning is necessary, resistance to both acidic and basic chemicals is essential.
- The membrane must be long-term operational stable, preserving both permeability and selectivity over time.
- Cost-effectiveness is critical the membrane must be economically viable for large-scale use.

5. Membrane distillation applications

To better understand the performance and requirements of membranes in membrane distillation (MD) processes, the Table II. 4 below lists a number of research studies published in the literature. These studies used a flat sheet membrane and examined different membrane types, physical properties (thickness, pore size), MD process configurations (DCMD, AGMD, VMD, SGMD), and feed solutions studied.

This section illustrates the diversity of membranes studied in membrane distillation processes, particularly in terms of materials (PVDF, PTFE, PVDE), geometries (thickness ranging from 55 to 178 µm), and pore sizes (0.1 to 0.8 µm). DCMD and VMD are the most widely utilized techniques, with extremely porous hydrophobic membranes favored. The feed solutions range from pure water to complex industrial effluents, demonstrating the versatility of MD.

Table II. 4: Membrane modules used in previous investigations [48]

MD Process	***Membrane Type***	***Thickness (µm)***	***Pore Size (µm)***	***Feed Solution***	***Reference***
DCMD	TF200	178	0.2	Pure water and humic acid	[53]
	PVDF	125	0.22		
DCMD	PVDF	125	-	Humic acid/NaCl	[54]
DCMD	PVDF	126	0.22	Pure water, NaCl, brackish and seawater	
DCMD	PTFE		0.2		
AGMD		175	0.5	Seawater and NaCl	[55]
DCMD	PTFE		0.1		
	PTFE	60	0.3	Pure water	[56]
	PVDE	60	0.2		
DCMD	PVDF	100	0.4		
DCMD	PVDF	120	0.2	Pure water, NaCl	[57]
	-	125			
	PTFE	125		Pure water and humic acid	[58]

DCMD		120	0.22	Heavy metals waste	[59]
DCMD			0.25		
	PTFE	-	0.8	LiBr and H_2SO_4	[60]
AGMD	PTFE	80		NaCl, H_2SO_4, NaOH, HCl, HNO_3	[61]
AGMD	PTFE	-	0.2	Acetone, ethanol, isopropanol, MTBE	[62]
VMD	3MC	60	0.2	Pure water, ethanol, degassing water	[63]
VMD	3MB	76	0.2	Pure water and ethanol	[64]
VMD	3MA	81	0.2		
	PTFE	91	0.51		
	PTFE	178	0.4	NaCl	[65], [66]
SGMD		178	0.29		
			0.2		
			0.45		

6. Different modules geometry for membrane distillation

The modules mechanically support and integrate the membranes in membrane distillation systems. They have a significant impact on the overall functioning of the process, impacting fluid distribution, mass and heat transfer performance, and the ease of cleaning and changing the membranes.

Currently, four major types of modules are available for membrane separation applications:

- Flat sheet (plate and frame)
- Hollow fiber
- Tubular membrane
- Spiral wound membrane

6.1 Flat sheet (plate and frame)

The membrane and spacers are layered between two plates, resulting in a flat sheet arrangement. This arrangement is extensively utilized on a laboratory scale because to its simplicity of cleaning and replacement. However, the packing density, or the ratio of membrane surface area to occupied volume, remains low, necessitating the use of a membrane support. Table II. 4 shows the properties of some flat sheet membranes utilized by various researchers. Flat sheet membranes are widely employed in membrane distillation applications, particularly desalination and water treatment.

6.2 Hollow fiber

The hollow fiber module, used in membrane distillation processes, is made up of thousands of hollow fibers arranged in a "shell" tube. Depending on the arrangement, the feed solution can flow inside or outside the fibers, with the permeate collected on the opposite side. This type of module has the advantage of a high packing density and low energy consumption. Nevertheless, it is challenging to maintain and clean, and it is susceptible to fouling. If the feed solution penetrates the membrane pores, especially in envelope and tube-type modules, the complete module must be changed. This arrangement has been effectively used for the treatment of apple juice, alcohols, and saline wastes [48].

6.3 Tubular membrane

In this type of module, the membrane is tubular and is positioned between two cylindrical chambers carrying hot and cold fluid, respectively. Commercially, tubular modules are appreciated for their low fouling sensitivity, ease of cleaning, and relatively efficient exchange surface. However, it has lower packing density and higher operational expenses than other modules. Tubular membranes, including ceramic membranes, have been utilized in various membrane distillation configurations (DCMD, AGMD, and VMD) to process saline solutions such as NaCl, with rejection rates surpassing 99% [2].

6.4 Spiral wound membrane

In this module, a flat membrane and spacers are spirally looped around a perforated center collection tube. The feed flow passes axially over the membrane's surface, while the permeate flows radially towards the center before being collected by the tube. This structure, known as a spiral module, has a high stacking density, moderate energy consumption, and a medium fouling rate [48].

7. Mechanism

MD process is based on temperature differential between two solutions separated by a hydrophobic membrane. This method permits the passage of water vapor while retaining liquids and non-volatile solutes. To understand and maximize its operation, it is necessary to investigate the underlying phenomena that regulate it.

The system involves two types of transfers as depicted in Fig II. 3 for DCMD module:

- Heat transfer, which maintains the thermal gradient required for evaporation
- Mass transfer, which corresponds to the flow of water vapor across the membrane.

These transfers take place sequentially through the membrane, from the feed side to the permeate side. Furthermore, it should be mentioned that MD systems use two types of fluid circulation configurations: co-current, in which the feed and permeate flow in the same direction, and counter-current, in which both flows move in opposite directions. This latter design is often more thermally efficient since it allows for a more consistent temperature gradient across the module.

The next sections go over these mechanisms, their relationships, and how they affect the overall performance of the membrane distillation (MD) process.

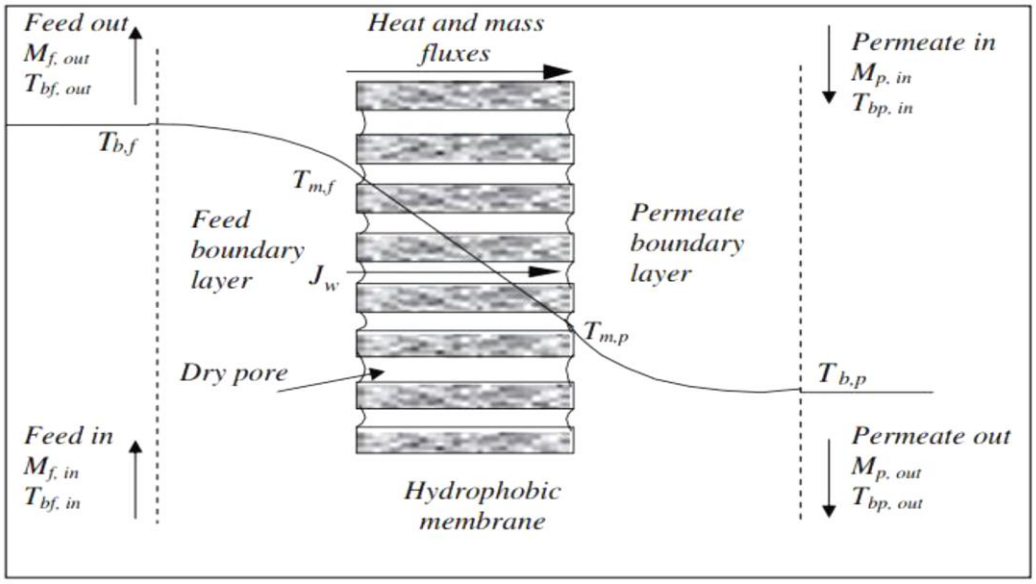

Fig II. 3: Mechanisms of phenomena in DCMD.

7.1 Mass transfer

This mass transfer occurs from the zone of higher vapor pressure on the heated feed side to the zone of lower vapor pressure on the colder permeate side. This allows for efficient separation without liquid water or dissolved solutes passing through. The non-isothermal nature of the process distinguishes MD from traditional membrane filtration processes, which rely on pressure-driven liquid flow.

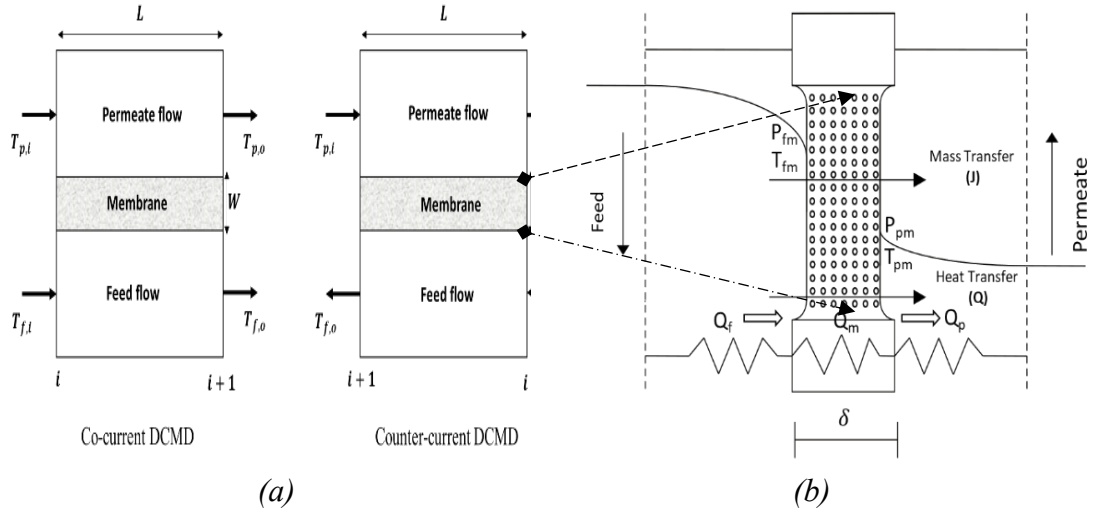

Fig II. 4: (a) Direct contact membrane distillation configurations, (b) Heat and mass transfer in DCMD module.

The driving force of mass transfer is determined by vapor pressure changes inside the dry porous membrane and the membrane water flux. By applying **Fick's first law**, the transmembrane mass flux is proportional to the partial vapor pressure difference, can be expressed using the following equation,[67]:

$$J_i = A_i . C_m . \Delta P^{sat} = A_i . C_m \left(P'^{sat}_{fm,i} - P^{sat}_{pm,i} \right) \quad (5)$$

The permeability coefficient of the membrane, denoted as C_m, is an important metric determined by the membrane's microstructural properties. Dong et al.[68] used the same method to calculate C_m using laboratory-scale experimental data. This method can predict the large-scale performance of units with a similar membrane and identical C_m. Then, a new method for estimating water flux J of the scaled-up was used. This method, based on the tanks-in-series approach, predicts the J iteratively. Raoult's law can be used to calculate the feed's partial vapor pressure in an aqueous NaCl solution, assuming 100% salt rejection on the feed side alone [38], [69].

$$P'^{sat}_{fm,i} = (1 - x_{NaCl,i}) . (1 - 0.5 . x_{NaCl,i} - 10 . x^2{}_{NaCl,i}) . P^{sat}_{fm,i} \quad (6)$$

Water saturation pressure at the feed and permeate membrane sides, P_{fm}^{sat} and P_{pm}^{sat}, were evaluated using the Antoine equation at the feed and permeate temperatures $T_{fm,i}$ and $T_{pm,i}$, where $x_{NaCl,i}$ is the mole fraction of NaCl in the feed solution as mentioned in reference [70]:

$$P_{m,i}^{sat} = 133.322 \times 10^{\left(8.07131-[1730.630/(T_{m,i}-39.724)]\right)} \quad (7)$$

7.2 Heat transfer

On the other hand, the heat transfer in the DCMD module is divided into 3 modes as illustrated in Fig II. 5:

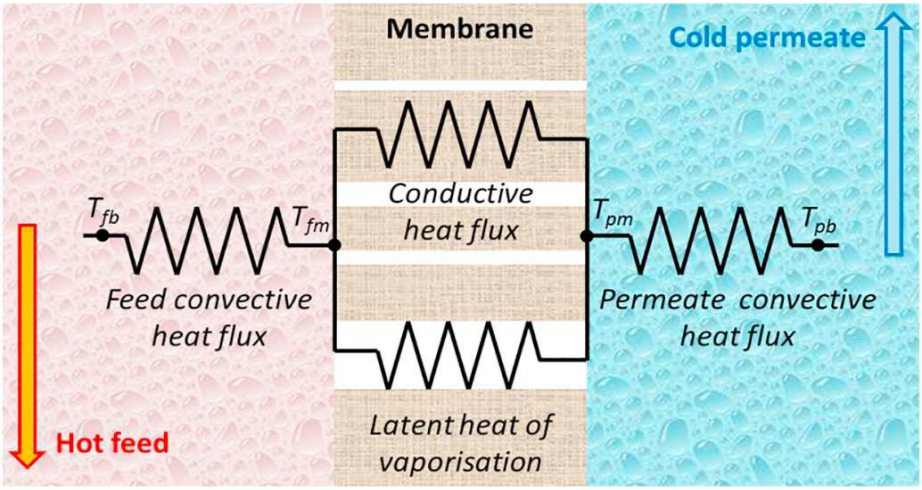

Fig II. 5: Heat transfer in DCMD module [71].

a) The convective heat transfer between the feed water and the membrane at the feed side is represented by Eq.(8) [72]:

$$Q_{f,i} = h_{f,i}(T_{fb,i} - T_{fm,i}) \quad (8)$$

b) The total heat transfer through the membrane ($Q_{m,i}$) is at the same time by conduction ($Q_{c,i}$) and latent exchange generated by water vapor passage ($Q_{v,i}$) [72][73].

c) The conductive heat flow over the flat sheet membrane can be calculated using Eq.(9):

$$Q_c = \frac{A_i . k_{mem}}{\delta} . (T_{fm} - T_{pm}) \quad (9)$$

$$Q_{m,i} = Q_{c,i} + Q_{v,i} = \frac{A_i . k_{mem}}{\delta} . (T_{fm} - T_{pm}) + J_i \Delta H_{v,i} \quad (10)$$

$\Delta H_{v,i}$ is the vaporation latent heat, given by Eq.(11) [49]:

$$\Delta H_{v,i} = 1.7535 . T_i + 2024.3 \quad (11)$$

The convective heat transfer between the permeate and the membrane at the permeate side is represented by Eq.(12), as provided in reference [11]:

$$Q_{p,i} = h_{p,i}(T_{pm,i} - T_{pb,i}) \quad (12)$$

Where k_{mem} is the membrane thermal conductivity, T_{bf} and T_{pf} are the bulk temperatures on the feed and permeate sides respectively, k_{mem} can be calculated using Eq. (2).

The convective heat transfer coefficients ($h_{f,i}$ and $h_{p,i}$) involve evaluating the Nusselt numbers. $h_{f,i}$ and $h_{p,i}$ varies based on operating conditions, the two convective heat transfer coefficients can be calculated using Eq.(13).

$$h_i = \frac{N_u . k}{D_i} \quad (13)$$

Where k is liquid conduction coefficient (W/m. K) and D_i is hydraulic diameter (m).

Semi-empirical equations based on dimensionless numbers, such as the Nusselt number (Nu), Reynolds number (Re), and Prandtl number (Pr), can be used to determine $h_{f,i}$ and $h_{p,i}$ coefficients. It should be noted that numerous empirical correlations have been developed to link these dimensionless numbers, and a variety of these correlations are shown in Table II. 5. It is important to note that each correlation is unique to a specific flow regime (laminar, transitional, or turbulent), as well as the module geometry (flat sheet, hollow fibers, etc.). The appropriate correlation is thus required for accurate thermal and hydrodynamic modeling of the system.

Table II. 5: Heat transfer correlations [68].

Membrane	***Flow Regime***	***Correlation***
Flat sheet	Laminar ($R_e < 10^4$)	$N_u = 0.664 {P_r}^{1/3} {R_e}^{1/2}$ (14)
	Turbulent$R_e > 10^4$	$N_u = 0.023 {R_e}^{0.8} {P_r}^{0.4}$ (15)
Hollow Fiber (shell side feed)	Laminar ($R_e < 10^4$)	$N_u = 0.664 {P_r}^{1/3} {R_e}^{1/2}$ (16)
	Turbulent$R_e > 10^4$	$N_u = 0.036 {P_r}^{1/3} {R_e}^{4/5}$ (17)
Hollow Fiber (bore side feed)	Laminar ($R_e < 10^4$)	$N_u = 0.027 {R_e}^{0.8} {P_r}^{1/3}$ (18)
	Turbulent$R_e > 10^4$	$N_u = 0.0.036 {R_e}^{0.8} P_r^{\frac{1}{3}} (\frac{2r}{L})^{0.055}$ (19)

In membrane distillation, the temperature difference between the feed/membrane interface (T_{mf}) and the permeate/membrane interface (T_{mp}) drives the transfer of water vapor through the membrane as depicted in Fig II. 6. However, thermal losses in the system cause temperatures at the interfaces to be lower than those measured in the bulk of the fluids. This reduces the theoretical driving force, which is defined as the difference between the bulk temperatures of the feed fluid (T_{bf}) and the permeate (T_{bp}), resulting in temperature polarization. This loss of efficiency can be evaluated using the temperature of polarization coefficient (Tpc). It is defined as the ratio of the actual driving force (calculated from interface temperatures) to the theoretical driving force (based on bulk temperatures) [72] (see Eq.(20)).

$$Tpc = \frac{T_{mf} - T_{mp}}{T_{bf} - T_{bp}} \quad (20)$$

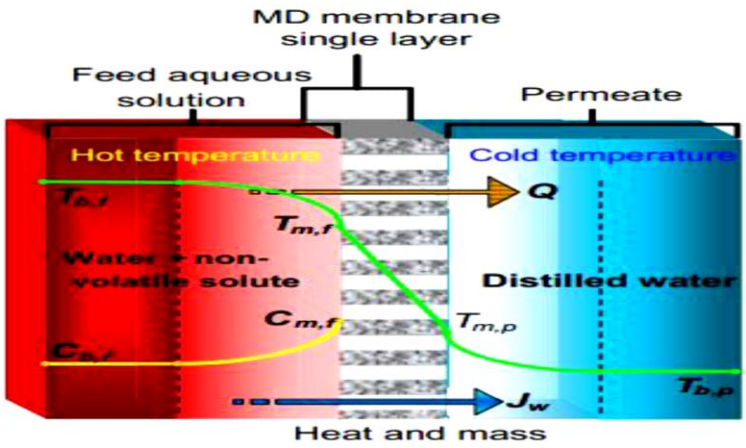

Fig II. 6: Polarization temperature in DCMD configurations [52].

8. Solar Membrane Distillation (SMD)

SMD can significantly reduce water scarcity while minimizing negative environmental effects [74]. However, due to MD's low feed temperature requirements, which include solar energy [75], which is consistently abundant in areas with a scarcity of freshwater, it appears to be a viable solution to this problem [76], making it suitable for Algeria, which has a significant solar energy potential [77]. Solar and desalination units work together to provide clean water to remote areas that do not have access to water or electricity. Several experimental studies have been conducted to determine the feasibility of desalination applications using MD systems and solar energy on a small and large scale.

8.1 Small-scale SMD

In small-scale studies, Shim et al. [67] investigated the feasibility of using solar energy for saltwater desalination. They found that combining a DCMD module with a solar collector with a 4.7 m² FPC area and a 0.06 m² DCMD module area resulted in lower thermal efficiency. In this regard, several experimental studies have been carried out; one of these investigations is the SMADES project, which includes two small-scale pilots. The first model, built and tested in Irbid, Jordan [78], [79], has a 5.73 m² solar FPC area that directly heats the hot solution for an AGMD module with a ten m² membrane area. The system produces 19 l/m² of FPC area per day. The second pilot in Alexandria, Egypt [80] produced 11.2 l/m² of FPC area per day. In Aqaba, Jordan, two subsystems [81] were installed for the same project, including a 72 m² FPC field and a 40 m² AGMD system with heat recovery. A heat exchanger

connected the two subsystems, with the desalination subsystem providing 2-11 l/m² of solar collector.

8.2 Large-scale SMD

As for large-scale studies, a combined unit for saltwater desalination was built, with productivity ranging from 59 to 117 l/day on sunny days In PozoIzquierdo-Gran, Canary Island, Spain. The unit included an 8.5 m² permeation gap membrane distillation (PGMD) system area and internal heat recovery, linked to a 6.96 m² FPC area [82]. Selimli et al. conducted experiments on seawater distillation using a solar pond and a solar vacuum tube, demonstrating its environmental friendliness, cost-effectiveness, and efficiency. The solar tube increased heat energy, increased distilled water production, and required no additional energy, providing a promising and sustainable solution to water scarcity in low-energy areas [83]. In Almeria, Spain [84], pilot-scale AGMD modules of 2.8 and 9 m² were connected to a 500 m² compound parabolic collector (CPC) via heat exchangers. Guillén-burrieza et al. [84] emphasized the importance of heat recovery in improving the thermal efficiency and performance of desalination systems, as found on a small scale by Banat et al. [81], and suggested multi-staging as a practical solution. The Fraunhofer ISE research group [85] created three MD plant prototypes, two of which are solar-powered and located in Amarika and Gran Canaria. The Amarika system included 12 AGMD modules with a total membrane area of 168 m² and 232 m² of solar FPC area, yielding 2.08 m³/day. In contrast, the Gran Canaria system featured a 120 m² AGMD loop and a 186 m² FPC solar loop, producing 1.4 m³ per day. The thermal energy flux analysis revealed that only 28% and 30% of solar radiation reached desalination plants in Amarika and Gran Canaria, respectively [85].

Comparing the results of small and large-scale studies is difficult due to differences in MD composition, unit size, membrane properties, and other variables. The reviewed studies [67], [78], [79], [80], [81], [82], [83], [84], [85] in the small-scale case show consistent daily distillate production of 10-30 l/m².hr of solar collector surface area. In terms of overall surface area, this production rate was lower than in traditional MD systems with a constant auxiliary heating source. Large-scale studies revealed that significantly more energy was used than was produced on a

daily basis. To address these issues and improve productivity, the researchers believed that creating a comprehensive productivity forecasting simulation would be preferable.

9. Conclusion

Comparing the results of small and large-scale studies is difficult due to differences in MD composition, unit size, membrane properties, and other variables. The reviewed studies in the small-scale case show consistent daily distillate production of 10-30 l/m².hr of solar collector surface area. In terms of overall surface area, this production rate was lower than in traditional MD systems with a constant auxiliary heating source. Large-scale studies revealed that significantly more energy was used than was produced on a daily basis.

To address these limitations and increase system productivity, some researchers have proposed creating robust simulation models that can accurately forecast performance under a variety of conditions. In the following chapter, we will look at this issue in greater depth and present potential solutions. Our work contributes to this effort by proposing a practical and effective approach that improves energy efficiency and output while also providing a promising solution to the scalability and performance challenges that solar-powered MD systems face

Chapter III: Modeling and simulation of a solar heating system integrated with membrane distillation

1. Introduction

The primary goal of this chapter is to model a direct contact membrane distillation (DCMD) system driven by renewable energy sources utilizing a co-simulation approach combining TRNSYS (Transient System Simulation Tool) and MATLAB. The system's core components, such as solar collectors, storage tanks, pumps, regulators, and heat exchanger, are selected from the standard TRNSYS library.

However, certain components, such as the DCMD module, are not included in the TRNSYS library. A model of the DCMD module was created in MATLAB and then imported into TRNSYS as an external program. This approach takes advantage of TRNSYS' dynamic thermal modeling capabilities while also utilizing MATLAB's versatility for simulating complex processes at the component level. The developed components will be validated before added to TRNSYS simulation, using a theoretical predictions and mathematical modeling and data gathered from scientific literature publications.

TRNSYS is largely dedicated to the modeling of global energy systems, hence it is critical to assess its ability to simulate detailed phenomena at the component level.

2. General description of the system

This research was designed and conducted an autonomous desalination system that depends mostly on renewable energy sources, specifically solar thermal energy. The goal is to create a sustainable, energy-efficient system ideal for remote regions or communities with limited access to the electrical grid, where obtaining drinking water is a big difficulty.

Fig III. 1 depicts the overall schematic of the examined system, which is based on direct contact membrane distillation (DCMD) technology and a solar

heating system. This integration enables the direct exploitation of the sun's heat to feed the membrane separation process.

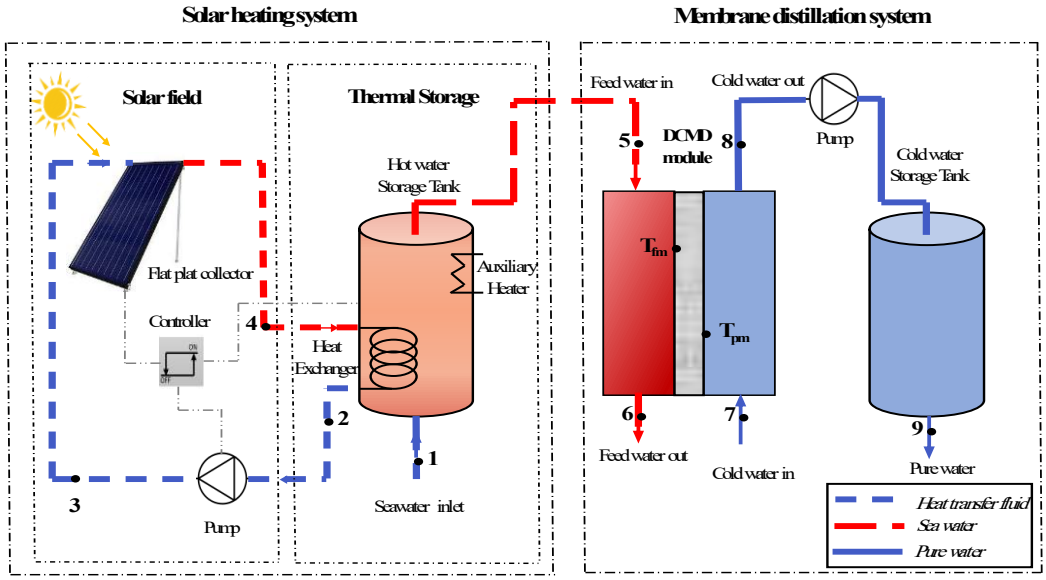

Fig III. 1: Schematic overview of the integrated system.

The system primarily comprises of two major thermal subsystems(loops):

- The solar heating loop collects and transfers solar energy to the feed water through the flat collector. This water is heated to a suitable temperature (usually between 50°C and 80°C) and then sent to the distillation module.

- The membrane distillation loop uses heat from the feed fluid to evaporate water vapor via a hydrophobic membrane, separating salts and contaminants. The vapor flows across the membrane and condenses on the permeate side, producing fresh water.

This type of installation has various advantages, including simplicity of design, adaptability, compatibility with plentiful solar resources, and the possibility of off-grid operation. However, it also introduces new technological issues, such as maximizing heat exchange, temperature management, and system stability in real-world scenarios, which will be addressed in the next parts.

2.1 Solar thermal subsystem

The solar subsystem consists of two primary components: the solar collector field and the thermal storage system. The solar field is made up of a series of flat solar collectors connected to an insulated storage tank equipped with a supplementary heating unit. Flat-plate collectors convert solar energy into heat, which is then transmitted to a heat transfer fluid (HTF), in this case a glycol combination. This fluid gathers heat from the collectors and carries it to the hot part of the direct contact membrane distillation (DCMD) module using the sun heating circuit [86].

2.1.1 Solar collectors

Flat-plate solar collectors are commonly employed in low-temperature applications such as home hot water, HVAC, and industrial processes. The measurement apparatus consists of a rectangular box with a glass lid and a dark absorber panel within. The absorber plate is made of metal with a selective surface that absorbs solar radiation and converts it into heat. This heat is then transferred to a liquid via the absorber circuit pipes. The collector absorber circulates a fluid, usually water or a mixture of water and antifreeze, via several pipelines or channels. The heated fluid is used to heat solar tank water for heating applications or residential hot water consumption.

Flat-plate solar collectors are widely utilized in home and commercial applications due to their simplicity, dependability, and high efficiency [87]. Conventional flat-plate solar collectors were chosen as the primary heat source for the solar DCMD system due of their favorable properties. The solar collector field is oriented south and consists of one, two, or parallel flat-plate collectors with a slope of 35◦ usually. This value maximizes total sun radiation and impacts solar collectors based on local weather conditions.

In this study, this component was modeled using TRNSYS software. The useful thermal energy (Qu) captured and delivered to the heating system is an important metric for assessing the energy efficiency of this type of collector [87], [88]. (see Eq.(21)).

$$Q_u = \dot{m}_{HTF}.Cp_{HTF}.(T_3 - T_4) \quad (21)$$

where, Q_u signifies the heat collected via the FPC (kJ/hr), T_3 and T_4 T4 are, respectively, the HTF's inlet and outlet temperatures (K), $\dot{m}_{HTF}$ is the HTF's mass flow rate (kg/hr), and Cp_{HTF} is the HTF's specific heat capacity (kJ/kg. K)

In addition to useful thermal energy, solar collector efficiency is an effective way to assess FPC performance. It can be calculated using Eq.(22) .

$$\eta_{coll} = \frac{Q_u}{A_{SC}.I_T} \quad (22)$$

where, A_{SC} is the FPC area (m²), and I_T is the total incident solar radiation (kJ/hr.m²).

2.1.2 Solar tank

Integrating thermal energy storage (TES) in solar systems improves flexibility and consistency of heat delivery, lowering the requirement for backup heating sources [87]. TES can take different forms, such as insulated tanks loaded with high-heat capacity fluids, rocks, or other high thermal mass materials. The examined system uses a traditional low-temperature solar thermal system with an insulated tank filled with water. Solar energy charges the tank and heats the membrane, which discharges it. To construct a solar thermal system, it's important to properly size the thermal storage tank, which should range from 50 to 180 liters per square meter of collecting area, depending on the amount of heat to be stored. The solar system features a 300-liter water storage tank that can store 150, 75, and 50 liters of heat per 2,290, 4, and 6 square meters of solar collectors, respectively. These values were sufficient to achieve the solar DCMD system's goal of providing 100 liters of distilled water every day.

The hot water storage tank contains an internal heat exchanger (internal coil) and an auxiliary heater that provides the energy needed to reach the desired temperature. To determine the energy exchanges within this tank, which is divided into several layers (nodes) as shown in Fig III. 2, we used the energy equation (Eq.(23)) at each node based on the literature [89], [90]:

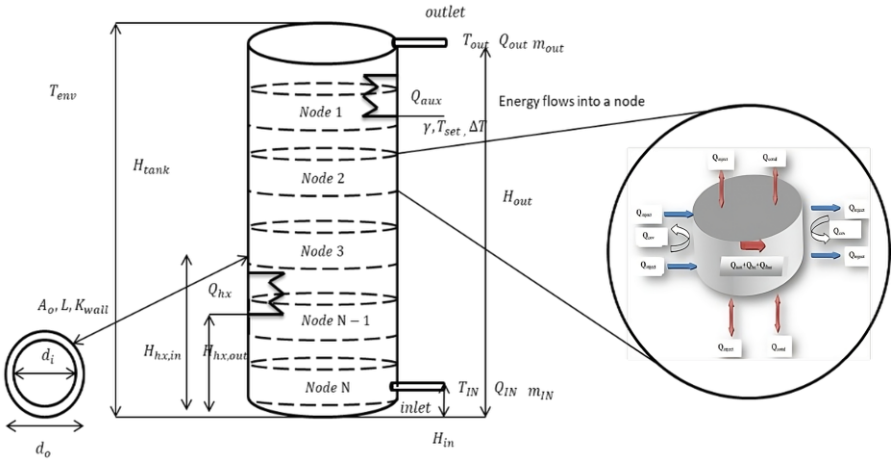

Fig III. 2: Stratified hot water storage tank.

$$M_i C_p . \frac{dT}{dt_i} = Q_{conve} + Q_{condu} + Q_{hx} + Q_{aux} + Q_{inject} \quad (23)$$

This equation includes the heat convection between the storage tank and the ambient air Q_{conve}, conduction transmitted through the tank's metal Q_{condu}, energy gained from the solar system by heat exchanger Q_{hx}, the energy produced by the auxiliary heater Q_{aux}, forced convective heat transfer from or to the segments above and below Q_{inject}. The M_i (kg) and C_p (kJ/kg. K) are, respectively, the mass and the specific heat of seawater. It is worth noting that each Q equation has been precisely expanded on in the literature, which aligns with the general equation used in this study [89], [90].

Another most important performance indicator is the solar fraction (denoted (S_F)) which identifies the fractional amount of heating energy provided by the energy delivered by solar collectors (Q_u) over the total energy demand to satisfy the load Q_{load}. The solar fraction is calculated as shown in Eq.(24) [91].

$$S_F = \frac{Q_u}{Q_u + Q_{aux}} \quad (24)$$

2.1.3 Other components

Other necessary hydraulic components and equipment are added in the integrated system. Pumps, piping networks, heat exchangers, and the appropriate

regulators and controllers are among the components that allow the entire system to function seamlessly. These parts work together to guarantee effective circulation of working fluids, precise adjustment of flow rates across different sections of the membrane (including both feed and permeate sides), and ideal operating conditions. This synchronized control is crucial for maintaining system stability and optimizing overall performance.

2.2 DCMD subsystem

The DCMD module is divided into two additional loops (feed water loop and permeate water loop), as shown in Fig III. 3(a). The feed water loop introduces hot saltwater from the storage tank directly into the feed side of a hydrophobic membrane; in contrast, the permeate water loop pumps fresh water and mixes it with permeate water that has passed through the membrane pores. The freshwater from the DCMD system is collected, and the brine is released into the sea. Because mathematical modeling is one of the necessary tools for evaluating the thermophysical performances of such systems, the model of Dong et al. [68] is well adopted in the current study, owing to its accuracy in predicting such phenomena as well as its good quality in terms of flexibility and application from small to large scales. This model works under the following conditions: the membrane can completely reject salt without wetting, the membrane module is well insulated, the transfer phenomena are in a steady state, and the effects of fluid entry and exit of the membrane are ignored.

In this study, only the flat sheet DCMD module of Dong et al. [68] was used, re-coded in MATLAB, and thoroughly tested against the same authors' experimental results. This model uses laboratory test results as inputs to estimate the performance of scaled-up MD systems in various configurations (co-current and counter-current), as shown in Fig III. 3(b). The final modeling step used tanks-in-series, a mathematical approach, to simulate membrane separation. This method divides the membrane into multiple tanks of equal lengths. Figure 2b depicts the heat and mass transfer across the membrane in the DCMD module.

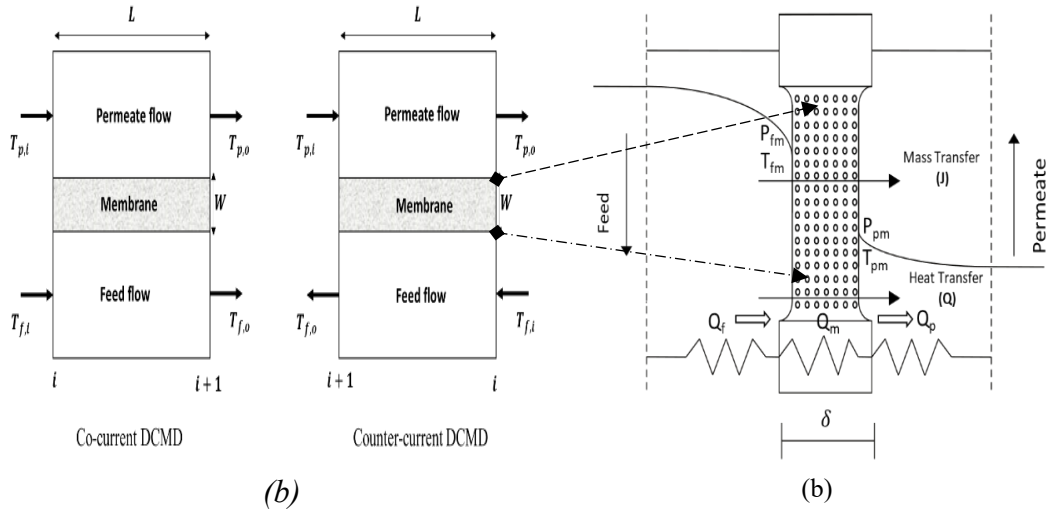

Fig III. 3: (a) Direct contact membrane distillation configurations, (b) Heat and mass transfer in DCMD module.

2.2.1 Mathematical modeling

Tanks-in-series [92], [93] mathematical model used for membrane separation simulations, mostly for gas separation through either flat sheet or hollow fiber membranes. This mathematical method accurately predicted steady-state membrane desalination for MD. Fig III. 4 shows the schematic overview of "Tanks-in-series" model in two configurations co-current and counter current.

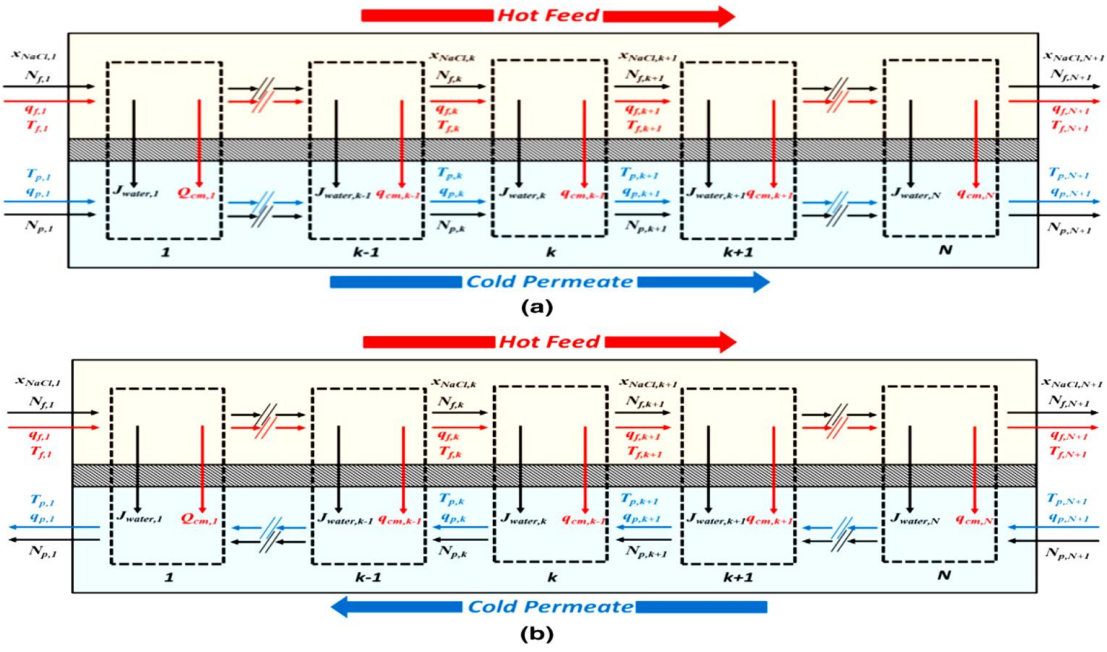

Fig III. 4: Schematic overview of the "tanks-in-series" model for DCMD simulation: (a) co-current and (b) counter-current configuration [68].

In this work, we used the "Tanks-in-Series" model to simulate a flat-sheet DCMD module. Dong et al. [68]. used laboratory-scale experimental data to calibrate the model and calculate the membrane's permeation coefficient Cm. To complete this, we used the open-source simulator created by Dong et al. [68], which was intended for steady-state analysis. However, we rebuilt and recoded the original software using MATLAB to increase its capability and enable it to handle non-steady-state (transient) situations. This update allows for the simulation of alternative DCMD setups that have the same physical features but differ in orientation (co-current or counter-current), module dimensions, and dynamic operating parameters.

2.2.2 Thermophysical properties in DCMD module

The model developed in this study aims to predict the behavior of the DCMD process under a wide range of operating conditions. For this purpose, the equations established in the previous chapters (Eq. (2), and from Eq. (5) to Eq. (25)) have been integrated into this section, covering aspects related to heat and mass transfers within the module.

It should be noted that the temperatures of the feed fluid and the permeate, as well as the NaCl concentration in the feed solution, strongly influence the thermophysical properties of the fluids involved. These properties such as density, dynamic viscosity, thermal conductivity, and specific heat capacity vary significantly with temperature and salinity, both for pure water and saline aqueous solutions. These variations have a direct impact on dimensionless quantities, particularly the Nusselt number, as well as on the heat transfer coefficients. It is therefore imperative to take these parameters into account to ensure the accuracy and reliability of the simulations.

Table III. 1 gathers the main semi-empirical correlations used in this work for the evaluation of thermophysical properties as a function of temperature and salinity. These correlations allow for the dynamic adjustment of physical property values to local conditions within the DCMD module, thereby enhancing the robustness of the model under real operating conditions.

Table III. 1: Correlations for evaluating the thermophysical characteristics of NaCl Feed solution and permeate water solution [68], [94], [95], [96], [97].

Property	***Correlation***	
Density *(Feed)*	$\rho_{NaCl} = 999.842594 + 6.793952\times10^{-2}\cdot t - 9.09529\times10^{-3}\cdot t^2 + 1.001685\times10^{-4}\cdot t^3 - 1.120083\times10^{-6}\cdot t^4 + 6.536336\times10^{-9}\cdot t^5 + (0.824493 - 4.0899\times10^{-3}\cdot t + 7.6438\times10^{-5}\cdot t^2 - 8.2467\times10^{-7}\cdot t^3 + 5.3875\times10^{-9}\cdot t^4)\cdot x_{NaCl} + (-5.72466\times10^{-3} + 1.0227\times10^{-4}\cdot t - 1.6546\times10^{-6}\cdot t^2)\cdot x_{NaCl}1.5 + 4.8314\times10^{-4}\cdot x_{NaCl}$	(25)
Density *(Permeate)*	$\rho_{water} = 999.842594 + 6.793952\times10^{-2}\cdot t - 9.09529\times10^{-3}\cdot t^2 + 1.001685\times10^{-4}\cdot t^3 - 1.120083\times10^{-6}\cdot t^4 + 6.536336\times10^{-9}\cdot t^5$	(26)
Dynamic Viscosity *(Feed)*	$log_{10}(\mu_{NaCl}/\mu_{water}) = 0.0428\cdot I + 0.00123\cdot I^2 + 0.000131\cdot I^3 + (-0.03724\cdot I + 0.01859\cdot I^2 - 0.00271\cdot I^3)\cdot log_{10}(10^3\cdot\mu water)$	(27)
Dynamic Viscosity *(Permeate)*	$\mu_{water} = 2.414\times10^{-5}\times10^{(247.8/(T-140))}$	(28)
Thermal Conductivity *(Feed)*	$k_{NaCl}/k_{water} = 1 - [2.3434\times10^{-3} - 7.924\times10^{-6}\cdot(T-273.15) + 3.924\times10^{-8}\cdot(T-273.15)^2]\cdot S_o + [1.06\times10^{-5} - 2\times10^{-8}\cdot(T-273.15) + 1.2\times10^{-10}\cdot(T-273.15)^2]\cdot S'^2$	(29)
Thermal Conductivity *(Permeate)*	$k_{water} = -0.92247 + 2.8395\cdot T/273.15 - 1.8007\cdot(T-273.15) + 0.52577\cdot(T-273.15)^2 - 0.07344\cdot(T-273.15)^3$	(30)
Specific Heat Capacity *(Feed)*	$Cp_{NaCl} = Cp_{water} + (-13.81 + 0.1938\cdot t - 0.0025\cdot t^2)\cdot Cl + (0.43 - 0.0099\cdot t + 0.00013\cdot t^2)\cdot Cl^{1.5}$	(31)
Specific Heat Capacity *(Permeate)*	$Cpwater = 4217.4 - 3.72\cdot t + 0.141\cdot t^2 - 2.654\times10^{-3}\cdot t^3 + 2.093\times10^{-5}\cdot t^4$	(32)

The temperature is expressed either in degrees Celsius (t, °C) or in Kelvin (T, K), depending on the context of the equations. The salinity (S), its adjusted form (S') can be calculated using the relation S' = 58.443M /(1000 + 58.443M), where (M) is

the molarity of sodium chloride (mol/L). The mass concentration of x_{NaCl} is in g/kg. The ionic strength (I) is determined using the equation I = [1 − 1.00487·(S/1000)] / [19.915·(S/1000)]. Additionally, the chlorine concentration (Cl) is expressed in g/kg.

2.2.3 Approach using MATLAB coding

The simulation process for direct contact membrane distillation (DCMD) involves three main parts. As illustrated in Fig III. 5.

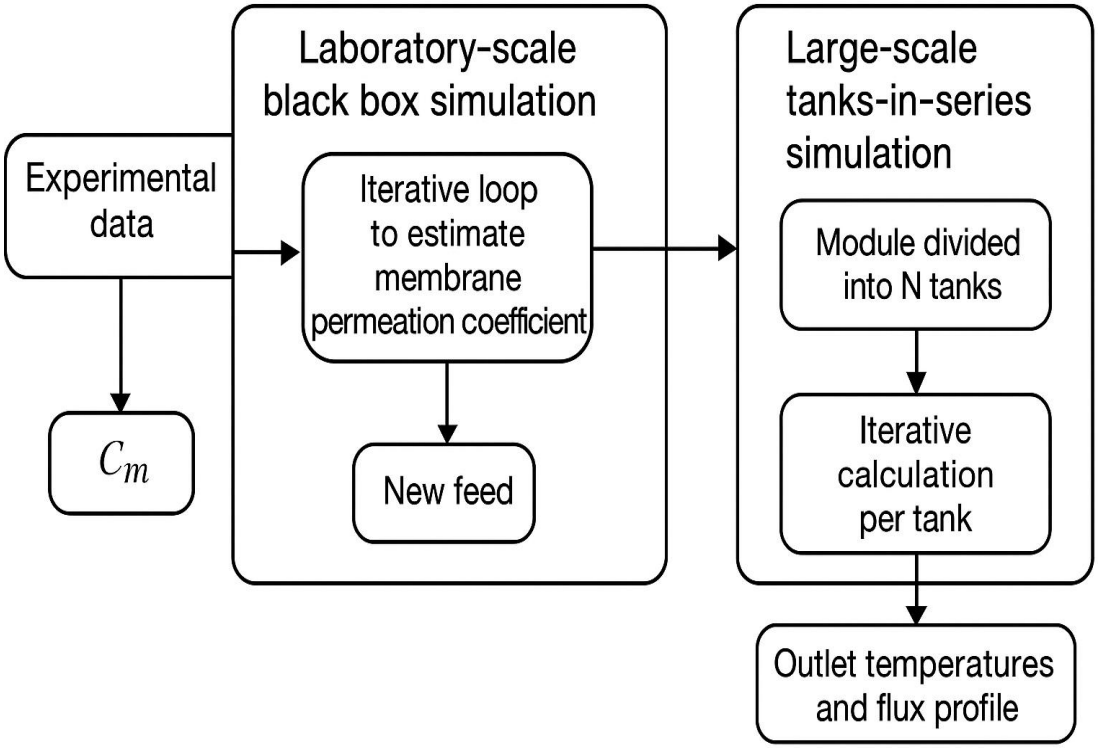

Fig III. 5: General Flowchart for DCMD MATLAB coding.

First, a laboratory-scale "black box" simulation is conducted using experimental data to estimate the membrane water vapor permeation coefficient as depicted in Fig III. 6. This involves iteratively guessing outlet temperatures, calculating heat and mass transfer, and refining estimates until the error is minimized. The output from this stage is the membrane permeation coefficient, which is then used as input for the large-scale simulation.

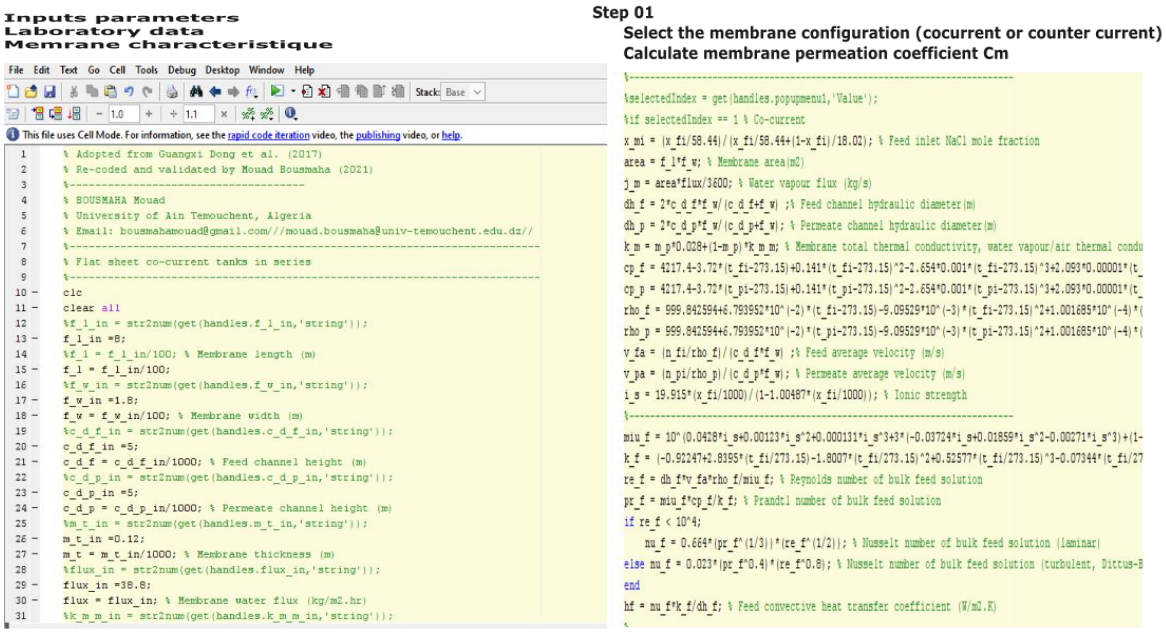

Fig III. 6: Inputs data and first loop in MATLAB code.

In the second step, the large-scale "black box" simulation applies the previously determined coefficient to new operating conditions, recalculating outlet temperatures, thermal properties, and flow rates to predict system performance at scale as depicted in Fig III. 7 . The results provide updated outlet conditions and thermal characteristics.

The final step is the "tanks-in-series" simulation, where the module is divided into multiple segments (tanks). Each tank's outlet conditions serve as the inlet for the next, and calculations for temperature, heat, and mass transfer are repeated for each segment. This approach generates a detailed profile of temperature and flux along the module. The process can be adapted for both co-current and counter-current flow configurations, with specific convergence criteria for each direction to ensure accurate energy and mass balances.

Step 02
Large scale calculation
Loop 02

```
%% Loop
for i = 1:1:10000; % Start of the i loop
t_fo_guess(i) = t_fi-i*(t_fi-t_pi)/10000; % Guessed feed outlet temperature (K)
q_f_calc(i) = n_fi*cp_f*(t_fi-t_fo_guess(i)); % Feed heat transfer rate (W)
t_po_calc(i) = q_f_calc(i)/(n_pi*cp_p)+t_pi; % Permeate outlet temperature (K)
t_fb_calc(i) = (t_fi+t_fo_guess(i))/2; % Average bulk feed temperature (K)
t_pb_calc(i) = (t_pi+t_po_calc(i))/2; % Average bulk permeate temperature (K)
t_fmb_calc(i) = t_fb_calc(i)-q_f_calc(i)/(hf*f_l*f_w); % Bulk feed boundary layer temperature (K)
t_pmb_calc(i) = t_pb_calc(i)+q_f_calc(i)/(hp*f_l*f_w); % Bulk permeate boundary layer temperature (K)
q_v_calc(i) = 1000*(1.7535*t_fmb_calc(i)+2024.3)*j_m; % Latent heat transfer rate (W)
q_c_calc(i) = f_l*f_w*k_m*(t_fmb_calc(i)-t_pmb_calc(i))/m_t; % Conductive heat transfer rate (W)
q_m_calc(i) = q_v_calc(i)+q_c_calc(i); % Membrane heat transfer rate (W)
t_fo_calc(i) = t_fi - q_m_calc(i)/(cp_f*n_fi); % Feed outlet temperature (K)
if t_fo_guess(i) < t_fo_calc(i);
   break
end
end % End of the i loop
```

Step 03
Tanks in series model
Loop 03
& Final outputs

```
   t_pi_tis = t_po_tis_calc_vec(k-1);
end
%-----------------------------------------------------------------
for j = 1:1:100000; % Start of the j loop
t_fo_tis_guess(j) = t_fi_tis-j*(t_fi_tis-t_pi_tis)/100000; % Guessed feed outlet temperature in tank k (K)
q_f_tis_calc(j) = n_fi_tis*cp_f_new_1*(t_fi_tis-t_fo_tis_guess(j)); % Feed heat transfer rate in tank k (W)
t_po_tis_calc(j) = q_f_tis_calc(j)/(n_pi_tis*cp_p_new_1)+t_pi_tis; % Permeate outlet temperature in tank k (K)
t_fb_tis_calc(j) = (t_fi_tis+t_fo_tis_guess(j))/2; % Average bulk tank k feed temperature (K)
t_pb_tis_calc(j) = (t_pi_tis+t_po_tis_calc(j))/2; % Average bulk tank k permeate temperature (K)
t_fmb_tis_calc(j) = t_fb_tis_calc(j)-q_f_tis_calc(j)/(hf_new_1*0.01*f_w_1); % Bulk feed boundary layer temperat
t_pmb_tis_calc(j) = t_pb_tis_calc(j)+q_f_tis_calc(j)/(hp_new_1*0.01*f_w_1); % Bulk permeate boundary layer temp
j_m_tis_calc(j) = f_w_1*0.01*cm_dis*((1-x_mb_pre_1)*(1-0.5*x_mb_pre_1-10*x_mb_pre_1^2)*133.322*10^(8.07131-1730
q_v_tis_calc(j) = 1000*(1.7535*t_fmb_tis_calc(j)+2024.3)*j_m_tis_calc(j); % Latent heat transfer rate (W)
q_c_tis_calc(j) = 0.01*f_w_1*k_m*(t_fmb_tis_calc(j)-t_pmb_tis_calc(j))/m_t; % Conductive heat transfer rate in
q_m_tis_calc(j) = q_v_tis_calc(j)+q_c_tis_calc(j); % Membrane heat transfer rate in tank k (W)
t_fo_tis_calc(j) = t_fi_tis - q_m_tis_calc(j)/(cp_f_new_1*n_fi_tis); % Feed outlet temperature in tank k (K)
n_fo_tis_calc(j) = n_fi_tis-j_m_tis_calc(j); % Feed mass outlet flow rate in tank k (kg/s)
n_po_tis_calc(j) = n_pi_tis+j_m_tis_calc(j); % Permeate mass outlet flow rate in tank k (kg/s)
x_fo_tis_calc(j) = x_fi_tis*n_fi_tis/n_fo_tis_calc(j); % Tank k feed outlet NaCl concentration (kg/kg)
if t_fo_tis_guess(j) < t_fo_tis_calc(j);
   break
```

Fig III. 7: Large scale loop and tank in series model in MATLAB code.

3. Numerical integration of DCMD integrated with solar thermal energy

3.1 TRNSYS Software overview

TRNSYS, a commercially available transient systems simulation program since 1975 [90], is being developed by an international collaboration of the United States (Thermal Energy System Specialists and the University of Wisconsin Solar Energy Laboratory), Germany (TRANSSOLAR Energietechnik), and France (Centre Scientifique et Technique du Bâtiment). TRNSYS is a flexible energy modeling software that allows for the inclusion of mathematical models.

- The availability of additional components.
- The ability to connect to other simulation applications.

TRNSYS has been extensively utilized to simulate solar energy applications, biological systems, and conventional buildings. TRNSYS simulates complicated thermal systems such as Energy 10, HVACSIM +, and CA SIS using its general solver, model parts, or both [98].

The TRNSYS simulation software is a collection of mathematical models of physical components from the TRNSYS library. The components can be built with the FORTRAN program, however TRNSYS 17 allows the use of any programming language capable of generating a Windows C DLL, C ++, etc...

TRNSYS 17 has a large number of standard models (solar collectors, thermal storage, heat exchangers, regulators, electrical/photovoltaic components, hydraulics, loads and structures, etc.). To create a simulation project, simply join them in a project editor. Furthermore, there are many building models that can simulate the thermal behavior of a multi-zone building in great detail (ambient temperature, air humidity, energy requirements for each surface and zone; gains from ventilation, convective coupling with other zones; latent energy needs; appreciable variation in energy; solar energy entering through the windows, etc.). The TRNSYS standard library contains a wide range of components, including solar (photovoltaic and thermal), HVAC, hydrogen systems, and many more. TRNSYS has been operating since 1975. It has spawned various advancements in other simulation programs (Energy +).

The TRNSYS program offers numerous advantages, including [5]:

- Comprehensive documentation and feedback.
- Editable source code for model customization.
- Connectivity to other software, like MATLAB, SketchUp, Excel, ESS, etc.
- Simulation control, including starting and ending time step selection.
- The user must enter all building system information.
- Use a common temperature technique to simplify heat exchange gradients.

On the other hand, TRNSYS does not verify the accuracy of the regions and volumes entered into the software. As a result, several drawbacks must be considered in the program while making assumptions and evaluating findings.

3.2 Dynamic simulation

3.2.1 The main component of the integrated system

The TRNSYS software was used to design the proposed solar heating and membrane distillation system. Fig III. 8 and Fig III. 9 show the system's primary components.

To evaluate the system's performance, two simulation cases were considered:

1. **Case (01)**: without an economizer as illustrated in Fig III. 8.

2. **Case (02)**: Including an economizer to assess its impact on thermal efficiency and overall productivity, as illustrated in Fig III. 9.This case will be discussed in Chapter V as an optimization part.

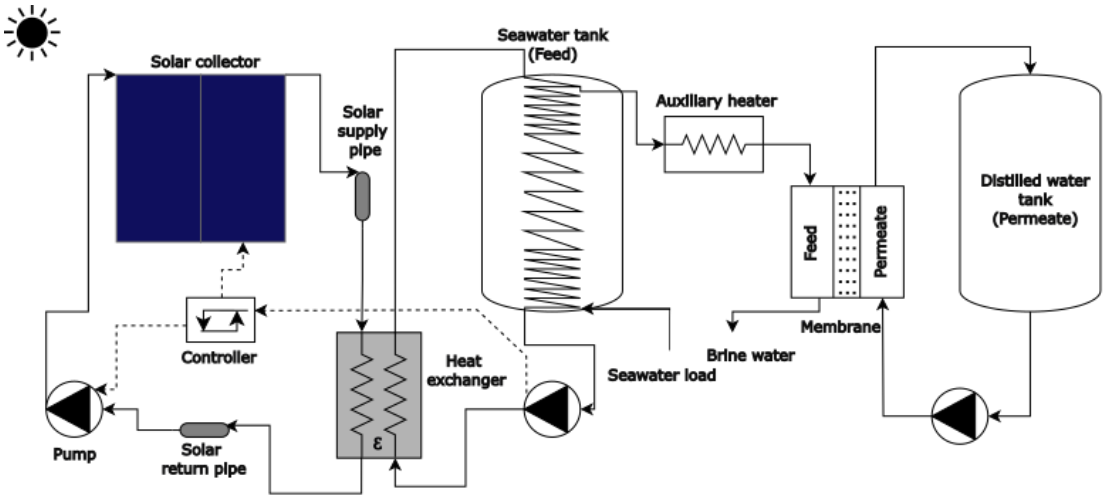

Fig III. 8: Schematic diagram of the integrated solar DCMD system without an economizer.

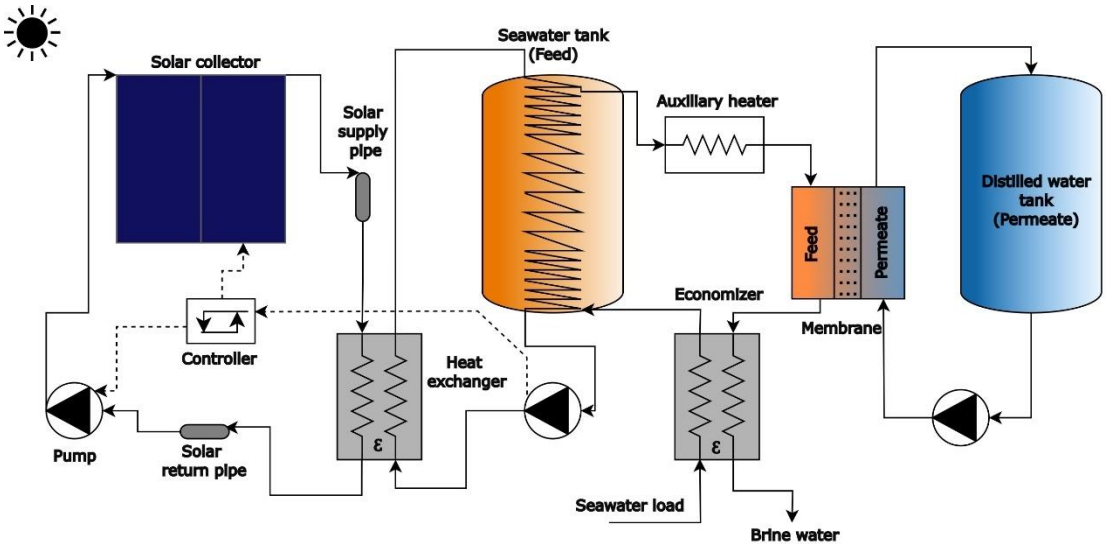

Fig III. 9: Schematic diagram of the integrated solar DCMD system with an economizer.

3.2.1.1 The main component of the solar thermal system

The solar field system consists of meteorological data reading and processing (Type109-TMY2), a flat plate collector (Type 1b), a solar water pump (Type 3b), and a differential temperature controller (Type 2b). The thermal storage system consists

of a stratified fluid storage tank (Type 60d) with optional internal heaters, internal heat exchangers with one input and output, and a general forcing function (Type 14h). Table III. 2 summarizes the different parameter values for the FPC component used in this simulation. Table III. 3 lists the hot storage tank's main parameters, such as its dimensions and thermal characteristics.

Table III. 2: Main parameters for FPC

Component (Type)	***Parameters***	***Value***	***Unit***
Flat plat collector (Type1b)	*Collector area*	*2*	*m²*
	Specific heat of fluid	*3.627*	*kJ/Kg. K*
	Tested flow rate	*40*	*Kg/hr.m²*
	Intercept efficiency	*0.788*	*-*
	Efficiency slope	*4.15*	*W/m². K*
	Efficiency curvature	*0.017*	*W/m². K*

Table III. 3: Main parameters for Hot water storage tank

Component (Type)	***Parameters***	***Value***	***Unit***
Hot water storage tank (Type60d)	*Volume*	*300*	*L*
	Height	*1.42*	*m*
	Specific heat of fluid	*3.911*	*kJ/kg.K*
	Density of fluid	*1040*	*Kg/m³*
	Thermal conductivity of fluid	*0.6041*	*W/m.K*
	Set point temperature for element 2	*60*	*°C*
	Fraction of glycol	*0.5*	*-*
	Heat exchanger length	*32*	*m*
	The total surface area of HX	*1.2*	*m²*
	Wall conductivity of HX	*390*	*W/m.K*

3.2.1.2 The main component of the DCMD module

Because the membrane distillation model is not available in TRNSYS, the previously created mathematical model of the DCMD flat sheet is used by calling an external application via MATLAB (Type 155). The DCMD model used in the simulation is an external component coded by MATLAB and called within TRNSYS; the main parameters, such as the number of inputs, outputs, and calling modes, are

listed in Table III. 4. On the other hand, Table III. 5 shows the main operating conditions used for experimental validation based on literature results [32], also includes our own set of operating conditions (for Ain Témouchent) that were used on a large scale.

Table III. 4: Main parameters for the DCMD system.

Component (Type)	***Parameters***	***Value***
DCMD system (Type155)	*Mode*	*0*
	Number of inputs	*22*
	Number of outputs	*20*
	Calling Mode	*0*
	Keep Matlab open after the simulation	*1*

Table III. 5: Main operating conditions.

Parameters	***Value***	***Unit***
Feed inlet NaCl concentration	*35*	*g/kg*
Feed inlet temperature	*50-60-70*	*°C*
Permeate inlet temperature	*20*	*°C*
Feed inlet mass flow rate	*1*	*kg/s*
Permeate inlet mass flow rate	*1*	*kg/s*

3.3 Co-simulation TRNSYS – MATLAB

3.3.1 Co-simulation design

MATLAB and TRNSYS can be used to model the entire system, including the solar heating and membrane distillation modules. TRNSYS is used to model the energy and solar system, and MATLAB is used to simulate the DCMD process. By combining both software, a more precise and effective model can be created, allowing for predictive control of various parameters such as feed and permeate inlet temperatures, feed and permeate flow rates, solar heating system efficiency, and DCMD system efficiency.

The following Fig III. 10 provides an overview of the integrated solar heating and membrane distillation system, detailing the main components of each subsystem.

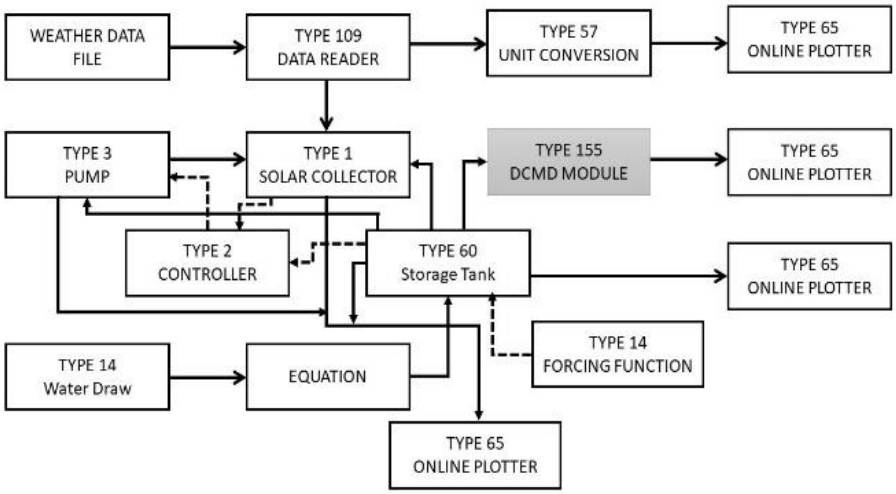

Fig III. 10: Workflow diagram including all components

Fig III. 11 depicts the layout design of the complete system in TRNSYS for case study (01) which does not include an economizer. Furthermore, the Fig III. 12 illustrated below, corresponds to case study (02) and this time incorporates a heat economizer into the circuit, allowing for improved energy use and an increase in total system efficiency. These two simulations enable a comparison of the economizer's impact on the thermal performance and productivity of the installation.

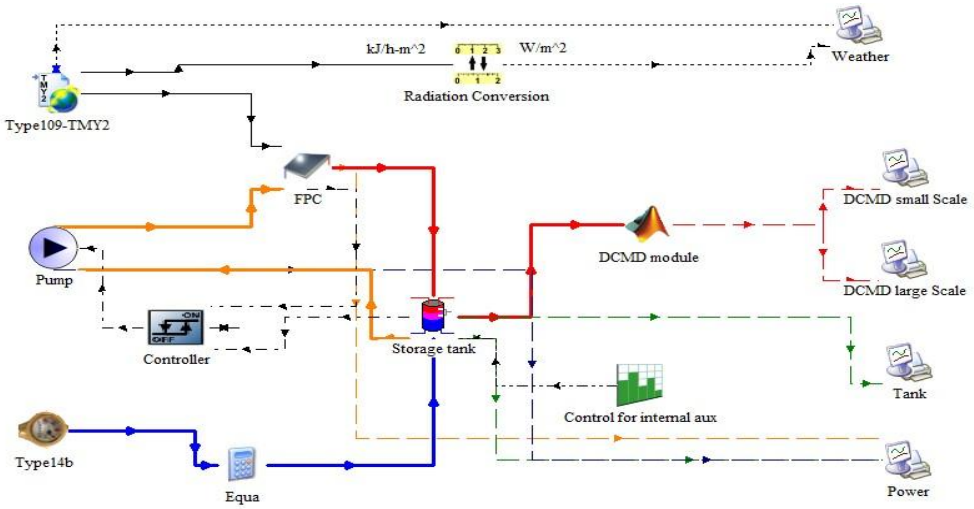

*Fig III. 11: Complete TRNSYS model simulation (**Case (01)**).*

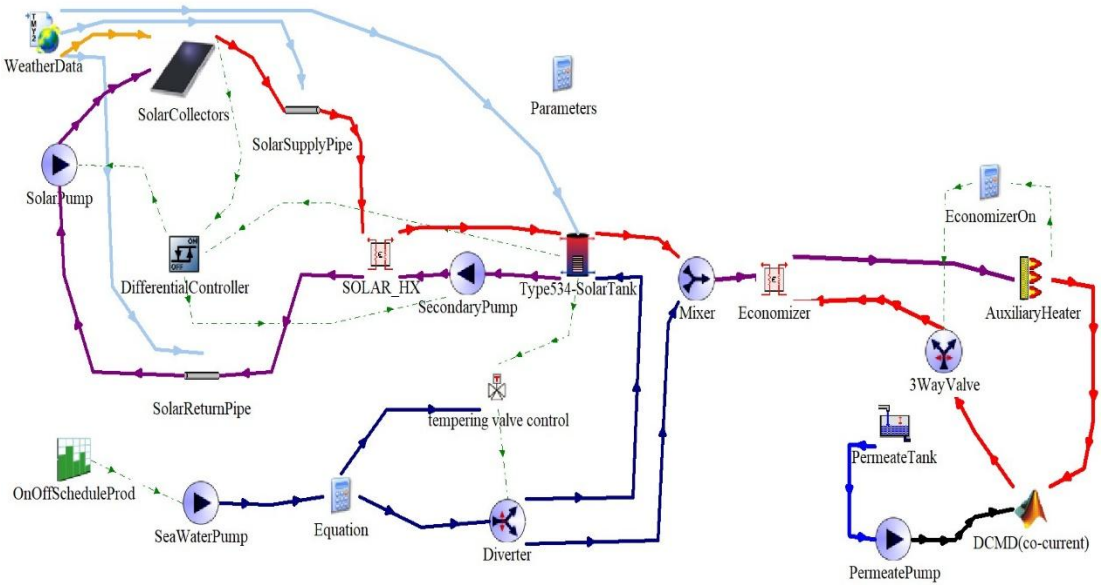

*Fig III. 12: Complete TRNSYS model simulation (**Case (02)**).*

3.3.2 Co-simulation coding (Integration and calling between MATLAB and TRNSYS

Before proceeding with the complete system simulation, particular attention must be paid to the integration of the MATLAB model into the TRNSYS environment. Indeed, the MATLAB code, initially developed independently, must be restructured and adapted to ensure effective communication with TRNSYS via the Type 155 component (Calling External File).

This adaptation requires a partial reprogramming of the code, taking into account the specifics of data exchange between the two platforms. More specifically, it is essential to clearly define the inputs and outputs of the MATLAB model so that they correspond to the variables manipulated by the different components of the TRNSYS scheme. Each variable must be explicitly linked to an input or output recognized in the TRNSYS External File component, adhering to the required formats and orders as depicted in Fig III. 13.

```
%                          end to indicate that the call w
% trnOutputs (nOx1)      : TRNSYS outputs
%trnInputs               : TRNSYS Inputs

% TRNSYS sets mFileErrorCode = 1 at the beginning of the
% This file increments mFileErrorCode at different place
% be indicated by mFileErrorCode, which is displayed in
% At the very end, the m-file sets mFileErrorCode to 0 t

mFileErrorCode = 100     % Beginning of the m-file

% --- Roof  parameters----------------------------------

mFileErrorCode = 110     % After setting parameters

% --- Process Inputs -----------------------------------
% ------------------------------------------------------

f_l_in   = trnInputs(1);
f_w_in   = trnInputs(2);
c_d_f_in = trnInputs(3);
c_d_p_in = trnInputs(4);
```

```
% --- Set outputs ---

trnOutputs(1) = t_fo_tis_dis;% Feed outlet temperature of the last tank (degree C)
trnOutputs(2) = t_po_tis_dis;% Permeate outlet temperature of the last tank (degree C)
trnOutputs(3) = x_fo_tis_dis;% Feed outlet NaCl concentration of the last tank (g/kg)
trnOutputs(4) = n_fo_tis_dis; % Feed outlet mass flow rate of the last tank (kg/s)
trnOutputs(5) = n_po_tis_dis; % Permeate outlet mass flow rate of the last tank (kg/s)
trnOutputs(6) = j_m_total_dis;% Total cross-membrane water flux (kg/m2.hr)
trnOutputs(7) = t_e_dis;% Thermal efficiency
trnOutputs(8) = cm_dis;% Membrane water vapour permeation coefficient (kg/m2.Pa.s)
trnOutputs(9) = tpc;% Temperature polarisation coefficient
trnOutputs(10) = re_f_new_1;% New Reynolds number of bulk feed solution
trnOutputs(11) = re_p_new_1;% New Reynolds number of bulk permeate solution
```

Fig III. 13: MATLAB code for TRNSYS calling external component.

Once this reprogramming is complete, the external file call command is configured in TRNSYS to call the MATLAB script during the simulation. It is also necessary to modify or add the required parameters at the Type 155 component level to ensure dynamic data exchange between the two environments.

This process thus allows for the launch of the global simulation of the integrated system, with precise modeling of the membrane distillation module handled in MATLAB, while benefiting from the flexibility of TRNSYS for the modeling of the solar circuit and thermal storage.

The external calling MATLAB from TRNSYS proceeds as follows:

1. **Reading TRNSYS inputs:** The script begins by extracting the values provided by TRNSYS via the "trnInputs" vector. These values are then converted into the necessary SI units (for example, °C → K, mm → m).
2. **Execution of calculations**: The core of the script performs the thermal and mass calculations necessary to simulate the behavior of the DCMD module, including:
   - The heat and mass balances,

- The dimensionless numbers (Re, Nu, Pr),
- The flows through the membrane,
- The outlet temperatures and thermal efficiency.

3. **Definition of outputs:** The results are stored in the "trnOutputs" vector, which is returned to TRNSYS. These outputs can be used in other components or for display.
4. **Return code:** The file ends with "mFileErrorCode = 0", indicating to TRNSYS that no error has been encountered.
5. **Necessary conditions:** a successful call from TRNSYS for this calling to work without error, the following conditions must be met:

- The file must absolutely contain a return line at the end.
- The file name must match the one referenced in Type 155 (e.g., DCMD_calcul.m).
- Dimension concordance:
- The number of inputs in trnInputs and the number of outputs in trnOutputs must be consistent with those specified in TRNSYS (user interface or .dck file). (see Fig III. 14).
- Presence of the MATLAB software:
- A valid MATLAB license must be installed on the machine.
- MATLAB and TRNSYS must be of the same architecture: either both 32-bit, or both 64-bit.
- TRNSYS must be configured to access MATLAB via the external link (Type 155 / MATLAB Link).
- The .m file must be placed in an accessible path and correctly referenced by TRNSYS. TRNSYS. (see Fig III. 14)

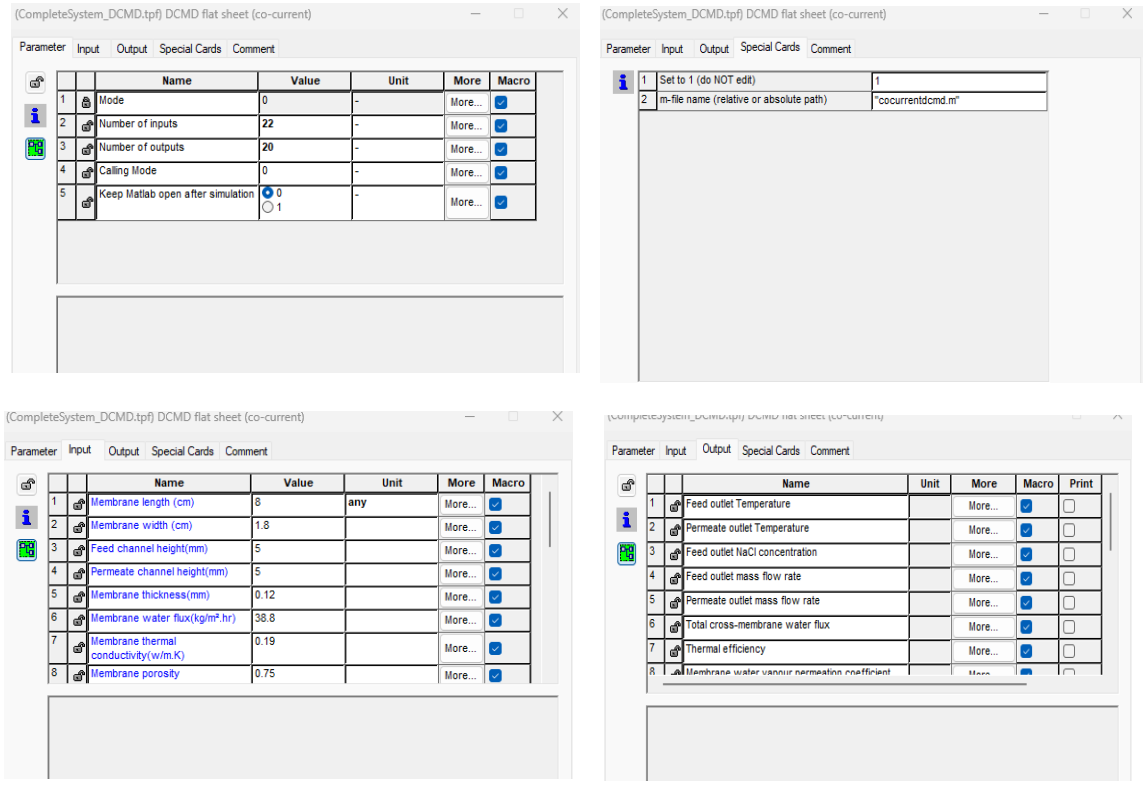

Fig III. 14: Overview of Parameters, Inputs, Outputs, and File Paths for TRNSYS–MATLAB co-simulation.

4. Conclusion

This study used MATLAB and TRNSYS to create a dynamic simulation of a direct contact membrane distillation (DCMD) system powered by renewable energy. The DCMD module, which is not directly available in TRNSYS, was developed in MATLAB with full physical and thermodynamic models. The coupling was accomplished using the Type155 interface, which allowed real-time data flow between the two platforms during simulation.

The MATLAB model calculates membrane performance using input factors such as temperature, flow rate, salinity, and membrane properties. TRNSYS receives these inputs at each time step, and the outputs, which include outlet temperatures, membrane flow, thermal efficiency, and important heat transfer parameters, are provided back to TRNSYS to dynamically update the simulation.

The process involved defining two system scales: a lab-scale flat-sheet DCMD module and a pilot-scale module, both of which were simulated using solar thermal input conditions. A TRNSYS-modeled flat plate collector (FPC) system with

a hot water storage tank and circulation loop delivered the required thermal energy. The entire structure resembles a realistic solar-powered desalination system.

To ensure compatibility and proper coupling function, both MATLAB and TRNSYS must have the same architecture, as well as a consistent version supported by Type155. The input/output structure, file directories, and exchange variable formatting were all taken into consideration.

Two situations were analyzed, an integrated system without and economizer (case 01) and another one with an economizer (case 02).

This study demonstrates the possibility and flexibility of expanding TRNSYS to model modern desalination technologies using other tools such as MATLAB. The technique allows for exact control over physical modeling while retaining TRNSYS's system-level advantages, making it appropriate for both research and design optimization of hybrid solar-desalination systems.

Chapter IV: Results and discussions

1. Introduction

The global water scarcity crisis has increased demand for sustainable and decentralized freshwater production. Membrane distillation (MD) is a potential thermal desalination method that operates efficiently at moderate temperatures. However, some MD systems often struggle with heat management, especially in variable sunlight conditions. Hybrid solar desalination systems, which combine solar thermal with MD, offer an alternative solution by providing thermal energy to feed solutions.

In this context, the current chapter discusses the modeling and dynamic simulation results of our DCMD powered by solar thermal system. The simulation uses a custom-developed interface (Type 155) to integrate the TRNSYS and MATLAB environments. The primary objectives of this study are to assess the system's feasibility, thermal behavior, and overall performance under realistic solar conditions. Key parameters such as feed and permeate temperatures, membrane water flux, thermal efficiency, heat transfer characteristics, and auxiliary heating demand are thoroughly investigated.

This chapter also includes the validation of the developed MATLAB model, where simulation results are compared with published experimental data to ensure model accuracy and reliability. Then, a multi-scale transient analysis of the system is presented:

- Daily performance simulations assess system behavior under different solar radiation profiles.
- Monthly performance analysis includes additional evaluations such as membrane water flux, outlet temperature, economizer outlet temperature, solar fraction, collector thermal efficiency, and accumulated freshwater production.

2. Validation of DCMD model

In the present study, the same types of membranes and the same experimental conditions as those reported by Dong et al. [68] were adopted. The membrane permeation coefficient (Cm) was calculated for two materials PVDF (using 38.8

kg/m²·s of experimental membrane water flux) and TR-PBOI (using 88.9 kg/m²·s of experimental membrane water flux) based on the experimentally obtained water fluxes (J). The thermophysical properties of the commercial membranes used in the membrane distillation process, such as porosity, thickness, thermal conductivity, among other parameters, were maintained in accordance with the data provided by Dong et al. Where the thickness of TR-PBOI is 0.06 mm. We used in this validation an input temperature of 70°C for the feed solution and 20°C for the permeate, as well as a feed solution salinity of 30g/kg NaCl.

2.1 Small scale validation of DCMD model

A preliminary validation of the model was carried out on a small scale, with a membrane surface area of 0.5 m² (small scale membrane). Table IV. 1 compares the simulated findings from the current model to the experimental data reported by Dong et al. [68] for the outlet temperatures of the permeate and feed, as well as the membrane water flux for two membrane materials PVDF and TR-PBOI.

The results reveal a high level of agreement between the model and the experimental data. The temperature deviation is less than 2%, and the flow value difference is less than 1%. These minor variations demonstrate the model's dependability and precision in simulating the thermal and mass performance of a DCMD module.

Table IV. 1: Small-scale validation results for mathematical DCMD model.

Membrane properties	***PVDF***			***TR-PBOI***		
Results	*Experimental* [68]	*Current work*	*Error %*	*Experimental* [68]	*Current work*	*Error %*
Feed out temp (°C)	*70.2*	*70.36*	*0.23*	*68.9*	*68.59*	*0.45*
Permeate out temp (°C)	*19.8*	*19.52*	*1.41*	*21.3*	*21.76*	*2.16*
Water flux (Kg/m². h)	*38.8*	*38.81*	*0.03*	*88.9*	*88.91*	*0.01*

2.2 Large scale validation of DCMD model

The model extended to a larger scale, with the aim of confirming the model's accuracy on different module sizes, particularly regarding output temperatures. A direct comparison was made with the results of Dong et al. [68], using their data which allowed for a confrontation of the water flux predictions.

compares the water flux as a function of the membrane surface area for PVDF and TR-PBOI membranes, based on the large-scale operating conditions described in Table III. 5, for surface areas ranging from 1 m² to 10 m². This analysis allows for a comprehensive evaluation of the water flux behavior for both materials. The results obtained for the PVDF membrane show an excellent agreement with the experimental data of Dong et al. [68], with an average deviation of about 1%. Regarding the TR-PBOI membrane, a moderate deviation of around 6% was observed, which remains acceptable. These deviations can be attributed to the instantaneous effect considered in the model developed in this study.

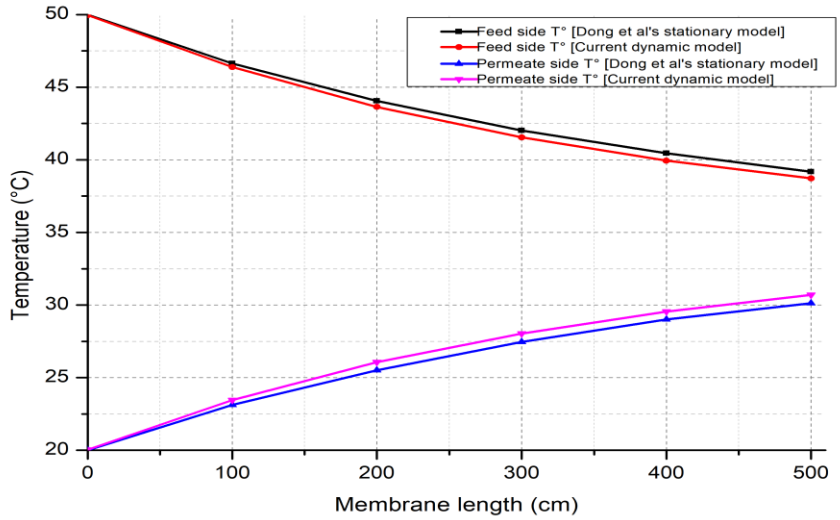

Fig IV. 1: Comparison of temperature distributions of the feed and the permeate sides with Dong et al.'s model.

Based on its more precise performance, the PVDF membrane was selected for the subsequent simulations. Fig IV. 2 illustrates the temperature profiles on the feed and permeate sides of a co-current configured module, with a membrane 5 m long, 1 m wide, feed and permeate mass flow rates of 1 kg/s, and a salinity of 35 g/kg, in accordance with the data in Table III. 5. These parameters are identical to

those used in the previous validation. The results obtained (see Fig IV. 2) show a good match with those reported by Dong et al. [68], thus confirming the reliability of the model for predicting the thermal and hydraulic behavior of the system under realistic conditions.

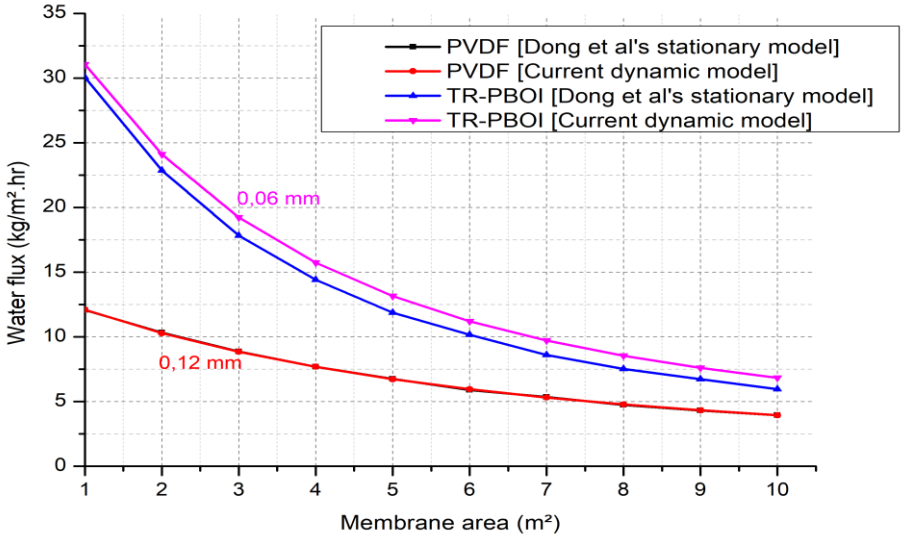

Fig IV. 2: Large-scale validation of water flux for co-current DCMD model.

2.3 Co-current model vs Counter-current model

The flat sheet membrane is suitable for both co-current and counter-current applications. The impact of these two configurations on water flux was assessed using a PVDF membrane. Fig IV. 3 depicts the effect of membrane area on water flux in co-current and counter-current membrane configurations. The results show that for all membrane areas considered, the counter-current configuration provides more water flow than the co-current configuration, with the difference between these configurations increasing as the membrane area increases.

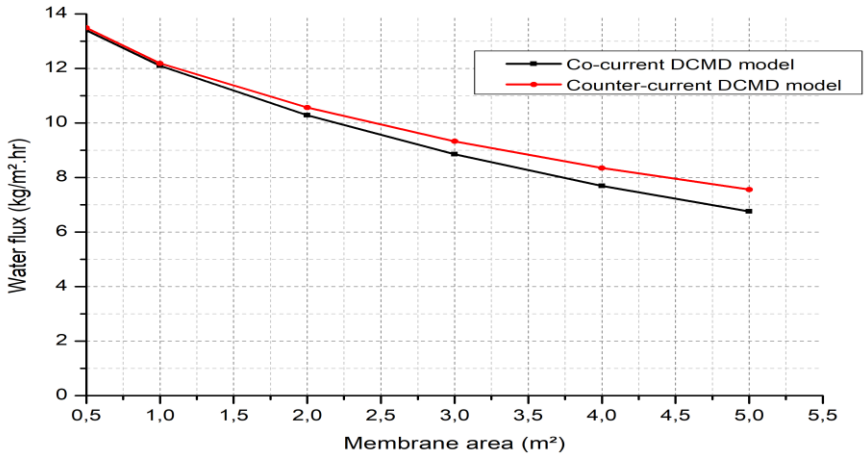

Fig IV. 3: Predicted co - and counter-current water flux as a function of membrane area.

3. Wheater data

This model was tested using the meteorological data from Ain Témouchent. Fig IV. 4 illustrates the variable climatic conditions throughout the year. The climate in Ain Témouchent is generally pleasant, warm, and mild. During the winter months, solar energy decreases to reach a lower value. Fig IV. 4 (a) shows the average temperatures, with an average of 26.4 °C. August is the hottest month. The temperature varies throughout the year, peaking at 37 °C in summer, with the highest recorded temperature being 36.35 °C on July 21, and the coldest month being January, with an average of 10.8 °C and a minimum temperature of 3.92 °C on January 15. Fig IV. 4 (b) displays monthly global horizontal radiation levels, with a peak of 331 Wh/m2 in July and a low of 110 Wh/m2 in December.

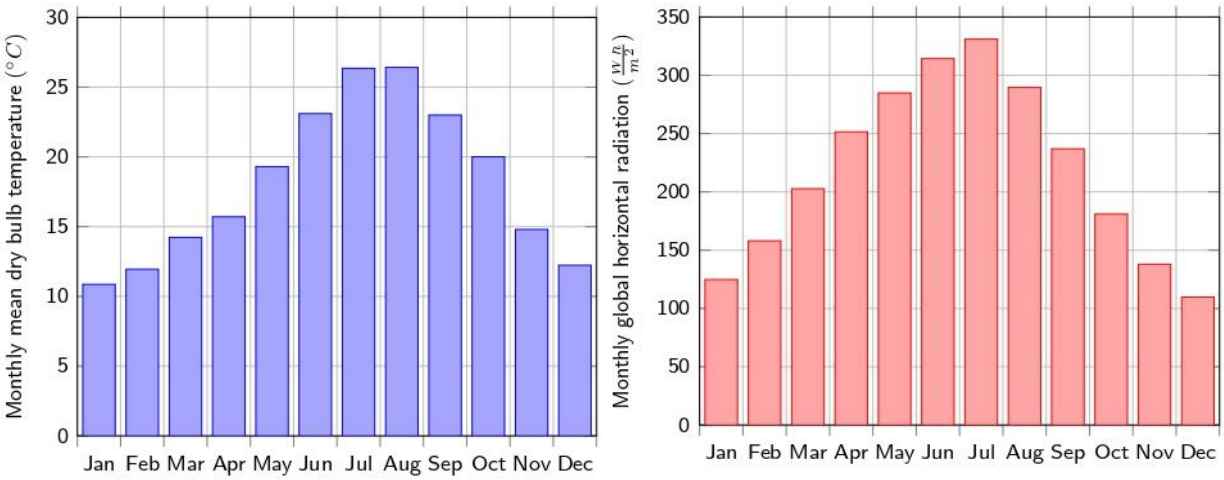

(a) (b)

Fig IV. 4: Weather data in Ain Témouchent city. (a) Mean ambient temperature, (b) Mean total radiation

3.1 Daily performance results

The integrated system results will be separated into two parts: the solar heating system and the DCMD module. As is well known, the DCMD feed temperature ranges from 50° to 80°C. To investigate the solar part, we will use a feed temperature of 60°C to ensure that the membrane receives the necessary energy. Fig IV. 5 shows the total radiation on the tilted surface (Q_{rd}), the useful energy gain (Q_u) to the HTF and the auxiliary heating rate supplied to the saltwater (Q_{aux}) over two significant days (January 21 and July 21). The plot shows that solar energy (Q_{rd}) peaks at 573 W/m² and 1006 W/m² during daylight on selected winter and summer days, respectively. The useful energy gain (Q_u) reaches its peak values of 5113 kJ/hr on January 21 and 5270 kJ/hr on July 21. This difference is due to seasonal variations in solar energy, as illustrated in Fig IV. 5. The behavior of useful thermal energy (Q_u) is primarily determined by solar radiation. As a result, an apparent effect is observed, with summer months exhibiting correspondingly higher useful thermal energy values, as reported by Remlaoui et al. [26]. The plot shows that the auxiliary heating rate (Q_{aux}) is significant for both days, with nearly identical values. This value is due to their useful energy gain (Q_u) has similar behavior and values. As a result, the internal auxiliary heater primarily provides the energy required for the saltwater to reach the required temperature (60°C). This issue will be addressed below by expanding the flat plate collector area.

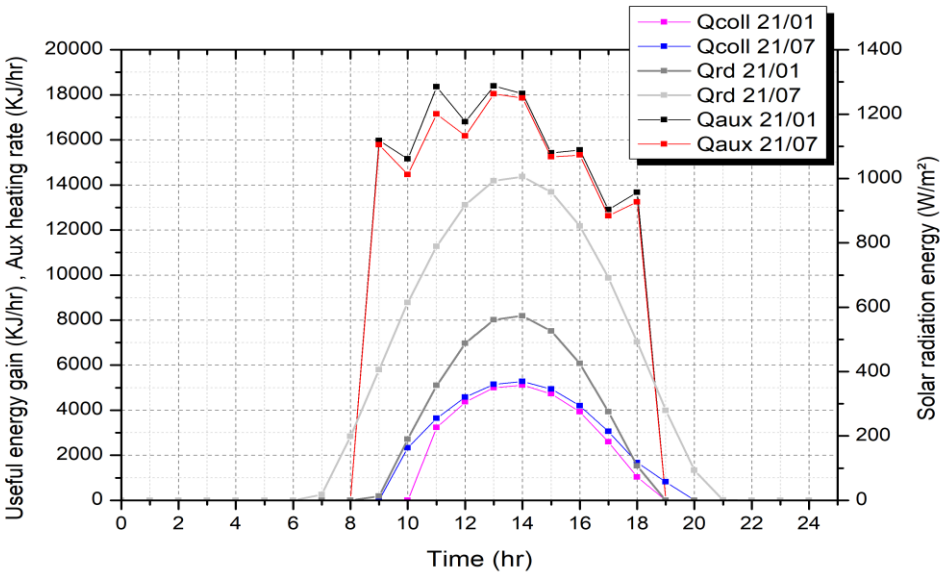

Fig IV. 5: Solar radiation, Energy provided by the FPC, and the auxiliary heating rate for definite days (January 21 and July 21).

3.1.1 Effect of feed inlet temperature

Fig IV. 6 depicts the effect of feed inlet temperature on outlet feed and permeate temperatures, as well as water flux in the DCMD system. This investigation was carried out on July 21, with feed inlet temperatures ranging from 50°C to 80°C supplied by the hot storage tank. The results show that changes in feed inlet temperature have a direct impact on water flux. Higher feed inlet temperatures, in particular, are associated with an increase in distilled water flux. Fig IV. 6 shows that the exit temperature on the feed side varies from 45.89°C to 60.08°C, indicating the effect of various settings in the hot water storage tank. On the permeate side, temperatures range from 22.35°C to 24.15°C. This examination provides a thorough understanding of the DCMD system's thermal behavior under various feed inlet temperature conditions.

3.1.2 Effect of feed inlet flow rate

Fig IV. 7 depicts the effect of the feed inlet mass flow rate on water production on July 21, with this rate ranging from 0.2 kg/s to 1 kg/s. The results show that the behavior of the water flux over time is nearly identical for the various mass flow rates studied and that this flux increases with the feed flow rate. At a flow rate of 1 kg/s, the average flux is 21 kg/m².hr, while at 0.2 kg/s, it is 12.5 kg/m².hr. This figure

shows how increasing the flow rate improves the transfer of heat and mass, resulting in more water.

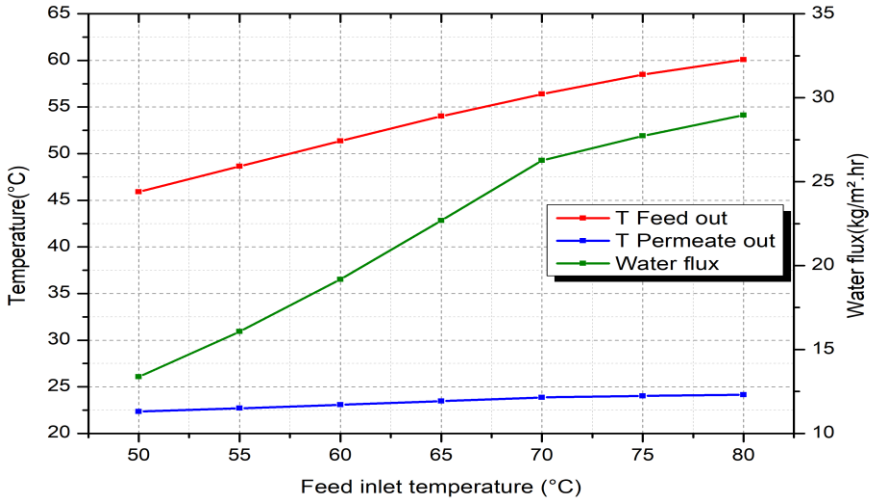

Fig IV. 6: Feed temperature, permeate temperature, and membrane water flux versus set temperature in hot storage tank over the day (July 21).

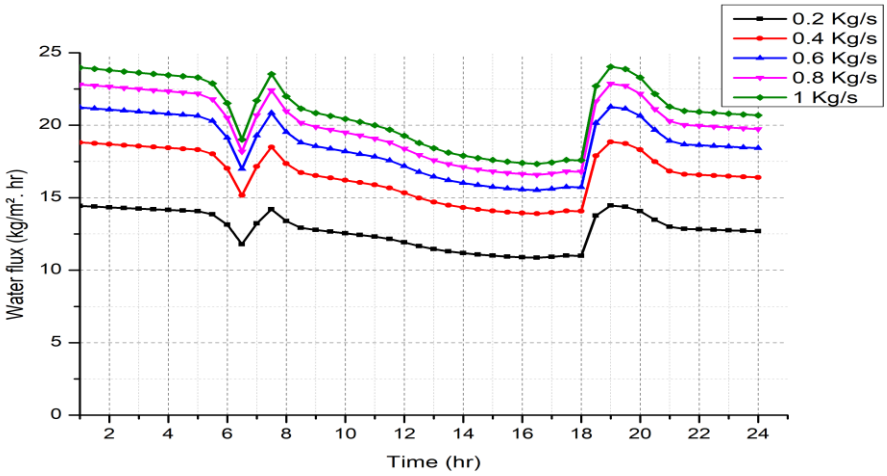

Fig IV. 7: Membrane water flux over July 21 with different feed inlet mass flow rates.

3.2 Monthly performance results

Fig IV. 8 illustrates the monthly average of total radiation on the tilted surface (Q_{rd}), useful energy gain (Q_u), and auxiliary heating rate (Q_{aux}) for feeding saltwater at 60°C. As previously observed, this figure highlights the appearance of seasonal peaks in summer for both (Q_{rd}) and (Q_u). Conversely, the auxiliary energy requirement (Q_{aux}) decreases. These findings highlight the importance of sunlight's duration and

intensity. According to that plot, the maximum order of the auxiliary heating rate is approximately 4.80 times the useful energy gain in December. In July, however, the minimum order is approximately 1.16. To address the previous issue, we attempted to increase the size of the thermal collector. Fig IV. 9 shows the energy consumption of the auxiliary heater (Q_{aux}) for four collector areas (2, 4, 6, and 8 m²). This figure shows that the order of the auxiliary heating rate decreases as the surface area of the thermal collector increases, and it also depends on the strength and duration of solar radiation. For an 8 m² collector area, the auxiliary heating rate decreased by approximately 14% in December and by nearly 44.27% in August compared to a 2 m² collector area.

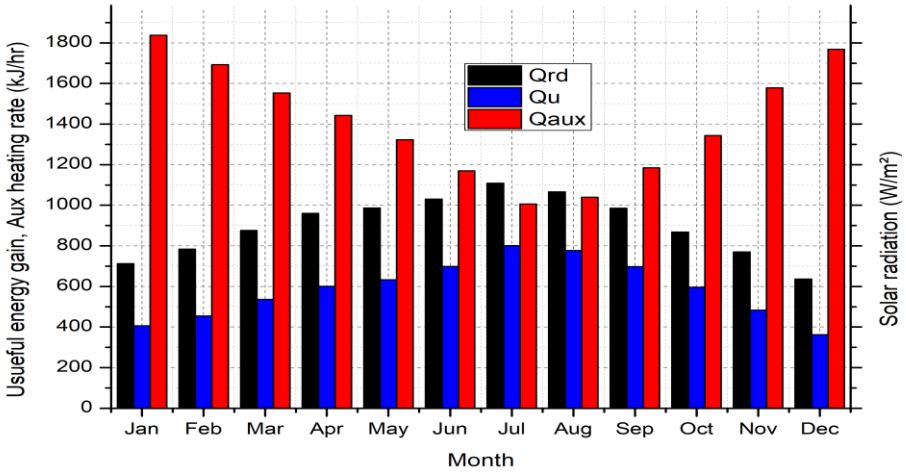

Fig IV. 8: Solar radiation, Energy provided by the FPC, and the auxiliary heating rate during the year.

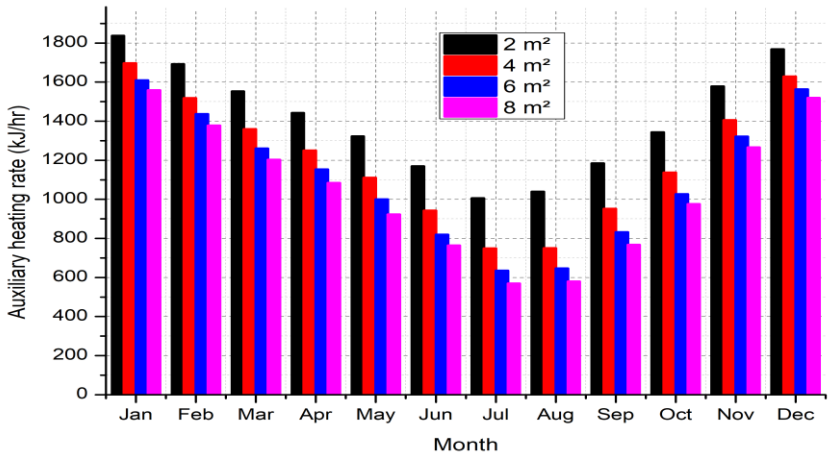

Fig IV. 9: The auxiliary heating rate during the year for the different collector areas.

When solar radiation is at its peak, the collector achieves its maximum collector outlet temperature and useful thermal energy. Summer provides the highest output temperature and useful thermal energy values. In terms of thermal system performance, Fig IV. 10 depicts how the collector's efficiency was evaluated over a year. Throughout the year, and based on Ain Témouchent's weather data, the monthly average of solar collector efficiency peaked in July at 64%. In comparison to the previous literature investigation [37], solar collector efficiency was recorded at 52% (January 24), 64% (June 24), and 55% (November 5). On the other hand, for the three selected days, the solar fraction was 41% (January 24), 52% (June 24), and 42% (November 5). This study evaluated the solar fraction of the thermal system over the year, as shown in the same figure, with a monthly average SF of 71% in July.

The module was tested under a variety of climatic conditions throughout the year for both co-current and counter-current configurations, with a feed temperature of 50°C from the hot storage tank. In contrast, the DCMD's cold inlet temperature is kept at 20°C, and the membrane length and width are 1 m and 0.5 m, respectively. Fig IV. 11shows the monthly water flux for two configurations: 50°C feed inlet, 20°C permeate inlet, and 0.5 m² membrane surface. We discovered that throughout the year, both counter-current and co-current configurations produced nearly identical water flow, with a difference of less than 1%. However, looking back at Fig IV. 3, where we investigated various membrane surface areas, we noticed that this minor difference becomes more noticeable with larger surfaces. We used a 0.5 m² membrane in this analysis, so the two water flows are closely matched.

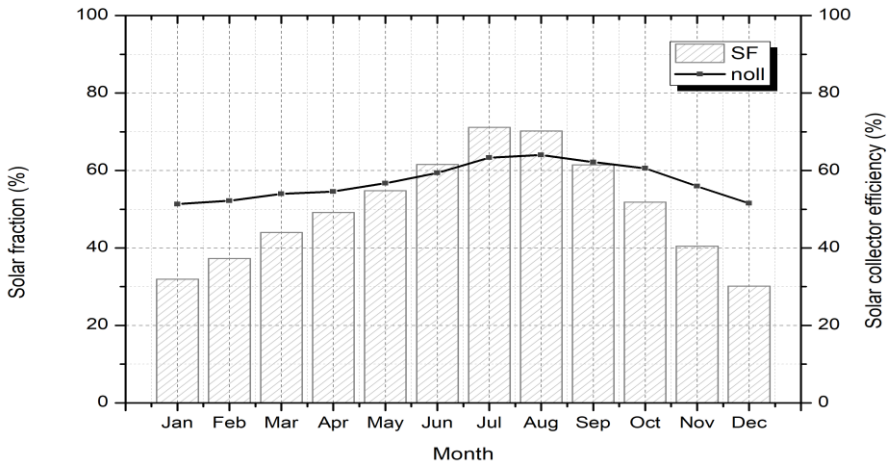

Fig IV. 10: Monthly average solar fraction and solar collector efficiency.

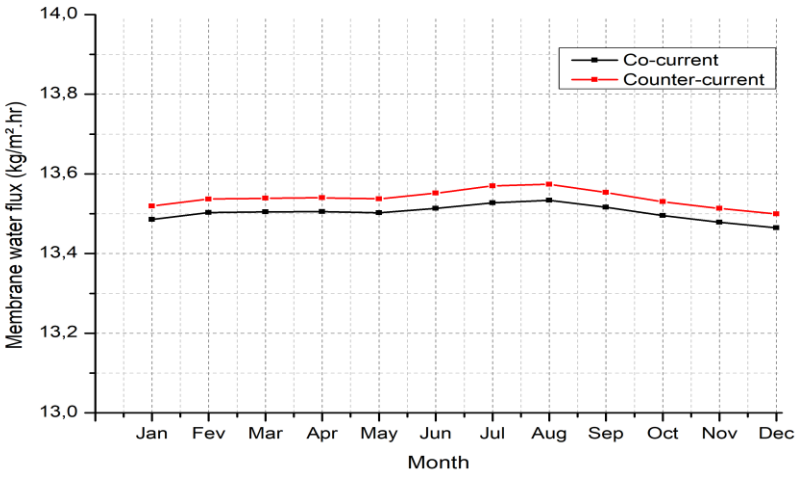

Fig IV. 11: Membrane water flux in two configurations during the year for set feed inlet temperature 50°C, permeate inlet temperature: 20°C, membrane area:0.5 m².

3.3 Comparison with other studies

Comparing our findings to previous research, particularly regarding the materials used and daily water production, can provide us with valuable insights and reassurance. As shown in Table IV.1 , our findings are consistent with the literature and demonstrate exemplary water productivity. Our water production rate is 108.56 l/m² mem, which is higher than the other technologies. This good performance confirms that our model has the potential for large-scale solar desalination applications, demonstrating its adaptability and effectiveness in addressing water scarcity challenges. Banat et al. [79] used a 5.73 m² FPC and a 10 m² AGMD module to produce 120 l of water per day at a rate of 12 l/m² for the membrane and 20.73 l/m² for the collector. Bouguecha et al. [99] used a 20 m² FPC and a 3.39 m² DCMD module to produce 18.4 l of water per day. Duong et al.'s [100] simulation study used a larger FPC and 7.2 m² DCMD module, achieving a significant daily water production of 140 l. Asim et al.'s [101] experimental and simulation study found a daily water production of 16 l, with rates of 80 l/m² of membrane and 1.34 l/m² of collector area. These findings imply that various configurations can increase water production efficiency and effectiveness. The simulation involves a 2 m² flat plate collector (FPC) connected to a 0.5 m² direct contact membrane distillation (DCMD) module. This setup produces 54.28 l of water per day, with a rate of 108.56 l/m² of membrane and 27.14 l/m² of collector area. This finding indicates a positive

interaction between the solar collector and the membrane, with the DCMD module efficiently converting heat energy to water.

Table IV.1: Comparison between the current simulation system and the literature studies

Method of study	***Solar Collector***		***Membrane***		***Daily Production (l)***	***Water Production (l/m² mem)***	***Water production (l/m² coll)***	***References***
	Type	***area(m²)***	***Type***	***area(m²)***				
Current simulation	*FPC*	*2*	*DCMD*	*0.5*	*54.28*	*108.56*	*27.14*	-
Experimental	*FPC*	*5.73*	*AGMD*	*10*	*120*	*12*	*20.73*	[79]
Experimental	*FPC*	*20*	*DCMD*	*3.39*	*18.4*	*5.43*	*0.92*	[99]
Simulation	*FPC*	*22.6*	*DCMD*	*7.2*	*140*	*19.4*	*6.19*	[100]
Experimental &Simulation	*FPC*	*11.9*	*AGMD*	*0.2*	*16*	*80*	*1.34*	[101]

4. Conclusion

In this study, a system combining solar heating and direct contact membrane distillation (DCMD) has been developed for the production of drinking water, particularly in regions with high sunlight and limited water resources. The DCMD model, based on heat and mass transfers, was recoded in MATLAB, then integrated into TRNSYS via co-simulation, allowing for dynamic system modeling. This approach was tested under real conditions in Ain Témouchent (Algeria), on an annual scale.

The results show a good agreement with the literature, both at small and large scales, for a flat PVDF membrane used in co-current and counter-current configurations. The latter proved to be more efficient, with an increased water flow, particularly for larger membrane surfaces. From an energy perspective, the solar fraction reached up to 71%, with the collector's efficiency around 63% in summer. The increase in the surface area of the solar collector significantly reduced the reliance on auxiliary heating, notably by 44% in August. These results confirm the effectiveness of the FPC–DCMD coupling and highlight the decisive impact of the capture surface, the type of membrane, and the hydraulic configuration on the overall performance of the system.

The simulation also demonstrated a good potential for adaptability to various applications, such as desalination of seawater or brackish water, wastewater reuse, or the integration of waste heat sources. The co-simulation approach TRNSYS–MATLAB thus paves the way for more precise, predictive, and optimized solar desalination systems.

Chapter V: System optimization & Comparative analysis

1. System optimization

The results from Chapter V confirmed that the membrane distillation system working with a solar thermal source is practical and effective. However, the energy analysis revealed significant heat losses at the output of the distillation module, particularly in the rejected brine flow. To improve the system's performance, we added a heat exchanger (economizer) to capture heat from the hot wastewater.

This new configuration aims to preheat the incoming supply using recovered heat, thereby reducing the auxiliary energy consumption needed to maintain operating temperatures. The optimized system retains the same basic structure (solar collector, storage tank, DCMD module), but now incorporates a heat exchanger placed between the module outlet and the feed tank (see Fig V. 1).

This chapter provides a detailed description of the optimized system's design, the modeling of the new heat exchanger, and a comparative performance analysis between the base system and the improved system. The objective is to demonstrate the gains in energy efficiency, the reduction in auxiliary energy consumption, and the productivity improvements related to this optimization.

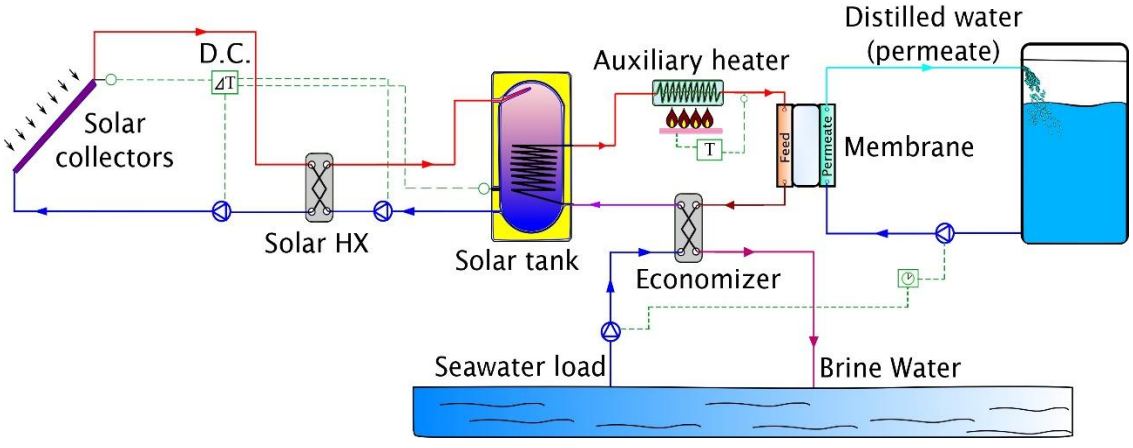

Fig V. 1: Schematic workflow for the optimized system.

In this optimized part, the integrated system is set to run for a defined **5-hour** period each day, from **13:00** to **18:00**, which corresponds to the peak solar availability. Outside of this time window, the system is inactive, and no distillate is

generated. This operational schedule is represented in all performance results, which only evaluate data for active operation hours. This method enables a true and focused assessment of how well the membrane performs during actual operating times, thereby reducing the likelihood of overestimating its performance due to inactive periods.

2. Main performance results

The performance of the DCMD module is significantly affected by operating conditions on both the feed and permeate sides, particularly the input feed temperature and flow rate. To further examine the membrane's dynamic behavior, the analysis focuses on the evolution of key performance parameters over specific time intervals. These include daily and monthly performance trends, with a focus on the system's current operating period.

3. Daily main performance results

3.1 Membrane water flux

The membrane water flux was evaluated in the same manner during the same period in August (Fig V. 2). The data obtained reveal a direct and significant relationship between the solar collector area and the water flux rate. Specifically, a solar collector area of 6 m^2 achieved a maximum flux exceeding 45 $kg/m^2.hr$, while smaller surfaces, such as 2 m^2, generated proportionally lower flux values. This observation confirms a positive correlation between the increase in solar collector area and the increase in distilled water flux production, highlighting the scalability of the system. However, temporal variations were recorded during the studied time range. These fluctuations could be attributed to external factors, such as variations in solar intensity or ambient conditions (temperature, humidity, etc.), which potentially influence the system's performance. These results underscore the importance of fully considering environmental parameters in the optimization and modeling of membrane systems for practical applications.

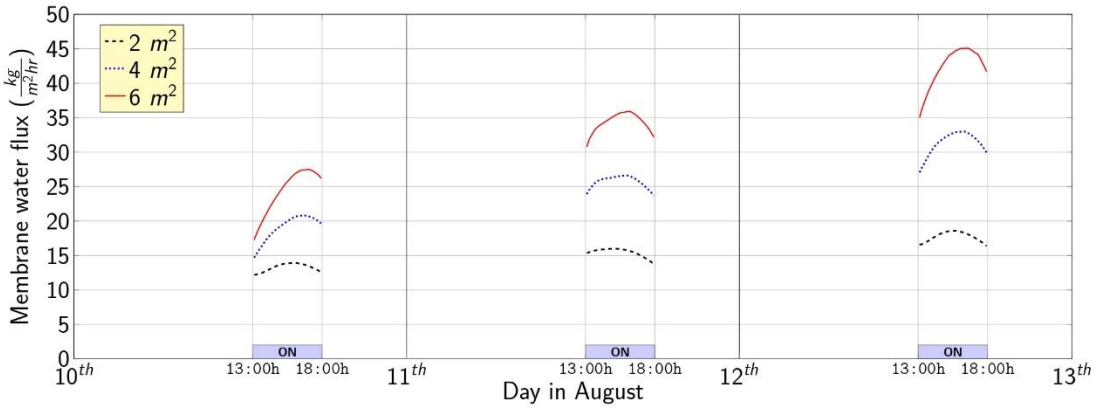

Fig V. 2: Membrane water flux during three-days operation in August.

3.2 Thermal efficiency

Thermal efficiency was evaluated over several days in August between 13:00 and 18:00 hr (Fig V. 3). Thermal efficiency remained relatively stable across all membrane surfaces, with variations ranging from approximately 0.4 to 0.6. Larger membrane surfaces exhibited slightly improved efficiency, suggesting better heat utilization in the desalination process. The stability observed during the study hours indicates that the system effectively maintains its performance under varying conditions. However, efficiency did not evolve as significantly as water flow, possibly due to limitations in heat transfer mechanisms.

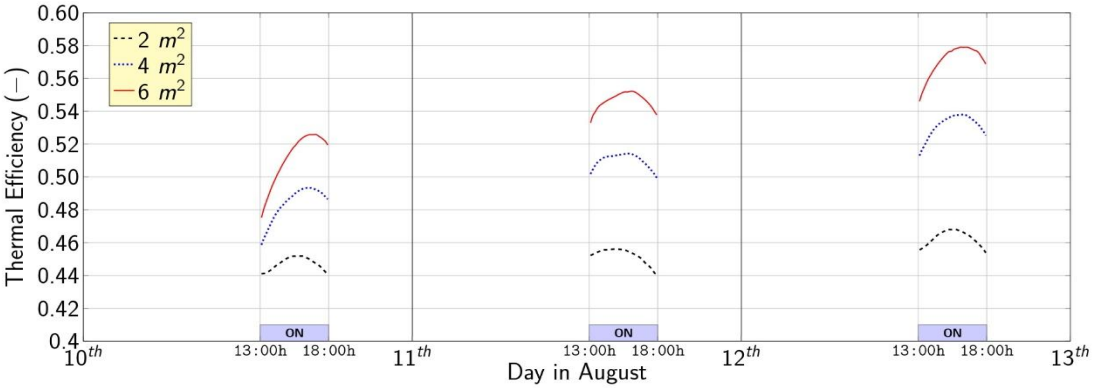

Fig V. 3 : Membrane thermal efficiency during three-days operation in August.

3.3 Feed outlet temperature

Fig V. 4 illustrates that the membrane outlet temperature is influenced by the solar collector surface area and operating hours. For a larger solar collector surface area (e.g., 6 m², the temperature reaches approximately 70°C during operating hours,

suggesting that increasing the surface area enhances thermal efficiency. However, beyond 6 m², temperature gains become less significant, indicating diminishing returns in efficiency. Daily temperature variations are also linked to environmental factors such as solar radiation intensity and ambient temperature. These results indicate that optimizing the surface area, orientation, and slope of solar collectors can improve the efficiency of thermal systems, particularly in solar desalination processes, by maximizing thermal capture while considering external conditions.

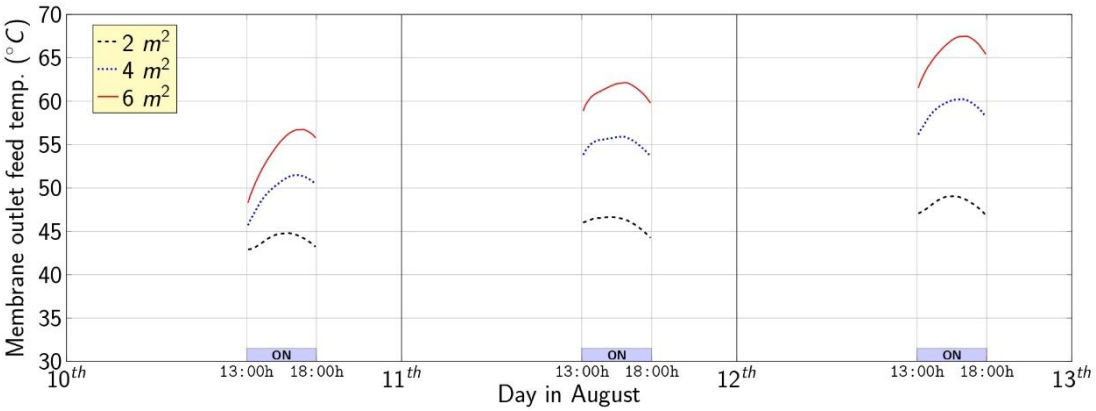

Fig V. 4: Membrane outlet feed temperature during three-days operation in August.

3.4 Economizer outlet temperature

The feed temperature at the economizer outlet exhibits a variation similar to that of the membrane (Fig V. 5), reaching maximum values close to 60°C for the economizer with a surface area of 6 m². Although its thermal efficiency is slightly lower than that of the membrane system, this difference could be attributed to variations in thermal retention and heat transfer efficiency. The simultaneous increase in temperature during the ON periods of both systems underscores the importance of coordinating operational programs to optimize energy use. These results suggest that increasing the surface area of solar collectors and economizers could enhance the thermal performance of solar systems. However, the diminishing temperature gains with increasing component sizes indicate practical and economical limits to scaling up.

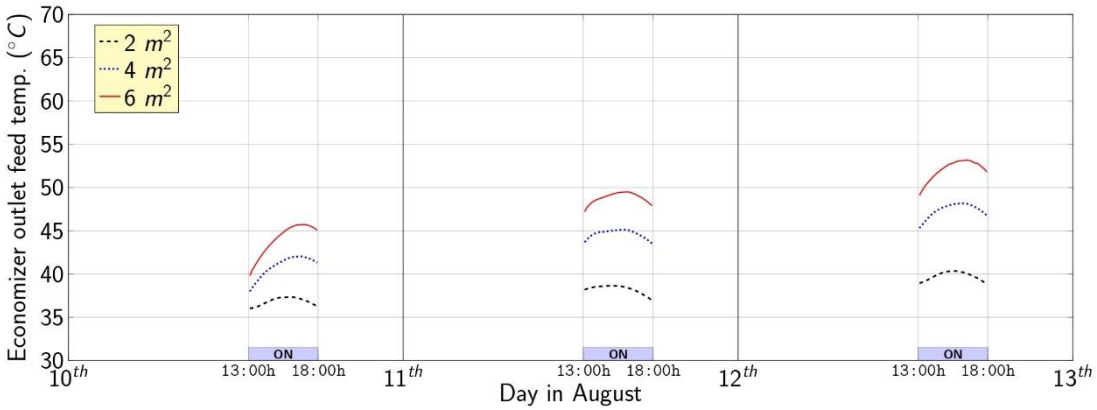

Fig V. 5: Economizer outlet temperature during three-days operation in August.

4. Monthly main performance results

Fig V. 6-Fig V. 8 present the most relevant performance indicators of the solar DCMD system for various solar collector areas and feed membrane temperatures. These figures combine simulation results for three different collector areas (i.e., integrating 1, 2, or 3 flat-plate collectors of 2 m² each) and set-point feed temperatures (50, 60, and 70°C respectively). A minimum activation temperature of 50°C is required for the DCMD membrane module to produce distilled water. On the other hand, the potential benefits of temperatures above 70°C are relatively small for the membrane technology used, as they involve substantially lower solar collector efficiencies, and the membrane must also withstand harsh operating conditions due to the higher temperature (which may impact its operational lifespan). Therefore, 70°C has been chosen as the upper set-point limit in our study. The other components of the solar DCMD system were kept constant for all simulations (i.e., the solar tank volume was 300 liters, and the membrane active area remained at 0.5 m²).

4.1 Collector efficiency

Fig V. 6 supports the previous findings, illustrating that the monthly solar collector efficiency consistently ranges between 20% and 40% across all configurations. As expected, higher efficiencies are observed at lower membrane feed set-point temperatures, due to reduced thermal demand and improved heat exchange conditions.

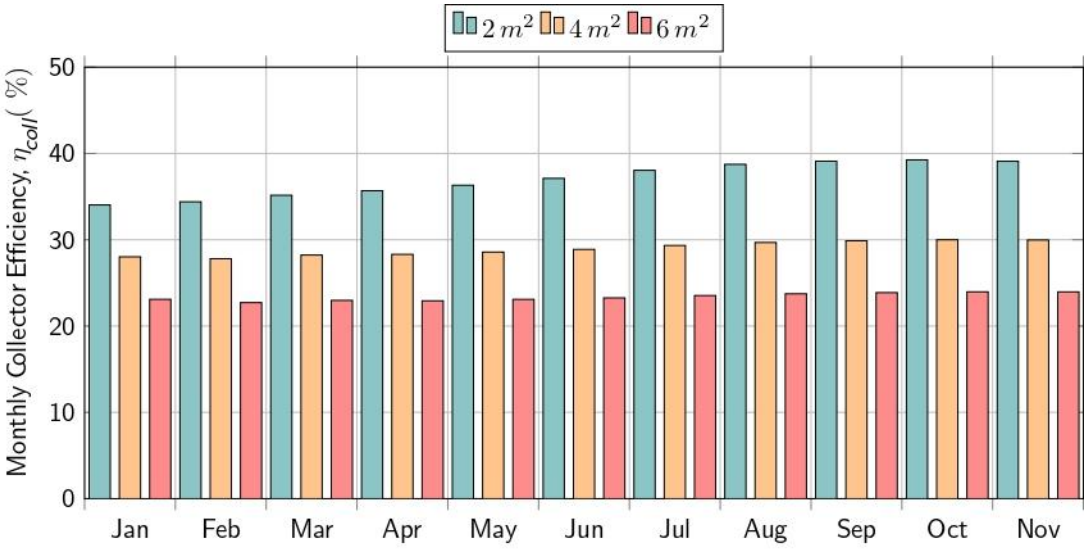

(a) $T_{set\ point}$ =50°C

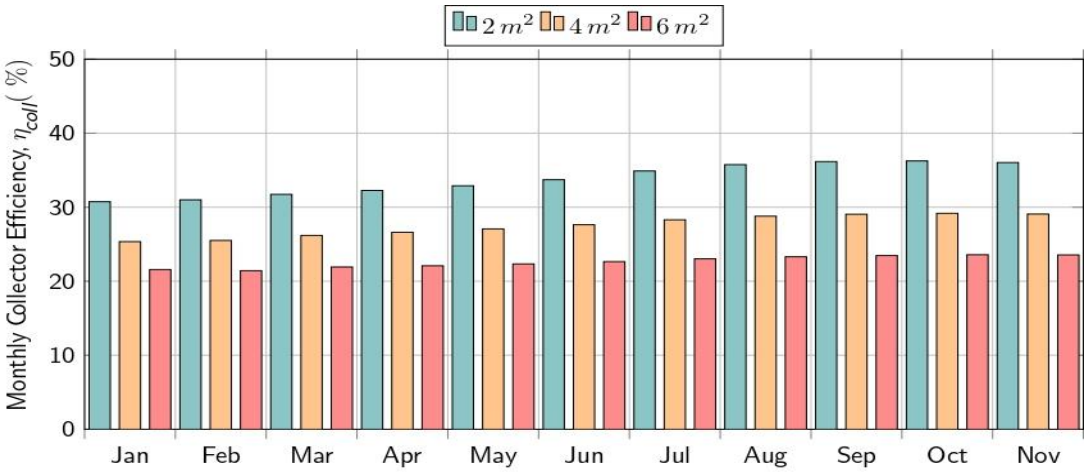

(b) $T_{set\ point}$ =60°C

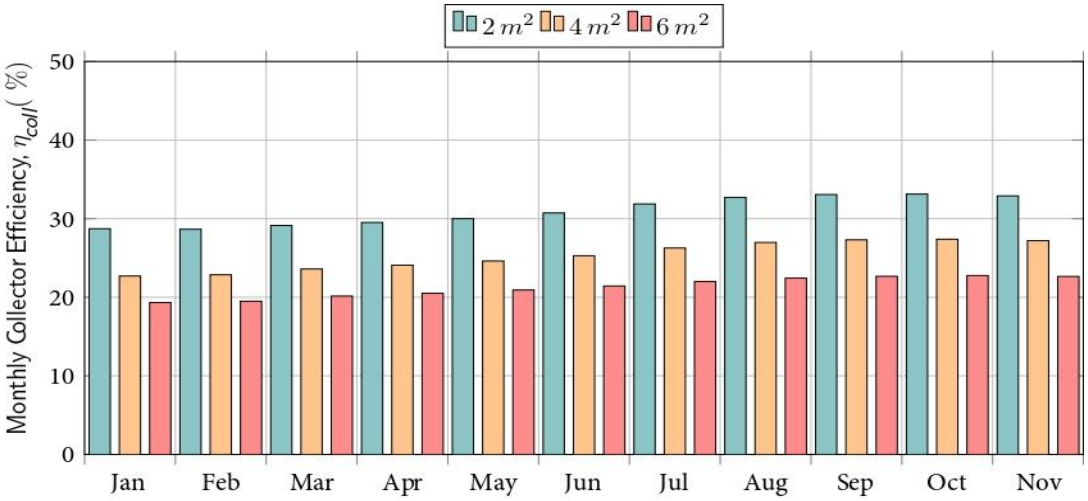

(c) $T_{set\ point}$ =70°C

Fig V. 6: Monthly average collector efficiency for different set-point feed membrane temperatures and collector areas.

4.2 Solar fraction

Fig V. 7 illustrates the monthly solar fraction provided by the solar subsystem. Several key insights can be drawn from this figure. Firstly, for the selected membrane, using a single solar collector is only effective at the minimum set-point feed membrane temperature. The solar contribution significantly decreases at higher set-point temperatures, where the membrane's distilled water production is higher. Secondly, integrating 2 or 3 collectors only produces noticeable variations at the maximum set-point temperature of 70°C. The solar contributions for 50 and 60°C set-point temperatures are similar for both collector areas. Fig V. 7 shows the monthly solar fraction for membrane temperatures of 50, 60, and 70°C, for surface areas of 2, 4, and 6 m². Annual data indicate that the solar fraction depends on the membrane surface area and seasonal insolation. For a 2 m² surface, it reaches 50% in summer (June-August) but drops below 20% in winter (December-February), indicating limited efficiency for small systems, especially during periods of low sunlight. Increasing the membrane surface area improves the solar fraction, reaching around 70% for 4 m² and over 80% for 6 m² in summer. However, in winter, it remains below 30% for 4 m² and above 40% for 6 m², indicating the need for additional thermal input. The gains become less significant above 4 m² especially in summer, suggesting a limit to optimization. Increasing the membrane surface area improves solar efficiency, but this improvement is limited by seasonal availability, necessitating optimization or auxiliary heat input.

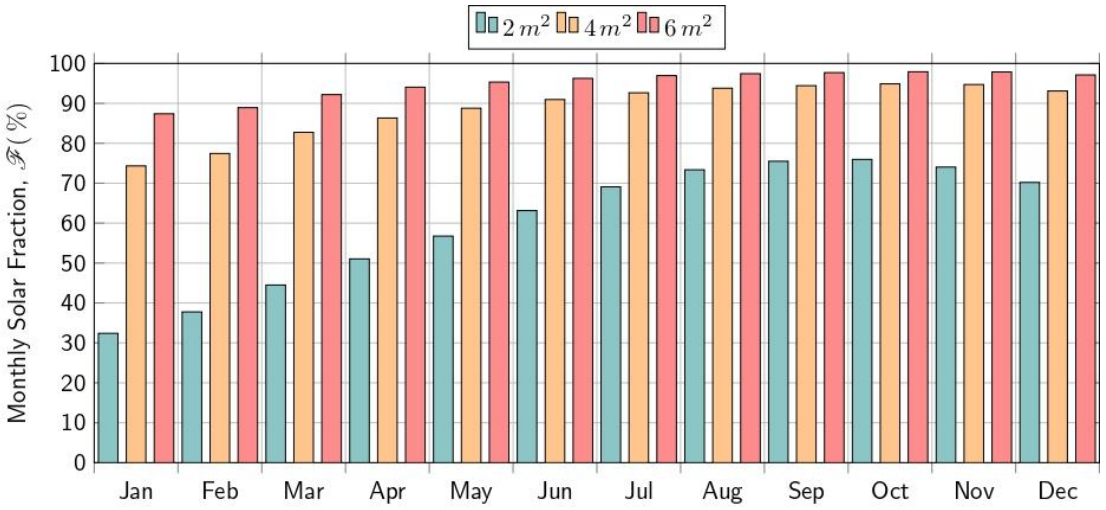

(a) $T_{set\ point}$ =50°C

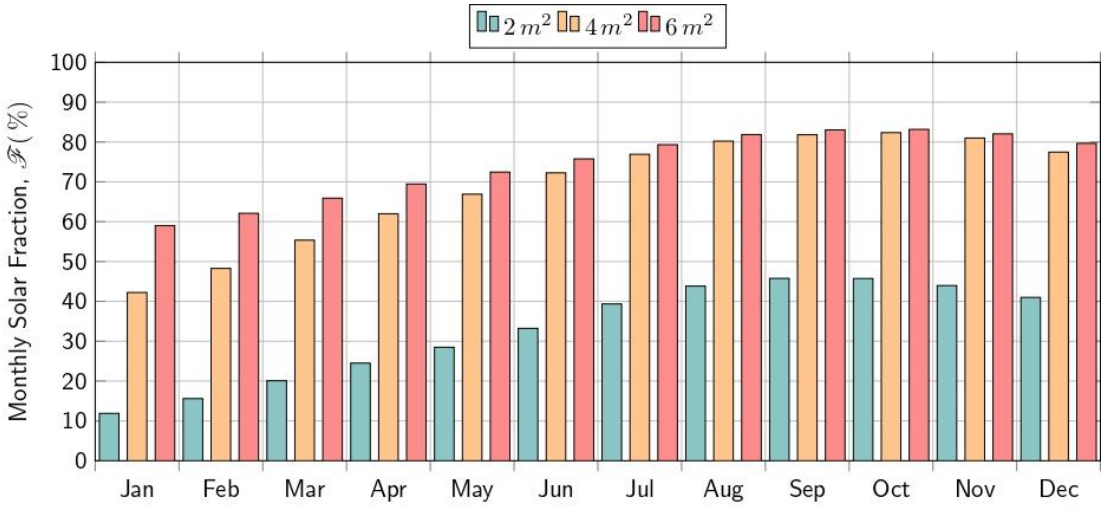

(b) $T_{set\ point}$ =60°C

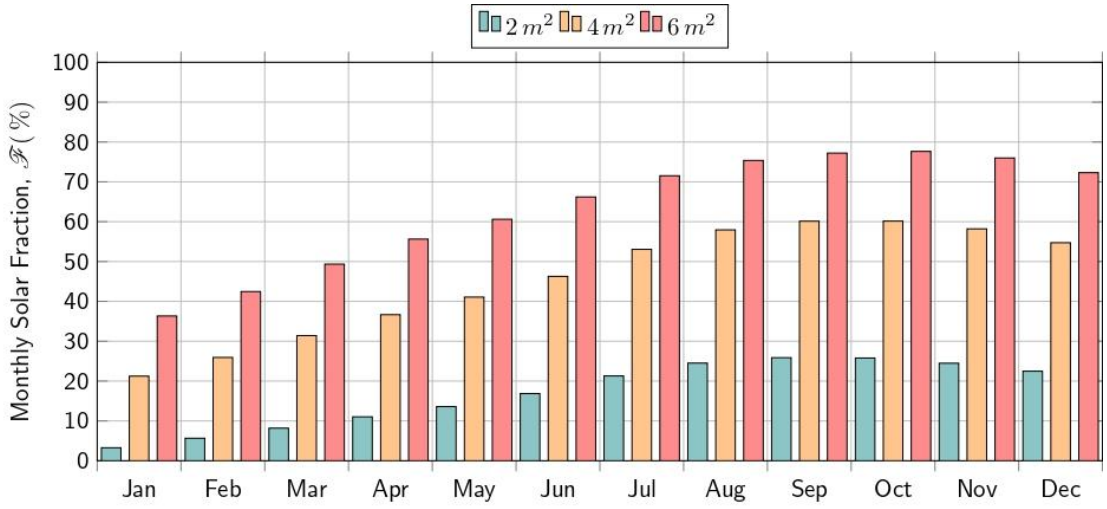

(c) $T_{set\ point}$ =70°C

Fig V. 7: Monthly average solar fraction for different set-point feed membrane temperatures and collector areas.

4.3 Membrane water flux

The performance of the distilled water side of the membrane is depicted in Fig V. 8. The solar DCMD system was designed to produce around 100 liters of distilled water per day at a feed temperature of approximately 70°C. This water production target is met at the higher set-point feed membrane temperature (70°C) with varying solar contributions depending on the different collector areas considered.

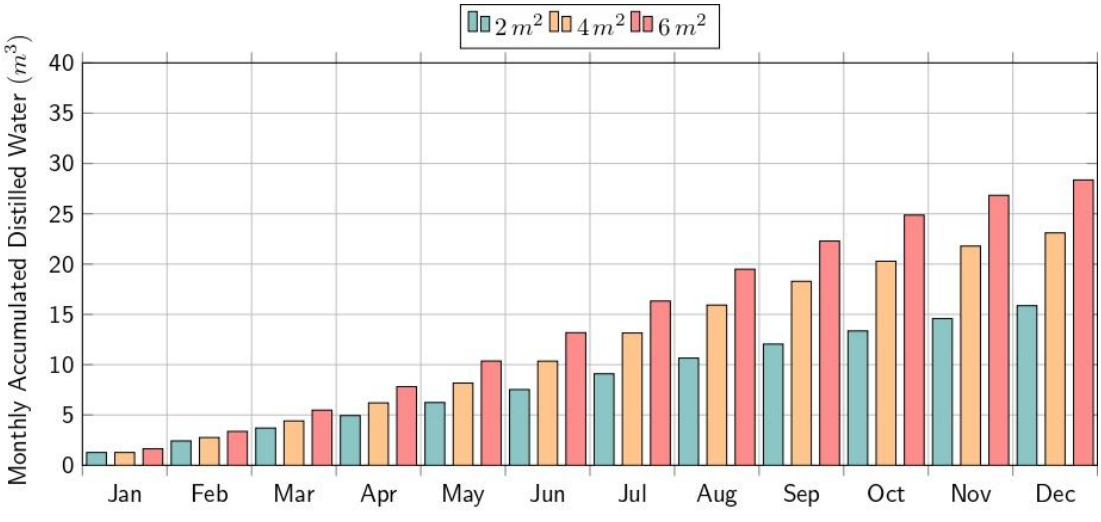

(a) $T_{set\ point}$ =50°C

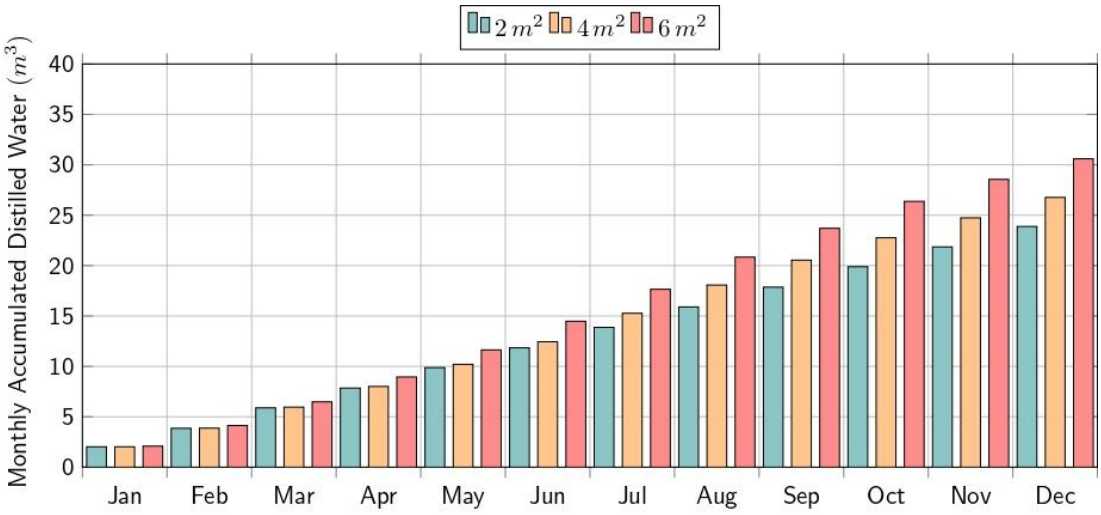

(b) $T_{set\ point}$ =60°C

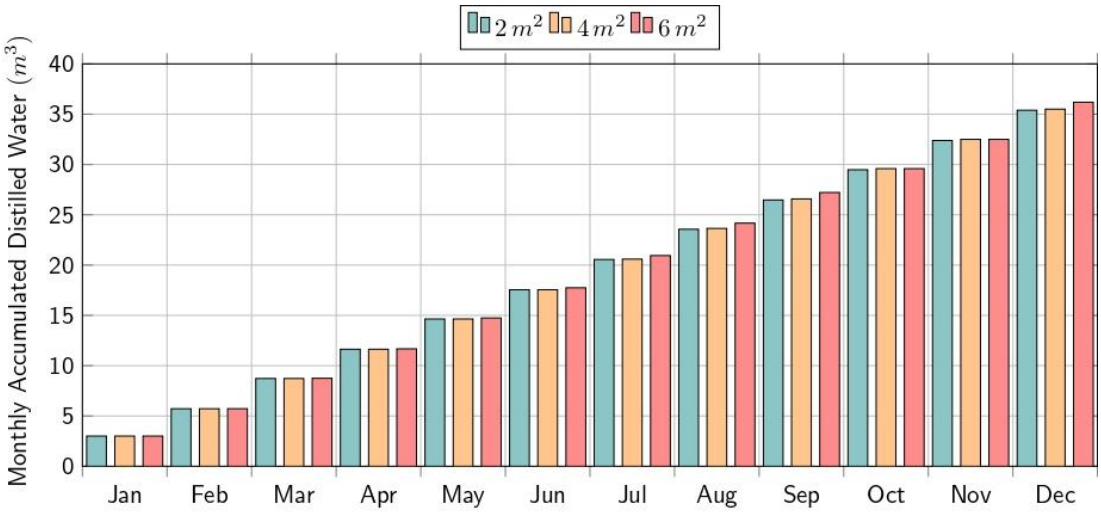

(c) $T_{set\ point}$ =70°C

Fig V. 8: Monthly accumulated water flux for different set-point feed membrane temperatures and collector areas.

5. Annual main performance results

Fig V. 9 - Fig V. 11 provides a detailed summary analysis of the performance of the proposed system as a function of the auxiliary heating set-point (i.e., the feed membrane temperature).

5.1 Collector efficiency

The results plotted in Fig V. 9 show the relationship between solar collector area, set-point temperature, and collector efficiency. As the solar collector area increases from 2 to 6 m², the collector efficiency decreases at all temperatures due to the fixed volume of the solar water tank (300 liters). For example, at 50 °C, the efficiency drops from 38% (2 m²) to 23% (6 m²). Similarly, at 60 °C, it drops from 35% to 23%, and at 70 °C, from 32% to 22%. This trend suggests that larger collector areas should be matched with larger storage tanks to maintain solar collection efficiency, especially given higher thermal losses at elevated operating temperatures. Additionally, higher set-point temperatures (from 50 to 70 °C) lead to slightly lower efficiencies for a given collector area, as more energy is required to reach and maintain the higher temperature.

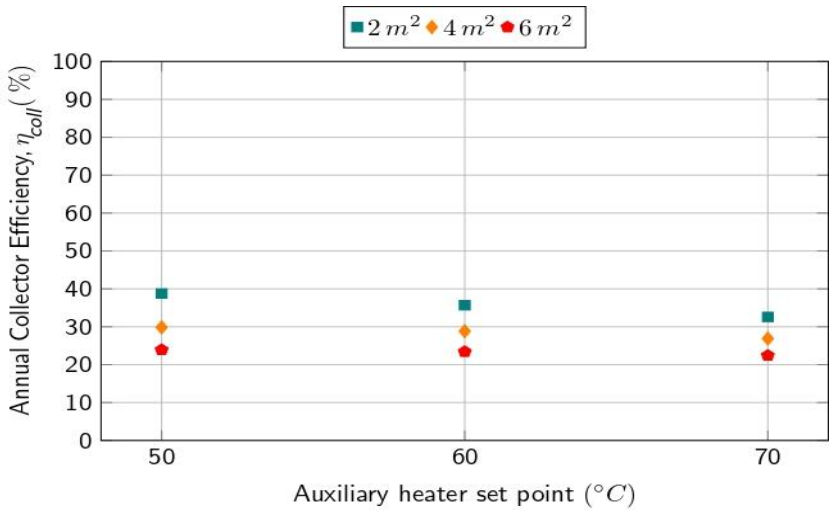

Fig V. 9: Annual collector efficiency for different set-point feed membrane temperatures and collector areas.

5.2 Solar fraction

Fig V. 10 illustrates the relationship between solar collector area, set-point temperature, and solar fraction (S_F). As the solar collector area increases from 2 to 6 m², the solar fraction improves significantly at all temperatures, indicating that a larger collector area captures more solar energy, thereby reducing the need for auxiliary heating. For instance, at 50 °C, the solar fraction rises from 70% (2 m²) to 97% (6 m²). However, higher auxiliary heating set-points (from 50 to 70 °C) reduce the solar fraction for the same collector area, as higher fluid temperatures degrade the performance of conventional flat-plate solar collectors (which are more sensitive than evacuated tube collectors). For example, with a collector area of 2 m², the solar fraction drops from 70% at 50 °C to only 22% at 70 °C. Additionally, while increasing the collector area boosts the solar fraction, the rate of improvement diminishes at larger sizes, suggesting diminishing returns. This underscores the need to optimize both collector size and set-point temperature to balance energy performance and cost-effectiveness.

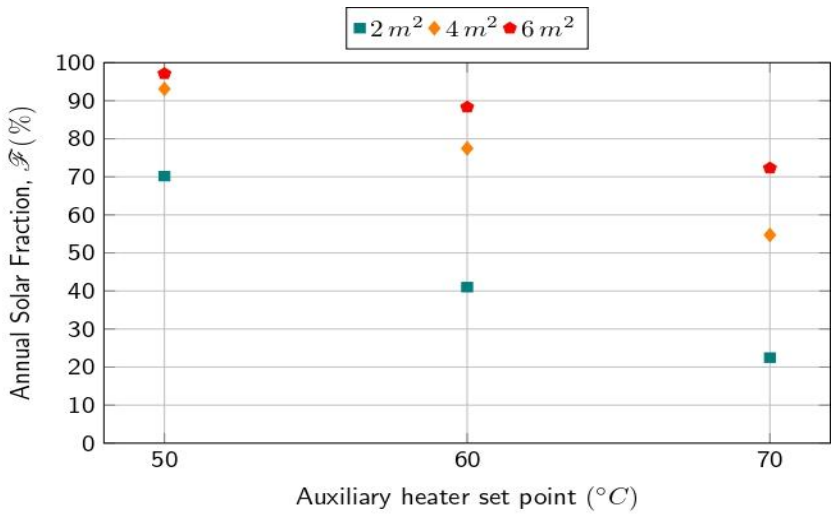

Fig V. 10: Annual solar fraction for different set-point feed membrane temperatures and collector areas.

5.3 Membrane water flux

Fig V. 11 shows the relationship between the auxiliary heating set-point and the annual accumulated volume (in cubic meters) of distilled water produced by the DCMD system. As the set-point temperature increases from 50 to 70 °C, there is a significant and consistent increase in the annual production of distilled water. At 50

°C, the system produces approximately 18–30 m³ of distilled water annually. This increases to around 25–30 m³ at 60 °C, and approximately 36 m³ at 70 °C, highlighting a notable gain in productivity at higher temperatures. The increase is not linear, with the most significant change occurring between 50 and 60 °C.

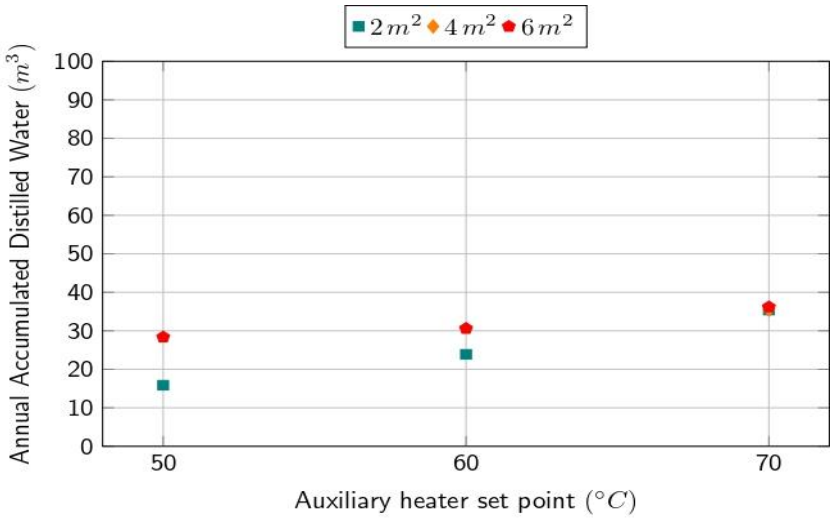

Fig V. 11: Annual accumulated water flux for different set-point feed membrane temperatures and collector areas.

6. Comparative analysis: case (01) vs case (02)

This section compares the collector efficiency and solar fraction results for different collector areas (2, 4, and 6 m² with our first system (case 01: without economizer), which analyzes a system very similar to the one studied in this Chapter, but without an economizer. This analysis provides an overall view of the improvements in the solar system compared to the previous work.

6.1 2m² of collector area

For a 2 m² collector area, there is no significant change in the average solar collector efficiency between the two studies. The results are almost identical, with only a variation of around 2%, indicating that the economizer does not provide much improvement for this configuration. However, the solar fraction shows a significant increase during certain periods (September-December), with a slight decrease in summer, as illustrated in Fig V. 12 .

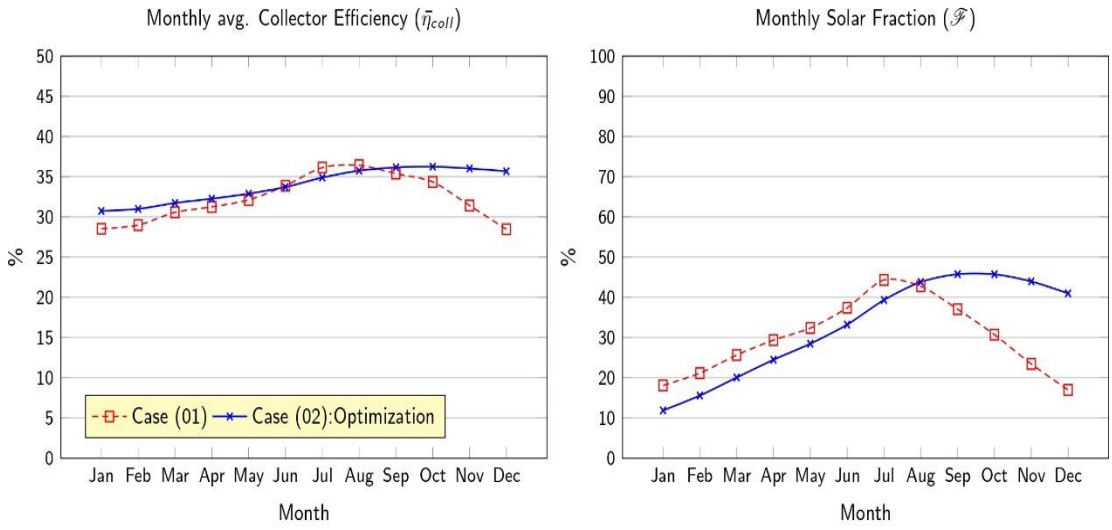

Fig V. 12: Monthly comparison of average collector efficiency and solar fraction for 2m² of collector area.

6.2 4m² of collector area

For a 4 m² collector area, as illustrated in Fig V. 13 the studied system offers a significant improvement, particularly in the solar fraction, which reaches higher values (up to +22% in October), reducing the need for auxiliary heating.

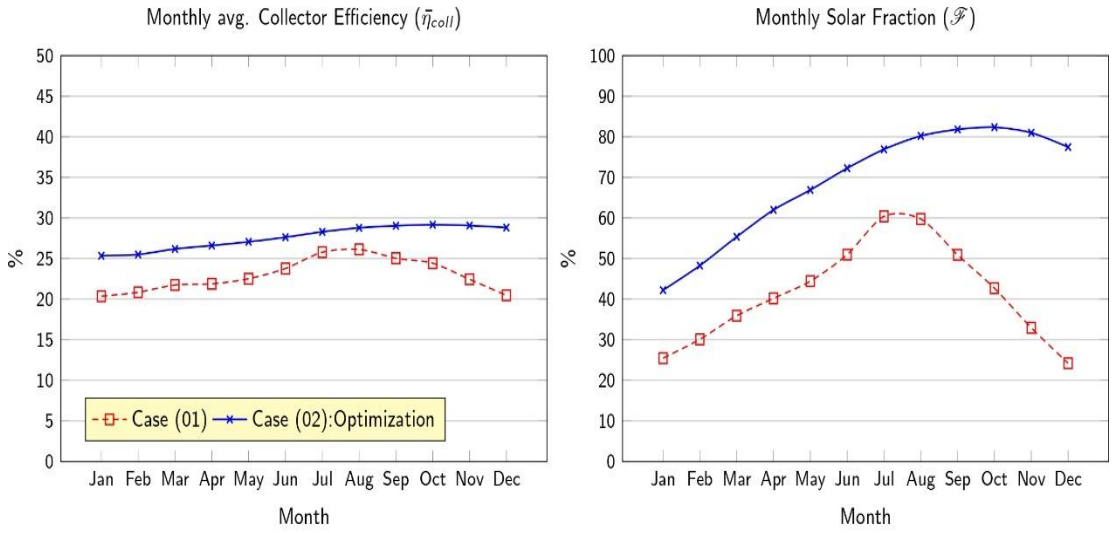

Fig V. 13: Monthly comparison of average collector efficiency and solar fraction for 4m² of collector area.

6.3 6m² of collector area

For a 6 m² surface, the improvement is even more pronounced, as shown in Fig V. 14.The solar fraction exceeds 90% in winter, with an increase in the average

yield of the solar collectors of up to 8% and in the solar fraction of 30%. This confirms that the system with the economizer optimizes the use of solar energy and significantly reduces the need for auxiliary heating.

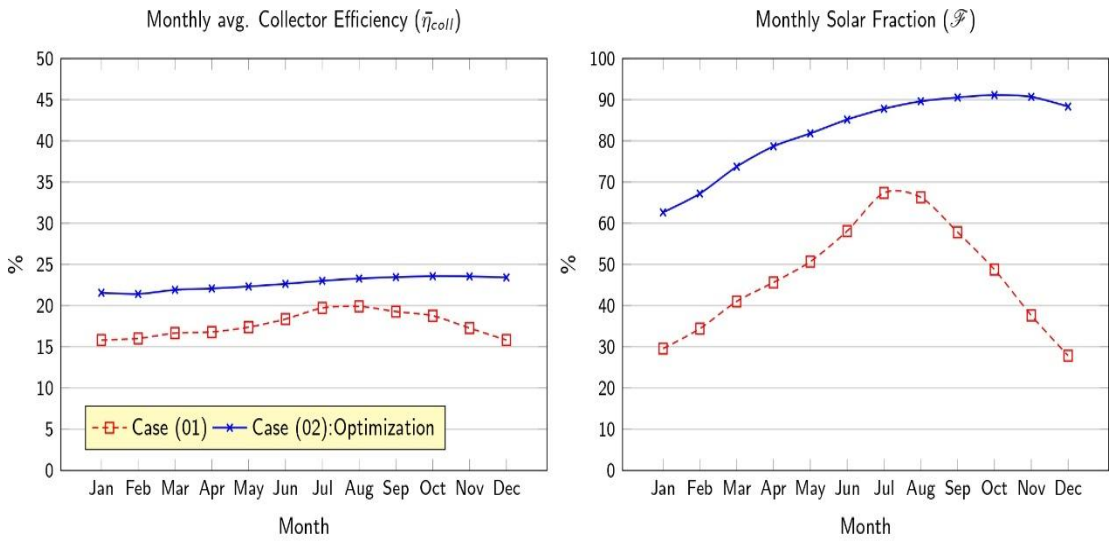

Fig V. 14: Monthly comparison of average collector efficiency and solar fraction for 6m² of collector area

This optimization resulted in a reduction in energy consumption, highlighting the overall improvement of the solar system. It is important to note that it is still difficult to compare the two systems directly due to certain differences between them. However, the improvement of the solar system and the reduction in auxiliary energy consumption compared to the previous work are clear. Additionally, daily water production increased from 54.28 liters/day to 100 liters/day, with operating time reduced from 8 hours to 5 hours, indicating a more efficient desalination process. This confirms that integrating an economizer optimizes solar energy use, making the recently integrated system more effective than the previous one.

7. Conclusion

The study investigates the integration of a DCMD module into a conventional low-temperature solar thermal system for producing distilled water. The system shares most components with a convectional small solar domestic hot water system,

with a simulated system consisting of flat-plate collectors, a 300-liter water storage tank, an auxiliary heater, an economizer, and 0.5 m² of flat sheet DCMD modules. The DCMD solar system showed high efficiency, particularly in summer, and the results show good performance in summer, with solar sensor yields between 20 and 40%. The increase in the surface area of the collectors improves water production and the solar fraction, although the gains become less significant beyond 4 m². A higher feed temperature (70°C) improves the production of distilled water but reduces the efficiency of the collectors.

The optimized system (case 02) produces approximately 100 liters of distilled water per day at 70°C. about double compared to (case 01).

General conclusion

This study demonstrates the feasibility and benefits of combining solar thermal energy with direct contact membrane distillation (DCMD) to produce sustainable water in sunny, abundant regions. The method used a thermal simulation in TRNSYS along with detailed membrane modeling in MATLAB, resulting in a reliable co-simulation that can forecast how the system will work in actual weather and operating conditions.

Through the comparative simulation of two configurations with and without a heat recovery economizer the study discovered that:

- The addition of an economizer improved system efficiency, especially for larger collector areas (4-6 m^2), which lowered auxiliary energy demand by up to 44% and increased the solar fraction to 71%.
- Daily distilled water production ranged from 50 to 100 L, depending on the collector area, feed temperature (50-70°C), and membrane arrangement.
- The counter-current membrane setup consistently worked better than the co-current setup, especially when there was more membrane surface area.
- The system-maintained collector efficiencies between 20–40%. However, increasing the feed setpoint temperature from 50 °C to 70 °C resulted in increased membrane productivity but decreased collector efficiency marginally.

These findings support the adaptability and scalability of solar-assisted DCMD systems, as well as their applicability in off-grid environments. The simulation platform enables detailed parametric study, including the impact of collector area, storage volume, membrane properties, and flow configurations.

This thesis paves the way for the creation of mobile desalination systems for rural or emergency use. We are implementing clever control strategies to maximize both energy and water output.

In the end, using advanced modeling tools and methods to recover heat helps create very efficient, self-sustaining, and eco-friendly desalination systems that align with worldwide goals for water security, sustainability, and renewable energy.

References

[1] W. JANTAPORN, “Technologies membranaires innovantes pours la réutilisatin des eaux”, PhD dissertation, Université Paul Sabatier-Toulouse III, 2016.

[2] R. Ahmed, “Etude et optimisation d’une installation thermo-solaire pour le dessalement d’eau de mer”, PhD dissertation, University Belhadj Bouchaib Ain Temouchent, 2020.

[3] O. CHARROUF, “Optimisation d’un système de dessalement renouvelable”, PhD dissertation, Université Mohamed Khider-Biskra, 2012.

[4] C. Le Guern, P. Lacassagne, Y. Noel, F. Persin, and L. De Buysscher, “Dessalement et recharge artificielle: synthèse techno-économique,” Rapport BRGM/RP-52262-FR, 2003.

[5] M. S. Abdelfatah, “Design of a seawater desalination unit working with solar energy” PhD dissertation, University Belhadj Bouchaib Ain Temouchent, 2023.

[6] P. Danis, Dessalement de l’eau de mer. Ed. Techniques Ingénieur, Paris, France, 2003.

[7] A. Al-Karaghouli and L. L. Kazmerski, “Energy consumption and water production cost of conventional and renewable-energy-powered desalination processes,” *Renew. Sustain. Energy Rev.*, vol. 24, pp. 343–356, 2013. doi.org/10.1016/j.rser.2012.12.064.

[8] P. Palenzuela and D. C. Alarcón-Padilla, *Concentrating solar power and desalination plants*. In *Solar Resources Mapping: Fundamentals and Applications* (pp. 327-340). Cham: Springer International Publishing, 2019.

[9] C. Galus, “Les techniques de dessalement de l’eau de mer prennent de l’essor,” *Extr. du monde*, vol. 23, 2000.

[10] A. Cipollina, M. G. Di Sparti, A. Tamburini, and G. Micale, “Development of a membrane distillation module for solar energy seawater desalination,” *Chem. Eng. Res. Des.*, vol. 90, no. 12, pp. 2101–2121, 2012. doi.org/10.1016/j.cherd.2012.05.021

[11] A. Alkhudhiri, N. Darwish, and N. Hilal, “Membrane distillation: A comprehensive review,” *Desalination*, vol. 287, pp. 2–18, 2012, doi: 10.1016/j.desal.2011.08.027.

[12] H. Mahmoudi, O. Abdellah, and N. Ghaffour, “Capacity building strategies and policy for desalination using renewable energies in Algeria,” *Renew. Sustain. Energy Rev.*, vol. 13, no. 4, pp. 921–926, 2009. doi.org/10.1016/j.rser.2008.02.001

[13] G.-R. Lourdes, “Seawater desalination driven by renewable energy: A review,” *Desalination*, vol. 143, pp. 103–113, 2002. doi.org/10.1016/S0011-9164(02)00232-1

[14] A. M. El-Nashar, “The economic feasibility of small solar MED seawater desalination plants for remote arid areas,” *Desalination*, vol. 134, no. 1–3, pp. 173–186, 2001. doi.org/10.1016/S0011-9164(01)00124-2

[15] E. S. Hrayshat and A. E. Al-Rawajfeh, “A solar multiple effect distiller for Jordan,” *Desalination*, vol. 220, no. 1–3, pp. 558–565, 2008. doi.org/10.1016/j.desal.2007.01.056

[16] D. Herold, V. Horstmann, A. Neskakis, J. Plettner-Marliani, G. Piernavieja, and R. Calero, “Small scale photovoltaic desalination for rural water supply-demonstration plant in Gran Canaria,” *Renew. energy*, vol. 14, no. 1–4, pp. 293–298, 1998. doi.org/10.1016/S0960-1481(98)00080-9

[17] A. Gotor, I. De la Nuez Pestana, and C. A. Espinoza, “Optimization of RO desalination systems powered by renewable energies,” *Desalination*, vol. 156, no. 1–3, p. 351, 2003. doi.org/10.1016/S0011-9164(03)00366-7

[18] J. A. Carta, J. González, and V. Subiela, “Operational analysis of an innovative wind powered reverse osmosis system installed in the Canary Islands,” *Sol. Energy*, vol. 75, no. 2, pp. 153–168, 2003. doi.org/10.1016/S0038-092X(03)00247-0

[19] M. Goosen, H. Mahmoudi, and N. Ghaffour, “Water desalination using geothermal energy,” *Energies*, vol. 3, no. 8, pp. 1423–1442, 2010. doi.org/10.3390/en3081423

[20] E. Mathioulakis, V. Belessiotis, and E. Delyannis, “Desalination by using alternative energy: Review and state-of-the-art,” *desalination*, vol. 203, no. 1–3, pp. 346–365, 2007. doi.org/10.1016/j.desal.2006.03.531

[21] H. M. Qiblawey and F. Banat, “Solar thermal desalination technologies,” *Desalination*, vol. 220, no. 1–3, pp. 633–644, 2008. doi.org/10.1016/j.desal.2007.01.059

[22] A. A. El-Sebaii, S. Aboul-Enein, M. R. I. Ramadan, and A. M. Khallaf, “Thermal performance of an active single basin solar still (ASBS) coupled to shallow solar pond (SSP),” *Desalination*, vol. 280, no. 1–3, pp. 183–190, 2011. doi.org/10.1016/j.desal.2011.07.004

[23] S. C. Bhatia, Advanced Renewable Energy Systems, (Part 1 and 2) (1st ed.). WPI Publishing, 2014. https://doi.org/10.1201/b18242

[24] C. Valderrama, J. L. Cortina, and A. Akbarzadeh, “Solar ponds,” in *Storing Energy*, Elsevier, 2016, pp. 273–289. doi.org/10.1016/B978-0-12-803440-8.00014-2

[25] D. González, J. Amigo, and F. Suárez, “Membrane distillation: Perspectives for sustainable and improved desalination,” *Renew. Sustain. Energy Rev.*, vol. 80, pp. 238–259, 2017. doi.org/10.1016/j.rser.2017.05.078

[26] A. Remlaoui, D. Nehari, M. Laissaoui, and A. Marni, “Performance evaluation of a solar thermal and photovoltaic hybrid system powering a direct contact membrane distillation : TRNSYS simulation,” vol. 194, pp. 37–51, 2020, doi: 10.5004/dwt.2020.25834.

[27] J. Zachary and C. M. Layman, “Adding desalination to solar hybrid and fossil plants,” *Power*, vol. 154, no. 5, 2010.

[28] P. R. Dos Santos and L. A. Daniel, “A review: organic matter and ammonia removal by biological activated carbon filtration for water and wastewater

treatment," *Int. J. Environ. Sci. Technol.*, vol. 17, no. 1, pp. 591–606, 2020. doi.org/10.1007/s13762-019-02567-1

[29] A. E. Khalifa, "Flux enhanced water gap membrane distillation process-circulation of gap water," *Sep. Purif. Technol.*, vol. 231, p. 115938, 2020, doi: 10.1016/j.seppur.2019.115938.

[30] B. R. Bodell, "Distillation of saline water using silicone rubber membrane," Jan. 02, 1968, U.S. Patent No. 3,361,645. 2 Jan. 1968.

[31] J. K. Adewole, H. M. Al Maawali, T. Jafary, A. Firouzi, and H. Oladipo, "A review of seawater desalination with membrane distillation: material development and energy requirements," *Water Supply*, vol. 22, no. 12, pp. 8500–8526, 2022. doi.org/10.2166/ws.2022.337

[32] N. Thomas, M. O. Mavukkandy, S. Loutatidou, and H. A. Arafat, "Membrane distillation research & implementation: Lessons from the past five decades," *Sep. Purif. Technol.*, vol. 189, pp. 108–127, 2017. doi.org/10.1016/j.seppur.2017.07.069

[33] I. Noor, "Waste Heat Driven Membrane Distillation for Industrial Wastewater Treatment", PhD dissertation, 2021.

[34] M. R. Qtaishat and F. Banat, "Desalination by solar powered membrane distillation systems," *Desalination*, vol. 308, pp. 186–197, 2013, doi: 10.1016/j.desal.2012.01.021.

[35] R. L. Ramos, Y. A. R. Lebron, V. R. Moreira, M. F. Martins, L. V. S. Santos, and M. C. S. Amaral, "Direct contact membrane distillation as an approach for water treatment with phenolic compounds," *J. Environ. Manage.*, vol. 303, p. 114117, 2022. doi.org/10.1016/j.jenvman.2021.114117

[36] A. S. Alsaadi *et al.*, "Modeling of air-gap membrane distillation process: A theoretical and experimental study," *J. Memb. Sci.*, vol. 445, pp. 53–65, 2013. doi.org/10.1016/j.memsci.2013.05.049

[37] I. Janajreh, K. El Kadi, R. Hashaikeh, and R. Ahmed, "Numerical investigation of air gap membrane distillation (AGMD): seeking optimal performance," *Desalination*, vol. 424, pp. 122–130, 2017. doi.org/10.1016/j.desal.2017.10.001

[38] K. W. Lawson and D. R. Lloyd, "Membrane distillation. II. Direct contact MD," *J. Memb. Sci.*, *120*(1), 123-133, 1996. doi.org/10.1016/0376-7388(96)00141-X

[39] M. K. Souhaimi, M. Khayet, and T. Matsuura, "Membrane distillation: principles and applications," 2011.

[40] M. S. El-Bourawi, Z. Ding, R. Ma, and M. Khayet, "A framework for better understanding membrane distillation separation process," *J. Memb. Sci.*, vol. 285, no. 1–2, pp. 4–29, 2006. doi.org/10.1016/j.memsci.2006.08.002

[41] M. Khayet, "Membranes and theoretical modeling of membrane distillation: A review," *Adv. Colloid Interface Sci.*, vol. 164, no. 1–2, pp. 56–88, 2011, doi: 10.1016/j.cis.2010.09.005.

[42] S. Al-Obaidani, E. Curcio, F. Macedonio, G. Di Profio, H. Al-Hinai, and E.

Drioli, “Potential of membrane distillation in seawater desalination: thermal efficiency, sensitivity study and cost estimation,” *J. Memb. Sci.*, vol. 323, no. 1, pp. 85–98, 2008. doi.org/10.1016/j.memsci.2008.06.006

[43] N. Ghaffour, J. Bundschuh, H. Mahmoudi, and M. F. A. Goosen, “Renewable energy-driven desalination technologies: A comprehensive review on challenges and potential applications of integrated systems,” *Desalination*, vol. 356, pp. 94–114, 2015. doi.org/10.1016/j.desal.2014.10.024

[44] J. H. Kim *et al.*, “Thermally rearranged polymer membranes for desalination,” *Energy Environ. Sci.*, vol. 9, no. 3, pp. 878–884, 2016, doi: 10.1039/c5ee03768a.

[45] M. A. E.-R. Abu-Zeid, Y. Zhang, H. Dong, L. Zhang, H.-L. Chen, and L. Hou, “A comprehensive review of vacuum membrane distillation technique,” *Desalination*, vol. 356, pp. 1–14, 2015. doi: 10.1016/j.desal.2014.10.033.

[46] A. C. M. Franken, J. A. M. Nolten, M. H. V Mulder, D. Bargeman, and C. A. Smolders, “Wetting criteria for the applicability of membrane distillation,” *J. Memb. Sci.*, vol. 33, no. 3, pp. 315–328, 1987. doi: 10.1016/S0376-7388(00)80288-4.

[47] J.-P. Méricq, “Approche intégrée du dessalement d’eau de mer: Distillation membranaire sous vide pour la réduction des rejets salins et possibilités de couplage avec l’énergie solaire,” 2009, *Institut National des Sciences Appliquées de Toulouse*.

[48] A. Alkhudhiri, N. Darwish, and N. Hilal, “Membrane Distillation : A cost effective process ’ Membrane distillation : A comprehensive review,” *DES*, vol. 287, no. January 2015, pp. 2–18, 2011, doi: 10.1016/j.desal.2011.08.027.

[49] J. Phattaranawik, R. Jiraratananon, and A. G. Fane, “Heat transport and membrane distillation coefficients in direct contact membrane distillation,” *J. Memb. Sci.*, vol. 212, no. 1–2, pp. 177–193, 2003, doi: 10.1016/S0376-7388(02)00498-2.

[50] J. Zhang, N. Dow, M. Duke, E. Ostarcevic, J. Li, and S. Gray, “Identification of material and physical features of membrane distillation membranes for high performance desalination,” vol. 349, pp. 295–303, 2010, doi: 10.1016/j.memsci.2009.11.056.

[51] M. Khayet and T. Matsuura, “Preparation and characterization of polyvinylidene fluoride membranes for membrane distillation,” *Ind. Eng. Chem. Res.*, vol. 40, no. 24, pp. 5710–5718, 2001. doi: 10.1021/ie010553y.

[52] A. Basile, A. Figoli, and M. Khayet, *Pervaporation, vapour permeation and membrane distillation: principles and applications*. Elsevier, 2015.

[53] M. Khayet, A. Velázquez, and J. I. Mengual, “Direct contact membrane distillation of humic acid solutions,” *J. Memb. Sci.*, vol. 240, no. 1–2, pp. 123–128, 2004. doi: 10.1016/j.memsci.2004.04.018

[54] S. Srisurichan, R. Jiraratananon, and A. G. Fane, “Humic acid fouling in the membrane distillation process,” *Desalination*, vol. 174, no. 1, pp. 63–72, 2005. doi: 10.1016/j.desal.2004.09.003.

[55] S. T. Hsu, K. T. Cheng, and J.-S. Chiou, “Seawater desalination by direct contact

membrane distillation," *Desalination*, vol. 143, no. 3, pp. 279–287, 2002. doi: 10.1016/S0011-9164(02)00266-7

[56] Z. Ding, R. Ma, and A. G. Fane, "A new model for mass transfer in direct contact membrane distillation," *Desalination*, vol. 151, no. 3, pp. 217–227, 2003. doi.org/10.1016/S0011-9164(02)00942-2

[57] Y. Yun, R. Ma, W. Zhang, A. G. Fane, and J. Li, "Direct contact membrane distillation mechanism for high concentration NaCl solutions," *Desalination*, vol. 188, no. 1–3, pp. 251–262, 2006. doi.org/10.1016/j.desal.2005.07.040

[58] S. Srisurichan, R. Jiraratananon, and A. G. Fane, "Mass transfer mechanisms and transport resistances in direct contact membrane distillation process," *J. Memb. Sci.*, vol. 277, no. 1–2, pp. 186–194, 2006. doi.org/10.1016/j.memsci.2005.10.047

[59] P. P. Zolotarev, V. V Ugrozov, I. B. Volkina, and V. M. Nikulin, "Treatment of waste water for removing heavy metals by membrane distillation," *J. Hazard. Mater.*, vol. 37, no. 1, pp. 77–82, 1994. https://doi.org/10.1016/0304-3894(94)85006-4

[60] H. Kurokawa, O. Kuroda, S. Takahashi, and K. Ebara, "Vapor permeate characteristics of membrane distillation," *Sep. Sci. Technol.*, vol. 25, no. 13–15, pp. 1349–1359, 1990. doi.org/10.1080/01496399008050411

[61] S. Kimura, S.-I. Nakao, and S.-I. Shimatani, "Transport phenomena in membrane distillation," *J. Memb. Sci.*, vol. 33, no. 3, pp. 285–298, 1987. doi.org/10.1016/S0376-7388(00)80083-6

[62] S. Bandini and G. C. Sarti, "Heat and mass transport resistances in vacuum membrane distillation per drop," *AIChE J.*, vol. 45, no. 7, pp. 1422–1433, 1999. doi.org/10.1002/aic.690450707

[63] S. Bandini, C. Gostoli, and G. C. Sarti, "Separation efficiency in vacuum membrane distillation," *J. Memb. Sci.*, vol. 73, no. 2–3, pp. 217–229, 1992. doi.org/10.1016/0376-7388(92)80152-P

[64] K. W. Lawson and D. R. Lloyd, "Membrane distillation. I. Module design and performance evaluation using vacuum membrane distillation," *J. Memb. Sci.*, vol. 120, no. 1, pp. 111–121, 1996. doi.org/10.1016/0376-7388(96)00140-8

[65] M. Khayet, P. Godino, and J. I. Mengual, "Nature of flow on sweeping gas membrane distillation," *J. Memb. Sci.*, vol. 170, no. 2, pp. 243–255, 2000. doi.org/10.1016/S0376-7388(00)00313-4

[66] M. Khayet, P. Godino, and J. I. Mengual, "Theory and experiments on sweeping gas membrane distillation," *J. Memb. Sci.*, vol. 165, no. 2, pp. 261–272, 2000. doi.org/10.1016/S0376-7388(99)00258-7

[67] W. G. Shim, K. He, S. Gray, and I. S. Moon, "Solar energy assisted direct contact membrane distillation (DCMD) process for seawater desalination," *Sep. Purif. Technol.*, vol. 143, pp. 94–104, 2015, doi: 10.1016/j.seppur.2015.01.028.

[68] G. Dong, J. F. Kim, J. Hoon, E. Drioli, and Y. Moo, "Open-source predictive simulators for scale-up of direct contact membrane distillation modules for seawater desalination," *DES*, vol. 402, pp. 72–87, 2017, doi:

10.1016/j.desal.2016.08.025.

[69] T. C. Chen, C. D. Ho, and H. M. Yeh, "Theoretical modeling and experimental analysis of direct contact membrane distillation," *J. Memb. Sci.*, vol. 330, no. 1–2, pp. 279–287, 2009, doi: 10.1016/j.memsci.2008.12.063.

[70] P. C. Lichtner, "Mass transfer," *In Encyclopedia of Geochemistry. Springer, Cham.*, pp. 892–895, 2018.

[71] G. Dong, W. Cha-umpong, J. Hou, C. Ji, and V. Chen, "Open-source industrial-scale module simulation : Paving the way towards the right configuration choice for membrane distillation," *Desalination*, vol. 464, no. April, pp. 48–62, 2019, doi: 10.1016/j.desal.2019.04.018.

[72] M. Qtaishat, T. Matsuura, B. Kruczek, and M. Khayet, "Heat and mass transfer analysis in direct contact membrane distillation," *Desalination*, vol. 219, no. 1–3, pp. 272–292, 2008. doi: 10.1016/j.desal.2007.05.019

[73] B. B. Ashoor, S. Mansour, A. Giwa, V. Dufour, and S. W. Hasan, "Principles and applications of direct contact membrane distillation (DCMD): A comprehensive review," *Desalination*, vol. 398, pp. 222–246, 2016. doi: 10.1016/j.desal.2016.07.043

[74] P. Behnam, M. Faegh, I. Fakhari, P. Ahmadi, E. Faegh, and M. A. Rosen, "Thermoeconomic analysis and multi-objective optimization of a novel trigeneration system consisting of kalina and humidification-dehumidification desalination cycles," *J. Therm. Eng.*, vol. 8, no. 1, pp. 52–66, 2022. doi: 10.18186/thermal.1180515.

[75] R. Ullah *et al.*, "Energy efficiency of direct contact membrane distillation," *Desalination*, vol. 433, pp. 56–67, 2018, doi: 10.1016/j.desal.2018.01.025.

[76] A. Kasaeian *et al.*, "Solar humidification-dehumidification desalination systems: A critical review," *Energy Convers. Manag.*, vol. 201, p. 112129, 2019. doi.org/10.1016/j.enconman.2019.112129

[77] B. T. Eddine and M. M. Salah, "Solid waste as renewable source of energy: Current and future possibility in Algeria," *Waste Manag. Valorization Altern. Technol.*, vol. 3, no. 1, pp. 115–141, 2017, doi: 10.1201/b19941-9.

[78] Q. Ma, Z. Xu, and R. Wang, "Distributed solar desalination by membrane distillation: current status and future perspectives," *Water Res.*, vol. 198, p. 117154, 2021. doi.org/10.1016/j.watres.2021.117154

[79] F. Banat, N. Jwaied, M. Rommel, J. Koschikowski, and M. Wieghaus, "Desalination by a 'compact SMADES' autonomous solarpowered membrane distillation unit," *Desalination*, vol. 217, no. 1–3, pp. 29–37, 2007, doi: 10.1016/j.desal.2006.11.028.

[80] H. E. S. Fath *et al.*, "PV and thermally driven small-scale, stand-alone solar desalination systems with very low maintenance needs," *Desalination*, vol. 225, no. 1–3, pp. 58–69, 2008, doi: 10.1016/j.desal.2006.11.029.

[81] F. Banat, N. Jwaied, M. Rommel, J. Koschikowski, and M. Wieghaus, "Performance evaluation of the 'large SMADES' autonomous desalination solar-driven membrane distillation plant in Aqaba, Jordan," *Desalination*, vol.

217, no. 1–3, pp. 17–28, 2007, doi: 10.1016/j.desal.2006.11.027.

[82] R. G. Raluy, R. Schwantes, V. J. Subiela, B. Peñate, G. Melián, and J. R. Betancort, "Operational experience of a solar membrane distillation demonstration plant in Pozo Izquierdo-Gran Canaria Island (Spain)," *Desalination*, vol. 290, pp. 1–13, 2012, doi: 10.1016/j.desal.2012.01.003.

[83] S. Selimli, Z. Recebli, and S. Ulker, "Solar vacuum tube integrated seawater distillation-An experimental study," *Facta Univ. Ser. Mech. Eng.*, vol. 14, no. 1, pp. 113–120, 2016. doi.org/10.22190/FUME1601113S

[84] E. Guillén-burrieza, G. Zaragoza, S. Miralles-cuevas, and J. Blanco, "Experimental evaluation of two pilot-scale membrane distillation modules used for solar desalination," *J. Memb. Sci.*, vol. 409–410, pp. 264–275, 2012, doi: 10.1016/j.memsci.2012.03.063.

[85] R. Schwantes *et al.*, "Membrane distillation: Solar and waste heat driven demonstration plants for desalination," *Desalination*, vol. 323, pp. 93–106, 2013, doi: 10.1016/j.desal.2013.04.011.

[86] K. B. Deshmukh and S. V Karmare, "A review on convective heat augmentation techniques in solar thermal collector using nanofluid," *J. Therm. Eng.*, vol. 7, no. 5, pp. 1257–1266, 2021. doi.org/10.18186/thermal.978064

[87] L. Acevedo *et al.*, "Dynamic Simulation of a Trigeneration Scheme for Domestic Purposes Based on Hybrid Techniques," 2016, doi: 10.3390/en9121013.

[88] B. SRIMANICKAM and S. KUMAR, "Drying investigation of coriander seeds in a photovoltaic thermal collector with solar dryer," 2021. DOI: 10.18186/thermal.1297575

[89] B. J. Newton, "Modeling of solar storage tanks", Master's thesis, University of Wisconsin--Madison. College of Engineering 1995.

[90] S. A. Klein *et al.*, "TRNSYS 17: A transient system simulation program, solar energy laboratory," *Madison, Madison, USA Univ. Wisconsin*, 2010.

[91] A. Hobbi and K. Siddiqui, "Optimal design of a forced circulation solar water heating system for a residential unit in cold climate using TRNSYS," *Sol. Energy*, vol. 83, no. 5, pp. 700–714, 2009, doi: 10.1016/j.solener.2008.10.018.

[92] O. Levenspiel, "Comparison of the tanks-in-series and the dispersion models for non ideal flow of fluid," *Chem. Eng. Sci.*, vol. 17, no. 7, pp. 576–577, 1962, doi: 10.1016/0009-2509(62)87010-9.

[93] Q. Yang, Q. Lin, S. Sammarchi, J. Li, S. Li, and D. Wang, "Water vapor effects on CO2 separation of amine-containing facilitated transport membranes (AFTMs) module: mathematical modeling using tanks-in-series approach," *Greenh. Gases Sci. Technol.*, vol. 11, no. 1, pp. 52–68, 2021. doi.org/10.1002/ghg.2031

[94] F. J. Millero and A. Poisson, "International one-atmosphere equation of state of seawater," *Deep Sea Res. Part A, Oceanogr. Res. Pap.*, vol. 28, no. 6, pp. 625–629, 1981, doi: 10.1016/0198-0149(81)90122-9.

[95] B. M. Fabuss, A. Korosi, and D. F. Othmer, "Viscosities of Aqueous Solutions

of Several Electrolytes Present in Sea Water," *J. Chem. Eng. Data*, vol. 14, no. 2, pp. 192–197, 1969, doi: 10.1021/je60041a025.

[96] M. H. Sharqawy, J. H. Lienhard V, and S. M. Zubair, "Thermophysical properties of seawater: A review of existing correlations and data," *Desalin. Water Treat.*, vol. 16, no. 1–3, pp. 354–380, 2010, doi: 10.5004/dwt.2010.1079.

[97] F. J. Millero, G. Perron, and J. E. Desnoyers, "Heat capacity of seawater solutions from 5° to 35°C and 0.5 to 22‰ chlorinity," *J. Geophys. Res.*, vol. 78, no. 21, pp. 4499–4507, 1973, doi: 10.1029/jc078i021p04499.

[98] M. J Duffy, M. Hiller, D. E Bradley, W. Keilholz, and J. W Thornton, "TRNSYS–features and functionalitity for building simulation 2009 conference," in *Building Simulation 2009*, IBPSA, 2009, pp. 1950–1954. doi.org/10.26868/25222708.2009.1950-1954

[99] S. T. Bouguecha, S. E. Aly, M. H. Al-Beirutty, M. M. Hamdi, and A. Boubakri, "Solar driven DCMD: Performance evaluation and thermal energy efficiency," *Chem. Eng. Res. Des.*, vol. 100, pp. 331–340, 2015, doi: 10.1016/j.cherd.2015.05.044.

[100] H. C. Duong, L. Xia, Z. Ma, P. Cooper, W. Ela, and L. D. Nghiem, "Assessing the performance of solar thermal driven membrane distillation for seawater desalination by computer simulation," *J. Memb. Sci.*, vol. 542, no. August, pp. 133–142, 2017, doi: 10.1016/j.memsci.2017.08.007.

[101] M. Asim, N. T. Uday Kumar, and A. R. Martin, "Feasibility analysis of solar combi-system for simultaneous production of pure drinking water via membrane distillation and domestic hot water for single-family villa: pilot plant setup in Dubai," *Desalin. Water Treat.*, vol. 57, no. 46, pp. 21674–21684, 2016, doi: 10.1080/19443994.2015.1125806.